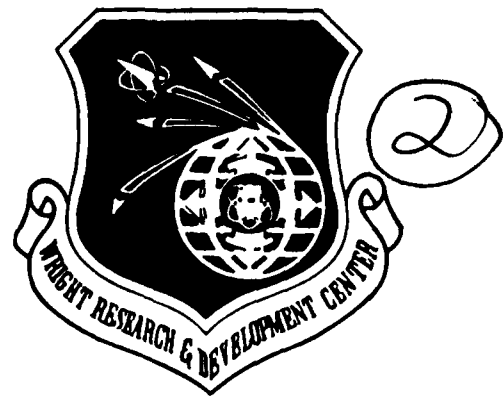


AD-A218 089

DTIC FILE COPY.

WRDC-TR-89-4035



**DETERMINATION OF FUNDAMENTAL THERMODYNAMIC PROPERTIES OF
CONSTITUENT MATERIALS AND PERFORMANCE SCREENING OF CANDIDATE
SYSTEMS**

J.T. Porter
G.H. Reynolds

MSNW, Inc.
P.O. Box 865
San Marcos, California

May 1989

DTIC
SELECTED
FEB 15 1990
S D

Final Report for Period October 1987 to December 1988

Approved for public release; distribution is unlimited.

MATERIALS LABORATORY
WRIGHT RESEARCH AND DEVELOPMENT CENTER
AIR FORCE SYSTEMS COMMAND
WRIGHT-PATTERSON AIR FORCE BASE, OHIO 45433-6533

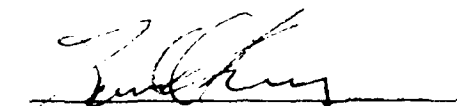
90 02 15 020


NOTICE

When Government drawings, specifications, or other data are used for any purpose other than in connection with a definitely Government-related procurement, the United States Government incurs no responsibility or any obligation whatsoever. The fact the government may have formulated or in any way supplied the said drawings, specifications, or other data, is not to be regarded by implication, or otherwise in any manner construed, as licensing the holder, or any other person or corporation; or as conveying any rights or permission to manufacture, use, or sell any patented invention that may in any way be related thereto.


This report is releasable to the National Technical Information Service (NTIS). At NTIS, it will be available to the general public, including foreign nations.

This technical report has been reviewed and is approved for publication.


Project Engineer
Processing and High Temperature
Materials Branch
Metals and Ceramics Division


Technical Area Manager
Processing and High Temperature
Materials Branch
Metals and Ceramics Division

FOR THE COMMANDER


Acting Chief
Processing and High Temperature
Materials Branch
Metals and Ceramics Division

If your address has changed, if you wish to be removed from our mailing list, or if the addressee is no longer employed by your organization please notify WRDC/MLLM, WPAFB, OH 45433-6533 to help us maintain a current mailing list.

Copies of this report should not be returned unless return is required by security considerations, contractual obligations, or notice on a specific document.

REPORT DOCUMENTATION PAGE

Form Approved
OMB No. 0704-0188

1a. REPORT SECURITY CLASSIFICATION Unclassified		1b. RESTRICTIVE MARKINGS N/A	
2a. SECURITY CLASSIFICATION AUTHORITY N/A		3. DISTRIBUTION / AVAILABILITY OF REPORT Approved for public release; distribution is unlimited.	
2b. DECLASSIFICATION / DOWNGRADING SCHEDULE N/A		4. PERFORMING ORGANIZATION REPORT NUMBER(S) N/A	
6a. NAME OF PERFORMING ORGANIZATION MSNW, Inc.		6b. OFFICE SYMBOL (if applicable)	7a. NAME OF MONITORING ORGANIZATION WRDC/MLLM
6c. ADDRESS (City, State, and ZIP Code) P.O. Box 865 San Marcos, CA 92069		7b. ADDRESS (City, State, and ZIP Code) Air Force Systems Command Wright-Patterson Air Force Base, Ohio 45433-6533	
8a. NAME OF FUNDING / SPONSORING ORGANIZATION WRDC/MLLM	8b. OFFICE SYMBOL (if applicable)	9. PROCUREMENT INSTRUMENT IDENTIFICATION NUMBER F33615-88-C-5401	
8c. ADDRESS (City, State, and ZIP Code) Air Force Systems Command Wright-Patterson Air Force Base, Ohio 45433-6533		10. SOURCE OF FUNDING NUMBERS	
	PROGRAM ELEMENT NO. 62102F	PROJECT NO. 2420	TASK NO. 01
			WORK UNIT ACCESSION NO. 15
11. TITLE (Include Security Classification) Determination of Fundamental Thermodynamic Properties of Constituent Materials and Performance Screening of Candidate Systems			
12. PERSONAL AUTHOR(S) Porter, John T., Reynolds, G.R.			
13a. TYPE OF REPORT Final	13b. TIME COVERED FROM 8710 TO 8812	14. DATE OF REPORT (Year, Month, Day) 8905	15. PAGE COUNT 75
16. SUPPLEMENTARY NOTATION			
17. COSATI CODES		18. SUBJECT TERMS (Continue on reverse if necessary and identify by block number)	
FIELD	GROUP	SUB-GROUP	Refractory Materials, Thermodynamics
			Vaporization,
			Composite Materials
19. ABSTRACT (Continue on reverse if necessary and identify by block number)			
<p>This document reports the Phase I results of a program directed at the validation of thermochemical modeling, combined with selected supplemental experimental techniques, as a basis for screening materials for application in ultra-high temperature composites. The experimental techniques employed were laser probe spectroscopy and high temperature mass spectrometry. Representative candidate constituents, drawn from oxides, carbides, borides, and intermetallics, were assessed under neutral and oxidizing conditions. The modeling approach can, in most cases, define probable limits for material stability. The experimental approaches provide a useful supplement to available data. Improved sensitivity in the laser spectroscopic measurement would be useful and the mass spectrometric technique would benefit from extended pressure sampling capability and reduced cell/heater interactions.</p>			
20. DISTRIBUTION / AVAILABILITY OF ABSTRACT <input type="checkbox"/> UNCLASSIFIED/UNLIMITED <input checked="" type="checkbox"/> SAME AS RPT. <input type="checkbox"/> DTIC USERS		21. ABSTRACT SECURITY CLASSIFICATION Unclassified	
22a. NAME OF RESPONSIBLE INDIVIDUAL R. J. Kerans		22b. TELEPHONE (Include Area Code) (513) 255-9823	22c. OFFICE SYMBOL WRDC-MLLM

FOREWORD

This program was performed under the sponsorship of Wright Research and Development Center, Wright-Patterson Air Force Base, Dayton, Ohio. Dr. Ronald J. Kerans was the Air Force Project Engineer.

The program was performed by MSNW, Inc., Drs. G. Reynolds and J. Porter, with the assistance of the Houston Area Research Center, Drs. M. Berry, T. Kunz, and L. Fredin and Messrs. R. Menefee and B. Krenek, and Rice University, Prof. J. J. Margrave, Drs. R. Hauge and J. Chu, and Ms. M. Sampson.



Accession For	
NTIS GRA&I	<input checked="" type="checkbox"/>
DTIC TAB	<input type="checkbox"/>
Unannounced	<input type="checkbox"/>
Justification	
By	
Distribution	
Availability Codes	
Dist	Availability or Special
A-1	

CONTENTS

<u>Chapter</u>	<u>Page</u>
1. INTRODUCTION AND SUMMARY	1
2. OBJECTIVES	4
2.1 MODELING	4
2.2 LASER PROBE SPECTROSCOPY	5
2.3 MASS SPECTROMETRY AND MATRIX ISOLATION FTIR SPECTROSCOPY	5
3. MATERIALS SELECTION	7
4. RESULTS	8
4.1 MODELING	8
4.1.1 IrAl	8
4.1.2 HfC	11
4.1.3 Y ₂ O ₃ Stabilized HfO ₂	14
4.1.4 SrO·HfO ₂	16
4.2 LASER PROBE SPECTROSCOPY	20
4.2.1 Experimental Apparatus	23
4.2.2 Spectroscopic Data	27
4.3 MASS SPECTROMETRY AND MATRIX ISOLATION FTIR SPECTROSCOPY	42
4.3.1 Experimental Apparatus	42
4.3.2 Experimental Results	49
5. DISCUSSION	63
5.1 MODELING	63
5.2 LASER PROBE SPECTROSCOPY	63
5.2.1 Emission Spectra	64
5.2.2 Absorption Spectra	64
5.3 MASS SPECTROMETRY AND MATRIX ISOLATION FTIR SPECTROSCOPY	65
5.4 MATERIALS AND METHODS COMPARISON	66
6. RECOMMENDATIONS	69
6.1 MODELING	69
6.2 LASER PROBE SPECTROSCOPY	72
6.3 MASS SPECTROMETRY AND MATRIX ISOLATION FTIR SPECTROSCOPY	74
7. REFERENCES	77

ILLUSTRATIONS

<u>Figure</u>	<u>Page</u>
4-1. CALCULATED VAPOR PRESSURES OVER Al/Al ₂ O ₃ AND IrAl/Al ₂ O ₃	10
4-2. PREDICTED VAPOR PRESSURES OF ELEMENTAL Hf AND C, Hf OVER HfC IN A NEUTRAL ATMOSPHERE, AND HfO ₂ IN EQUILIBRIUM WITH HfO ₂	12
4-3. PREDICTED VAPOR PRESSURES OVER Y ₂ O ₃ AND HfO ₂ UNDER NEUTRAL CONDITIONS AND UNDER 10 TORR O ₂	15
4-4. PREDICTED VAPOR PRESSURES OVER HfO ₂ /10 MOLE% Y ₂ O ₃	17
4-5. EQUILIBRIUM VAPOR PRESSURES OVER SrO	19
4-6. EQUILIBRIUM VAPOR PRESSURES OVER SrO·HfO ₂	21
4-7. CALCULATED PRESSURES OVER SrO AND SrO·HfO ₂ UNDER 10 TORR O ₂	22
4-8. HARC CO ₂ LASER TEST RESOURCE	24
4-9. COMPUTER CONTROLLED LASER ABSORPTION SPECTROMETER (CCLAS)	26
4-10. OPTICAL MULTICHANNEL ANALYZER (OMA) SYSTEM	28
4-11. PLUME EMISSION SPECTRUM FROM LASER HEATED Al ₂ O ₃	29
4-12. PLUME EMISSION SPECTRUM FROM LASER HEATED TiB ₂	31
4-13. PLUME EMISSION SPECTRUM FROM LASER HEATED Y ₂ O ₃ AND HfO ₂	32
4-14. PLUME EMISSION SPECTRUM FROM LASER HEATED HfO ₂ -Y ₂ O ₃	33
4-15. PLUME EMISSION SPECTRUM FROM LASER HEATED SrO	34
4-16. PLUME EMISSION SPECTRUM FROM LASER HEATED SrO·HfO ₂	35
4-17. PLUME EMISSION SPECTRUM FROM LASER HEATED HfC	36
4-18. PLUME EMISSION SPECTRUM FROM LASER HEATED ZrC	37
4-19. PLUME EMISSION SPECTRUM FROM LASER HEATED Ir _x Al _y	39
4-20. PLUME EMISSION SPECTRUM FROM LASER HEATED Al ₂ O ₃	40
4-21. CALCULATED VAPOR SPECIES PRESSURE OVER LASER HEATED Al ₂ O ₃	41
4-22. ABSORPTION SPECTRUM OF LASER HEATED Al	43
4-23. ABSORPTION SPECTRUM OF LASER HEATED Ir _x Al _y	44
4-24. SCHEMATIC OF RICE UNIVERSITY MASS SPECTROMETRY SYSTEM	45
4-25. SCHEMATIC OF MATRIX ISOLATION FTIR APPARATUS	46
4-26. FURNACE CONFIGURATIONS USED TO VAPORIZE SAMPLES	48
4-27. VAPORIZATION OF Al IN AN Al ₂ O ₃ CELL	50
4-28. VAPORIZATION OF B ₂ O ₃ IN AN Al ₂ O ₃ CELL	51
4-29. VAPORIZATION OF TiB ₂ + B ₂ O ₃ FROM Al ₂ O ₃	53
4-30. VAPORIZATION OF TiB ₂ WITH O ₂ IN ZrO ₂	54
4-31. MATRIX ISOLATION FTIR SPECTRA OF TiB ₂ + O ₂ IN ZrO ₂ CELL	55
4-32. VAPORIZATION OF Sr + O ₂ FROM SrHfO ₃ AND SrZrO ₃	56
4-33. VAPORIZATION OF Sr + O ₂ FROM SrZrO ₃ WITH VACUUM SEPARATION BETWEEN ZIRCONIA CELL AND Ta HEATER	58
4-34. APPEARANCE POTENTIAL OF Zr AND ZrO FROM THE VAPORIZATION OF SrZrO ₃	59
4-35. VAPORIZATION OF Al FROM Ir _{0.4} Al _{0.6}	61
4-36. VAPORIZATION OF Al FROM Ir _{0.4} Al _{0.6} WITH AND WITHOUT ADDED O ₂	62
6-1. HIGH TEMPERATURE MATERIALS EVALUATION APPROACH	70
6-2. HIGH PRESSURE MOLECULAR BEAM MASS SPECTROMETER PROBE	73

TABLES

3-1	MODEL MATERIALS.	7
4-1	PRELIMINARY LASER SPECTROSCOPIC OBSERVATIONS	23

CHAPTER 1

INTRODUCTION AND SUMMARY

The present program was undertaken to validate the application of thermochemical modeling, combined with specifically directed experimental measurements, as a screening tool in the development of ultrahigh temperature composite materials. If successful, this approach will permit the substantial existing information base to be used at an early stage of materials development and to supplement short time experimental measurements on small samples and under controlled environmental conditions. In this program, efforts were limited to single phase candidate constituent materials under conditions of varying O_2 pressure. Proposed future work will extend measurement to significant composite combinations.

The primary modeling approach employed is classical thermochemical analysis based upon compiled thermodynamic data. At the high temperatures of interest, this analysis can be extended to dynamic evaluation through incorporation of mass transport considerations.

In selecting experimental methods, the objective was to employ existing equipment and facilities that were expected to be available on a continuing basis without requiring dedicated systems. The experimental approaches selected are laser probe spectroscopy, employing the facilities at the Houston Area Research Center, and mass spectrometry, employing the facilities of the Chemistry Department of Rice University.

Laser probe spectroscopy examines, by either emission or absorption, the spectra of volatile species in the near surface region of a laser heated sample. Since the required temperature is achieved by direct energy absorption by the sample, the system does not require that extraneous materials be maintained at measurement temperatures. Samples can, in effect, be self-contained. Atmospheric composition and pressure are limited only by mechanical considerations of the experimental chamber and transparency to the heating and probing wavelengths. The chamber remains near ambient temperature.

Mass spectrometry has demonstrated capabilities for determining both simple and complex volatile species and, in conjunction with Knudsen cell methodology, for providing a significant portion of the currently available thermodynamic data for high temperature materials. The Rice University facility includes a capability for carrying out matrix isolation, Fourier transform infrared (FTIR) analysis. This provides a basis for distinguishing between alternatives when more than one origin of a particular charge/mass ratio peak in the mass spectrum is possible.

In selecting the experimental materials, an effort was made to achieve as wide a representation of suggested materials for ultrahigh temperature composites as possible. The materials employed included four combined or solid solution oxides, two carbides, one boride, and one intermetallic. Several pure oxides and aluminum metal were examined as reference materials.

The modeling effort was directed at estimating results for the conditions in the experimental investigations, in particular, the pressures of volatile species under a range of O_2 activity. One objective was to test the capability of analysis based on the existent data base in a range of conditions and materials. It was found that a wide range of conditions could be adequately treated, but only limited data are available for refractory intermetallic systems and ambiguity exists in treating systems involving compounds with extensive ranges of homogeneity. Comparison with experimental results encountered some difficulties arising from uncertainties in the effective O_2 pressures in the experiments.

The laser probe spectroscopic investigations demonstrated the ability of emission spectral analysis to identify volatile species in the near surface environment of laser heated samples. Further, temperature capabilities in excess of 3000K were shown. These extreme temperatures allow ready identification, at higher pressures, of species expected to contribute significantly to material performance at lower temperatures and pressures. Significant improvement in the quantification of concentrations in the laser plume was achieved, a first step toward interpretive quantification.

The mass spectrometric measurements verified the ability to determine a wide range of simple and complex vapor species simultaneously. It was found that measurement of oxides at high temperature and, in general, under significant O_2 pressures was hampered by interactions of the cell, sample, and heater. In some cases, significant thermodynamic data could be obtained despite these interferences, but in the present configuration they limit capabilities.

Overall, the results indicate that thermochemical modeling is a useful preliminary screening tool. It can be employed early in development and identifies the physical basis of any indicated limitation. The coordinated experimental techniques investigated are also applicable early in development. Only small samples are required, the environment can be controlled, and the measurements are of short duration.

Certain areas of development for both the modeling and experimental efforts can be identified from the work performed. The modeling needs to be extended to the consideration of kinetic parameters, in particular mass transport. The equilibria pressures developed in classical thermochemical analysis can be translated

into mass loss rate estimates when combined with appropriate mass transport models. Such models will be application specific. In particular, the aerodynamic boundary conditions will have to be established. This extension is also necessary for the continued development of the experimental methods being employed. Both are, or are evolving toward, open systems, as distinguished from the closed Knudsen cell type of system. Estimation of conditions at the defined surface and surface temperature, which can provide estimates of thermodynamic properties, requires the evaluation of the mass transport between that surface and the sampled vapor space.

The laser probe approach would benefit greatly from increased sensitivity. Temperatures in the 2500-3500K (4000°-5800°F) range were needed to obtain workable signal strength in several cases. Measurements down to 1500K (2240°F) would be desirable to characterize materials closer to application temperatures. Though present results are valuable, it is desirable to extend the measurements to temperatures and pressures of application. There is also a need to introduce an assessment of mass transport conditions to extract thermodynamic quantities from measured gas phase concentrations.

The usefulness of the mass spectrometric approach would be enhanced by a capability to carry out sampling from the near surface region of materials heated by laser irradiation in higher pressure environments. This development is in the direction of an open system. Again, mass transport analysis will be required to extract basic data.

CHAPTER 2

OBJECTIVES

This program was undertaken by MSNW, Inc., the Houston Area Research Center (HARC), and Rice University to demonstrate the applicability of thermochemical modeling, supported by selective experimental methods, to performance screening of multiphase composite materials for ultrahigh temperature application.

The experimental approaches selected are laser probe spectroscopy and a combination of mass spectrometry and matrix isolation, Fourier transform infrared (FTIR) spectroscopy. Laser probe spectroscopy permits very rapid determination of vapor species evolved when a sample is heated with a second laser source. Mass spectrometry is a versatile method for the simultaneous determination of a variety of species evolved from a heated sample, while matrix isolation FTIR spectroscopy provides a basis for distinguishing between alternatives in the occasional event of ambiguity of mass/charge ratios.

Examination was confined to single phase constituent materials. However, the projected complexities of true composite materials were addressed to some extent. Since both analytical and experimental efforts were concerned with neutral and oxidizing environments, in the case of materials forming stable condensed oxides, the systems in question have become multiphase.

2.1 MODELING

The thermochemical modeling effort was intended to examine how far assessment can be carried forward relying on available data from the major compilations supplemented by individual reports as appropriate. As part of a coordinated program of theoretical and experimental investigations, the modeling effort also attempted to predict and/or clarify the observations in the experimental studies.

Although thermodynamic analysis is not, in principle, limited to reactions involving gaseous species, the modeling was limited to these reactions. The experimental techniques considered involve the characterization and measurement of gaseous species. Further, the availability and reliability of thermodynamic data are such that modeling is most reliable under those conditions.

2.2 LASER PROBE SPECTROSCOPY

The major goals of the program at HARC were:

- (1) The development of a laser probe spectroscopy method suitable for studies on laser heated materials held in vacuum and low partial pressure oxidizing environments.
- (2) Demonstration of the utility of the method by studying atomic and diatomic species produced from laser heating model materials.

The ultimate goal of this program was to develop the capability to model and predict material performance in inert, oxidizing, and moist oxidizing environments based on data obtained from the laser probe spectroscopy method.

The laser probe spectroscopy method uses a computer controlled laser absorption spectrometer (CCLAS) and an optical multichannel analyzer (OMA) for measurement of emission spectra. The experimental facility is described in Section 4.2.

2.3 MASS SPECTROMETRY AND MATRIX ISOLATION FTIR SPECTROSCOPY

The principal objectives of the mass spectrometric and matrix isolation FTIR investigations at Rice University were:

- (1) To establish techniques for obtaining high temperature thermodynamic data for ultrahigh temperature materials under neutral and oxidizing conditions.
- (2) To obtain thermodynamic measurements on selected borides, carbides, oxides, and alloys at high temperatures under varying conditions.

Mass spectrometric and matrix isolation molecular beam monitoring of species evolved from resistively heated high temperature furnaces was used to identify species volatilized from the experimental materials. The furnace design permits the passage of O₂ directly over the sample when the sample is contained in oxide cells. Mass spectrometry was used to obtain quantitative measures of the volatile species as a function of temperature. The advantages of the two methods are as follows:

Mass Spectrometric Sampling

- (1) Identifies both simple and complex species.
- (2) Possesses high dynamic range and high sensitivity.
- (3) Real time monitor of species.

Matrix Isolation FTIR Sampling

- (1) Identifies both simple and complex species.
- (2) Possesses moderate dynamic range and sensitivity.
- (3) Can distinguish between species with the same mass, i.e., Al_2O_3 and B_2O_3 , SiO and CO_2 , or geometric isomers, i.e., HBO or BOH.

The high dynamic range and sensitivity of mass spectrometry makes it the preferred method for quantitative studies.

CHAPTER 3

MATERIALS SELECTION

Although the primary objective of the present program was the demonstration of the utility of certain analytical and experimental methodologies in the preliminary assessment of materials, an attempt was made to extend the demonstration to materials relevant to ultrahigh temperature composites. As the program was initiated, a letter soliciting recommendations was distributed to Air Force personnel and other contractors involved in this effort. In addition, discussions were held with various workers at the interim review.

Based on these recommendations and discussions and general technical considerations, the materials selected for investigation included both pure and mixed oxides, carbides, one boride, and one refractory intermetallic. These materials and reference materials examined are listed in Table 3-1.

TABLE 3.1. MODEL MATERIALS

Oxides

HfO₂ - Y₂O₃ Stabilized
ZrO₂ - Y₂O₃ Stabilized
SrO·ZrO₂
SrO·HfO₂

Carbides

HfC
ZrC

Boride

TiB₂

Intermetallic

IrAl (60 at% Al)

Reference Materials

Al Y₂O₃
Al₂O₃ B₂O₃

CHAPTER 4

RESULTS

4.1 MODELING

The thermochemical modeling was carried out to provide estimates of expected vapor species pressures to assist in understanding and provide a reference basis for the experimental investigations. This effort was in part an application exercise to determine how far it was possible to carry out analysis on the basis of existing data.

For the modeling effort, behavior was generally examined under neutral conditions and oxidizing conditions. Here neutral means that the surrounding atmosphere contains negligible pressures of any vaporization products or species that would react with those products. Experimentally this condition is most often met by vacuum operation, but a clean inert gas leads to the same thermochemical expectations. Oxidizing conditions have here been taken as 10 torr O_2 . It is noted that from a thermochemical view, the O_2 pressure enters logarithmically. The difference in going from 10 torr to 100 torr is of the same magnitude as in going from 1 torr to 10 torr.

The materials examined include an intermetallic, a carbide, and several oxides. For the intermetallic, the analysis indicates that mass spectrometry under neutral conditions provides an excellent basis for refining the available thermochemical data. Under oxidizing conditions the stable species for the intermetallic is the stable oxide. For the carbide, the neutral atmosphere behavior is that of the elements, with partial pressures reduced by compound formation. Under oxidizing conditions the stable species become CO and the oxide of the metal of the carbide. For oxides, two general trends can be observed in the analysis. First, since oxides in general decompose to the metal or a lower oxide and O under neutral conditions, vaporization is suppressed by even modest O activity. Second, where a mixed oxide compound or strongly interacting solid solution is formed, the vapor pressures of metal containing species are reduced.

4.1.1 IrAl

Mass spectrometric measurements of the temperature dependence of the Al(g) pressure over the IrAl material investigated have provided an estimate of the thermodynamic stability of this intermetallic.

In carrying out these measurements, Al_2O was also observed. The O observed may have originated from the background gas of the

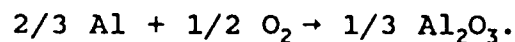
mass spectrometer or as an impurity in the sample. Oxygen in phase-pure IrAl can have an activity between zero and the minimum required for the stability of Al_2O_3 in equilibrium with IrAl. An upper limit can be established from the behavior of IrAl in equilibrium with Al_2O_3 . This limit is interesting both with respect to assessment of the experimental behavior and applications considerations.

As the concentration and activity of O_2 in IrAl are increased, a limit is reached when the most stable oxide, Al_2O_3 , separates. The O_2 activity for IrAl in equilibrium with Al_2O_3 represents the upper limit of O_2 activity that can be attributed to the sample in experiments. It also represents the lower O_2 activity limit to maintain a protective Al_2O_3 layer.

The phase diagram for IrAl is not well established. On the basis of the approximate diagram of Worrell,¹ the sample material lies in a single phase, Al-rich IrAl region. In this event, the Al activity is higher than for the stoichiometric IrAl compound but lower than for IrAl_3 . In the absence of data on the stoichiometric phases, one can attempt an estimate. Following Kubaschewski and Alcock,² one estimates that the heat of formation per gram atom would be some 20% or less smaller in magnitude than for stoichiometric IrAl.

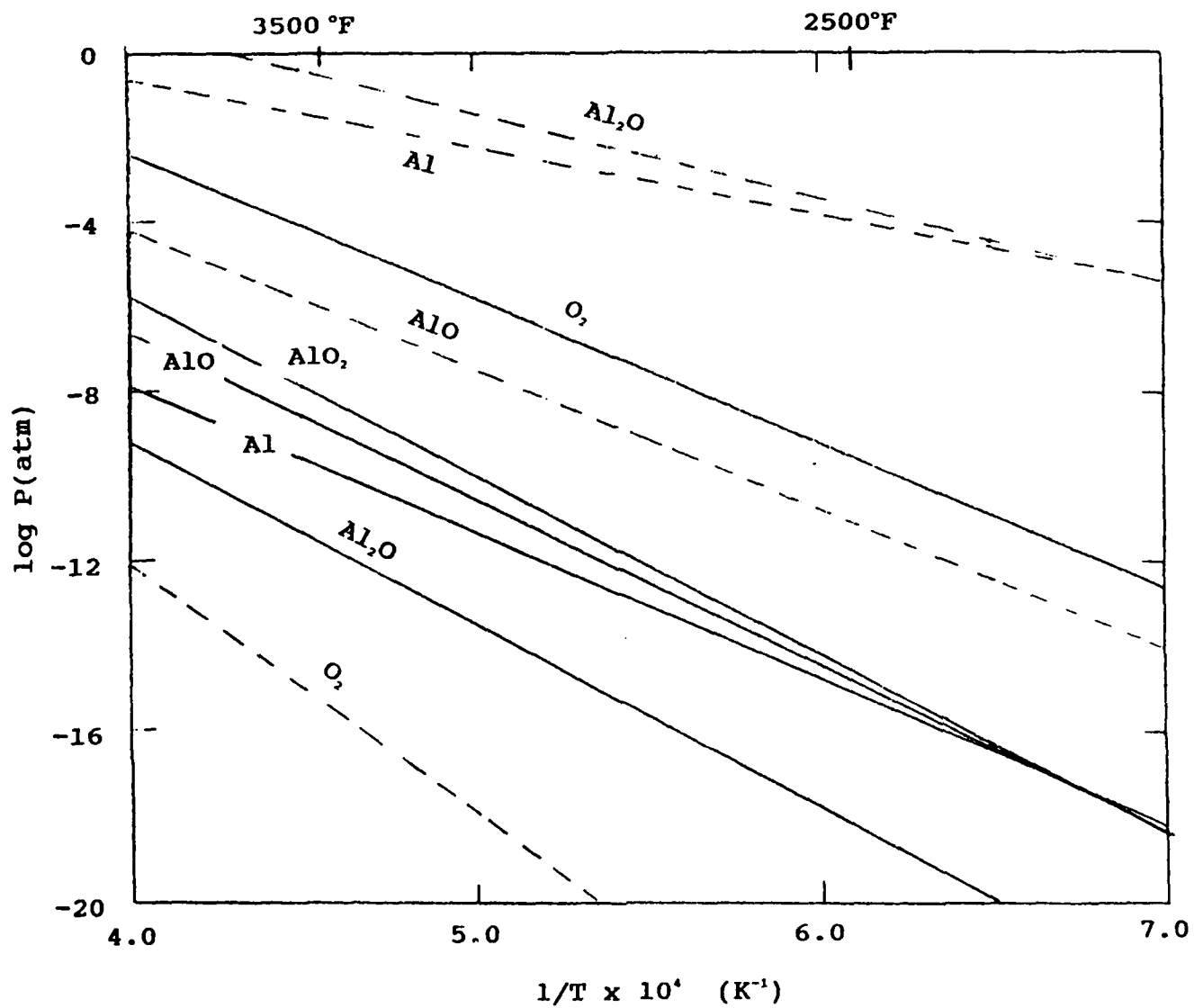
The free energy of formation of IrAl_x has been taken as -84 kcal per Al on the basis of early results from the mass spectrometric measurements at Rice University. As discussed in Section 4.3.2.5, experimental uncertainties, possibly associated with an initial oxide surface layer, have introduced uncertainties into the interpretation of the mass spectrometric data. It is presently the opinion of the Rice group that the heat of vaporization of Al from IrAl_x , and hence the heat of formation of IrAl_x , is lower than initially estimated. The result would be that the behavior of Al in IrAl_x would be closer to that of pure Al.

This process is to be compared with the reaction of pure Al,



The free energy of formation of the product is identical in the two cases, while for the reactants, the free energy of formation is zero in the case of elemental Al. The free energy of reaction for the aluminide will be less negative by the magnitude of the free energy of formation of the aluminide. As a result, the equilibrium O_2 activity for coexistence with the oxide is higher for IrAl, as shown in Figure 4-1.

For the coexistence of IrAl or Al with Al_2O_3 , the Al(g) activity can be calculated from the vaporization processes. For the aluminide, the activity is reduced by the free energy of



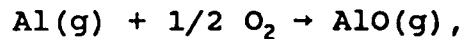
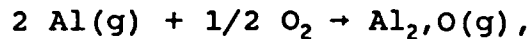
Vapor equilibrium species over:

Al/Al₂O₃ - - - - -
 IrAl/Al₂O₃ ———

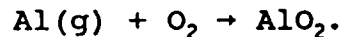
FIGURE 4-1. CALCULATED VAPOR PRESSURES OVER Al/Al₂O₃ AND IrAl/Al₂O₃

formation of the aluminide. The Al(g) pressures are shown in Figure 4-1.

With the O₂ and Al activities fixed, the activities of Al₂O, AlO, and AlO₂ are fixed by the reactions



and



The calculated pressures for these species, in equilibrium with IrAl/Al₂O₃ or Al/Al₂O₃, are also presented in Figure 4-1. In the IrAl case, the O₂ pressure is increased by ten or more orders compared with the Al case and the Al pressure is down some seven orders or more. As a consequence, the composition of the gaseous oxide species is fundamentally altered. In the IrAl case, the abundant O₂ containing Al species are O₂-rich AlO₂ and AlO, while in the Al case, the dominant species is the O₂-poor Al₂O, even AlO occurring at much lower concentration.

With respect to experimental investigation, these results suggest that as one departs from neutral conditions for pure material, in the direction of increasing O₂ activity, the dominant gas phase oxide species will be Al₂O at low O₂ activity. In the case of Al, this remains true up to Al₂O₃ separation. In the case of IrAl, however, the O₂ activity for O₂ at Al₂O₃ separation is so high that the dominant gas phase oxide species can be AlO₂ and AlO.

From an operational view, the volatility of any Al containing species is lower for IrAl than for Al. On the other hand, the O₂ activity in equilibrium with IrAl/Al₂O₃ is much higher. For temperatures in the range of 4000°F (1/T = 4x10⁻⁴), Al₂O₃ in contact with the aluminide becomes unstable with respect to decomposition to the aluminide and O₂ at O₂ partial pressures of the order of 1 torr. While relatively small, this O₂ pressure is not extreme compared with high altitude or fuel-rich environments.

4.1.2 HfC

It is anticipated that HfC will volatilize via decomposition; i.e., the primary expected species will be those associated with the elements. Both Hf and C are refractory and their activities will be further reduced through the formation of the carbide.

The upper lines in Figure 4-2 show the expected vapor pressures of the elements. Carbon is represented by the monatomic C, but there are significant pressures of C₂ and C₃ and lesser amounts

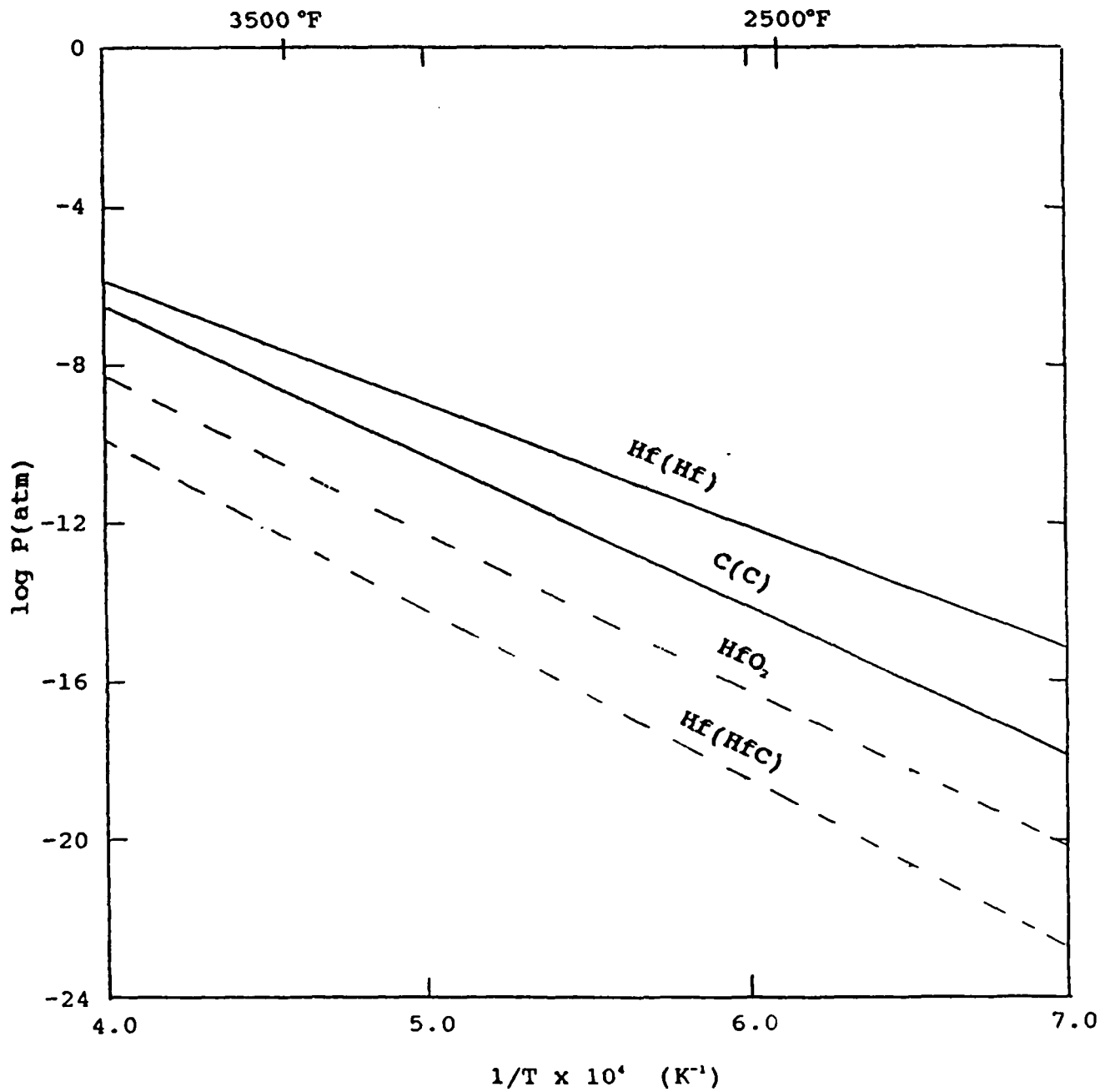
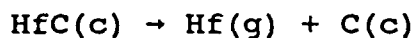


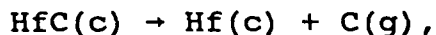
FIGURE 4-2. PREDICTED VAPOR PRESSURES OF ELEMENTAL Hf AND C, Hf OVER HfC IN A NEUTRAL ATMOSPHERE, AND HfO₂ IN EQUILIBRIUM WITH HfO₂. (CONDENSED PHASE IS INDICATED IN PARENTHESES.)

of C_4 and C_5 . In fact, at 2500K the pressure of C_3 exceeds that of C. At the reduced activities associated with the compound, however, more highly decomposed species are favored.

Both Hf and C are stabilized relative to the elements through the formation of the carbide. If the postulated vaporization processes were



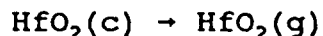
or



equal stabilization would be expected since the decomposition of one mole of HfC is involved in both cases.

Since the vapor pressure of Hf exceeds that of C, it is reasonable to treat the vaporization of Hf as the basic process. The loss of Hf would result in a more carbon-rich composition until the composition of the phase boundary with C was reached. At this composition, C would be left by further Hf loss. The vapor pressure of C is, however, greater than that of Hf over HfC; therefore, vaporization would continue congruently with the phase boundary composition. The lowest line in Figure 4-2 reflects the calculated pressure of Hf from HfC, the homogeneity range being ignored. The expected pressure of C would be essentially equivalent once the phase boundary composition was reached, the relative abundance of the polyatomic species being reduced at the low pressures.

In the presence of O_2 , the expected products are $\text{HfO}_2(c)$ and CO. For significant pressures of O_2 , the expected vaporization process for HfO_2 is



rather than the dissociative decomposition



observed for HfO_2 in a neutral atmosphere.

As can be seen in Figure 4-2, the expected vapor pressure of the oxide is greater than the Hf pressure predicted from the carbide under neutral conditions.

This analysis may account for the observation that in laser probe investigations, a structured emission was observed under vacuum conditions but only a weak and structureless emission under 10 torr O_2 . In vacuum, the vaporization occurs as the elements and the structured emission signal is of the sort that would be expected for elemental Hf. In the presence of O_2 , however, the gas

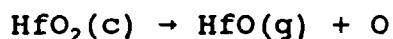
phase species are primarily HfO_2 and CO . Neither of these would be expected to exhibit strong emission.

Laser heating of the sample can be carried out with the beam impinging only the sample. When operating in this manner, no enclosure or support structure has to be heated to the experimental temperature, only the sample. This capability is illustrated by the HfC measurements. The spectra were obtained at 3500K (5800°F). Although this temperature is in excess of projected application, the ability to achieve such temperature allows the identification of limiting processes and processes that can be expected with lower pressures at reduced temperature.

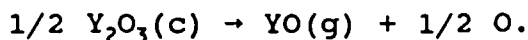
4.1.3 Y_2O_3 Stabilized HfO_2

Yttria stabilized hafnia is one of the most refractory oxide systems. Both constituents are of high stability, but there is a question as to whether the composition is fully stable at extreme temperatures. In particular, it is not known whether the relatively volatile Y_2O_3 will be lost preferentially with HfO_2 , leading to a compositional shift to a material subject to phase transition on thermal cycling.

The volatility characteristics of the pure components are illustrated in Figure 4-3. In neutral atmospheres, the vaporization processes are



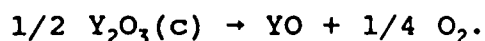
and



In the presence of O_2 , taken at 10 torr for the present analysis, HfO_2 becomes the dominant species for $\text{HfO}_2(\text{c})$, as discussed in relation to HfC behavior above:



The vaporization of Y_2O_3 as an oxide higher than YO has not been reported. In the presence of O_2 , however, the vaporization process becomes



The expected values in 10 torr O_2 are also shown in Figure 4-3.

In solid solution the vapor pressures would be expected to be less than those of the pure components. For Y_2O_3 in particular, even ideal solution would lead to an expected order of magnitude reduction in vaporization at concentrations of the order of 10 mole%. The evidence is, however, that there is a significant interaction

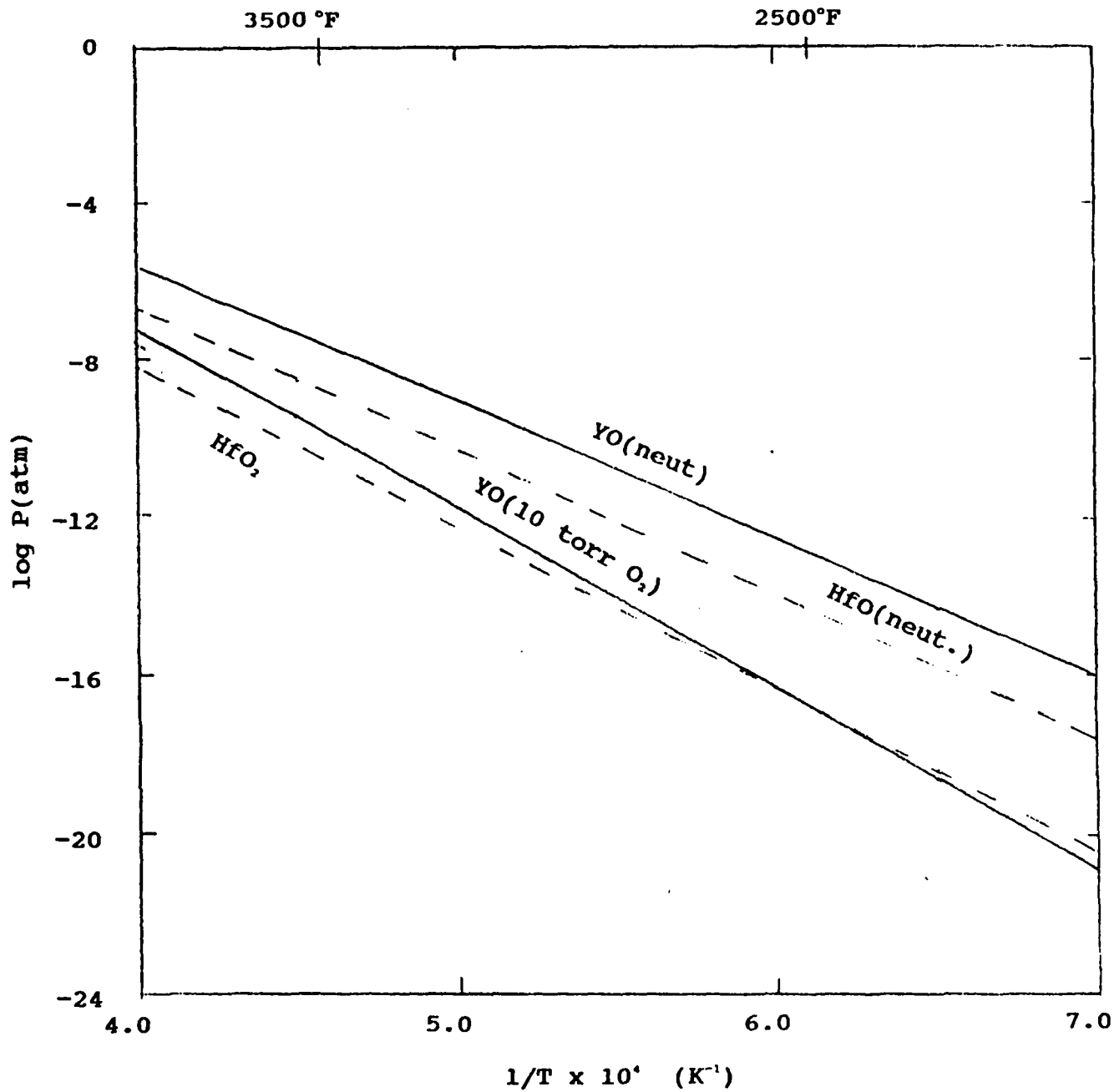
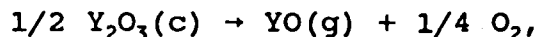


FIGURE 4-3. PREDICTED VAPOR PRESSURES OVER Y_2O_3 AND HfO_2 UNDER NEUTRAL CONDITIONS AND UNDER 10 TORR O_2

between Y_2O_3 and HfO_2 . On the basis of the results reported by Belov and Semenov,³ the activity coefficient for Y_2O_3 at 10 mole% is 0.01. (Although the results are strictly applicable at 2843K, it is expected that they should be reasonably good in the temperature range of interest.) The total reduction in activity is thus of the order of 10^3 . From the form of the vaporization equation



however, the YO pressure varies with the square root of the Y_2O_3 activity; therefore, the pressure reduction is approximately a factor of 30. For this composition, the activity coefficient estimated for HfO_2 is 0.8, giving an expected activity of HfO_2 of 0.7.

The estimated values for the solid solution are shown in Figure 4-4. It can be seen that the YO pressures have fallen below those of HfO or HfO_2 . This indicates that the activity reduction for Y_2O_3 should reduce or eliminate any tendency toward instability deriving from differential volatility of Y_2O_3 .

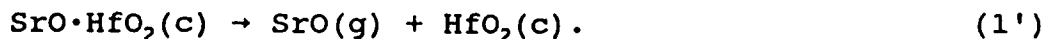
4.1.4 SrO·HfO₂

The vaporization of $SrO·HfO_2$ is expected to occur incongruently with the net loss of SrO . The process can be usefully compared with the vaporization of pure SrO . Thermochemically, one anticipates a reduction in the SrO activity as a result of compound formation. This will be accompanied by a reduction in the pressures of volatile species.

Considering the vaporization of SrO , either from strontia or from the hafnate, the initial vapor species can be formally taken as $SrO(g)$,



or



The $SrO(g)$ may dissociate,



At the temperatures and pressures of interest, it is also necessary to consider the dissociation of O_2 ,



under neutral conditions, i.e., with only the gaseous products from the vaporization present. The SrO dissociation reaction could be written in the alternative form



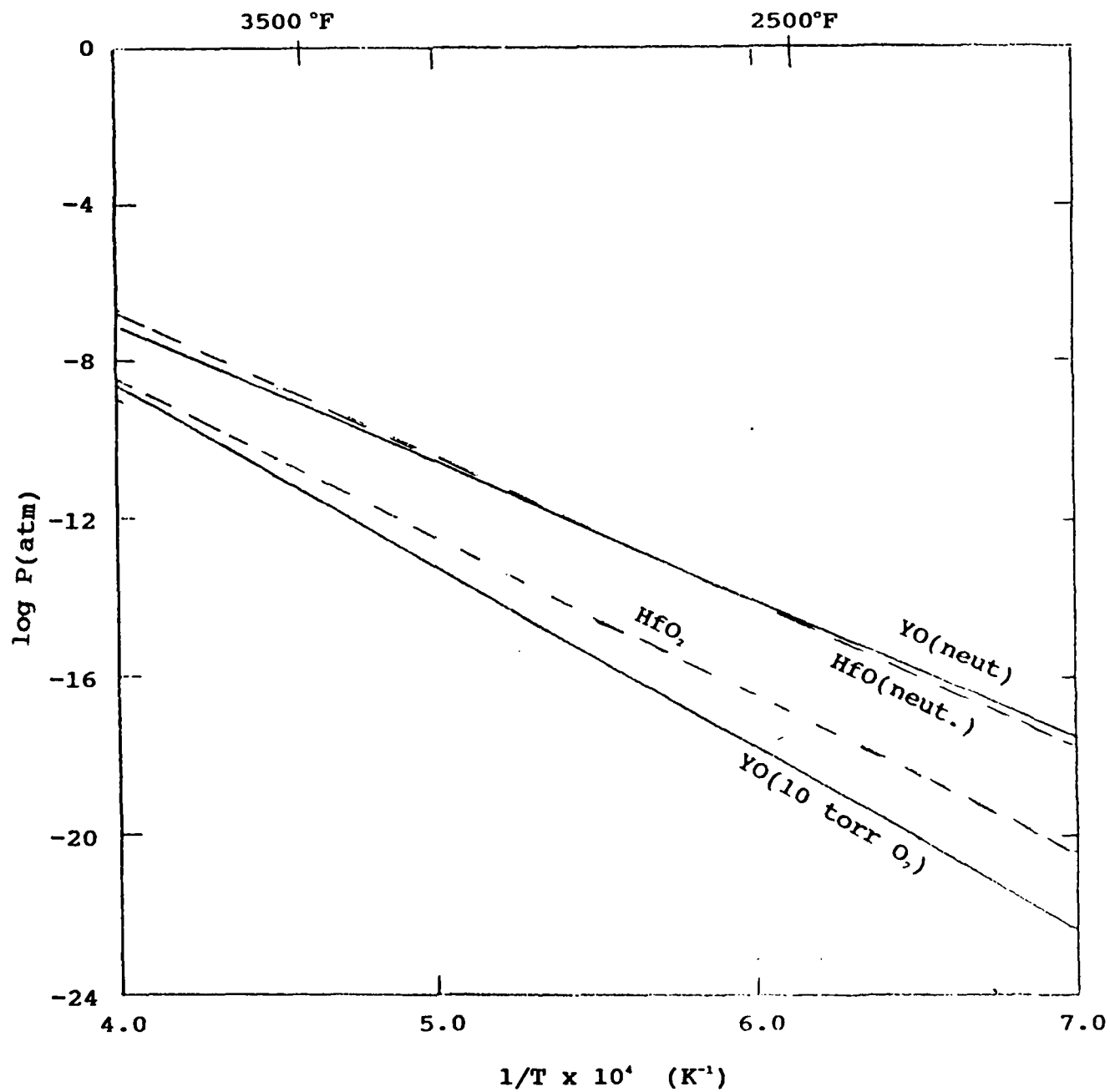


FIGURE 4-4. PREDICTED VAPOR PRESSURES OVER HfO₂/10 MOLE% Y₂O₃

The unknown concentrations to be determined under equilibrium conditions are

[SrO]
[Sr]
[O₂]
[O].

Standard algebraic requirements are that the number of independent equations equal the number of unknown, i.e., four. The choice is to some extent arbitrary.

Among the alternatives possible, the following were selected for the other three equations:

1. The SrO(g) pressure, taken from (1) or (1'). Since there is a single gaseous species involved, the equilibrium pressure is determined by the temperature.

2. Mass balance,

$$[\text{Sr}] = [\text{O}] + 1/2 [\text{O}_2],$$

from (2) and (2'). The Sr present must be compensated by O and O₂ under neutral conditions.

3. The equilibrium of (2'),

$$K_2 = [\text{Sr}][\text{O}]/[\text{SrO}].$$

4. The equilibrium of (3),

$$K_3 = [\text{O}]/[\text{O}_2]^{1/2}.$$

This results in a set of nonlinear equations which can be reduced to a cubic equation in [O].

The thermochemical data for the determination were drawn from the JANAF tables,⁴ the compilation of Schick,⁵ and, for the thermochemistry of formation of SrO·HfO₂, the report of L'vova and Feodos'ev.⁶ The measurements of L'vova and Feodos'ev provide only enthalpy of reaction at near ambient temperature. For present purposes, the entropy change has been taken as zero and the enthalpy change as independent of temperature. This approximation is expected to be reasonable. For condensed phase reactions, the entropy change and temperature dependence of the enthalpy change are small.

The results for SrO are presented in Figure 4-5. It is noted that the Sr pressure exceeds the SrO pressure over the entire, wide, temperature range, but to a greater extent at low

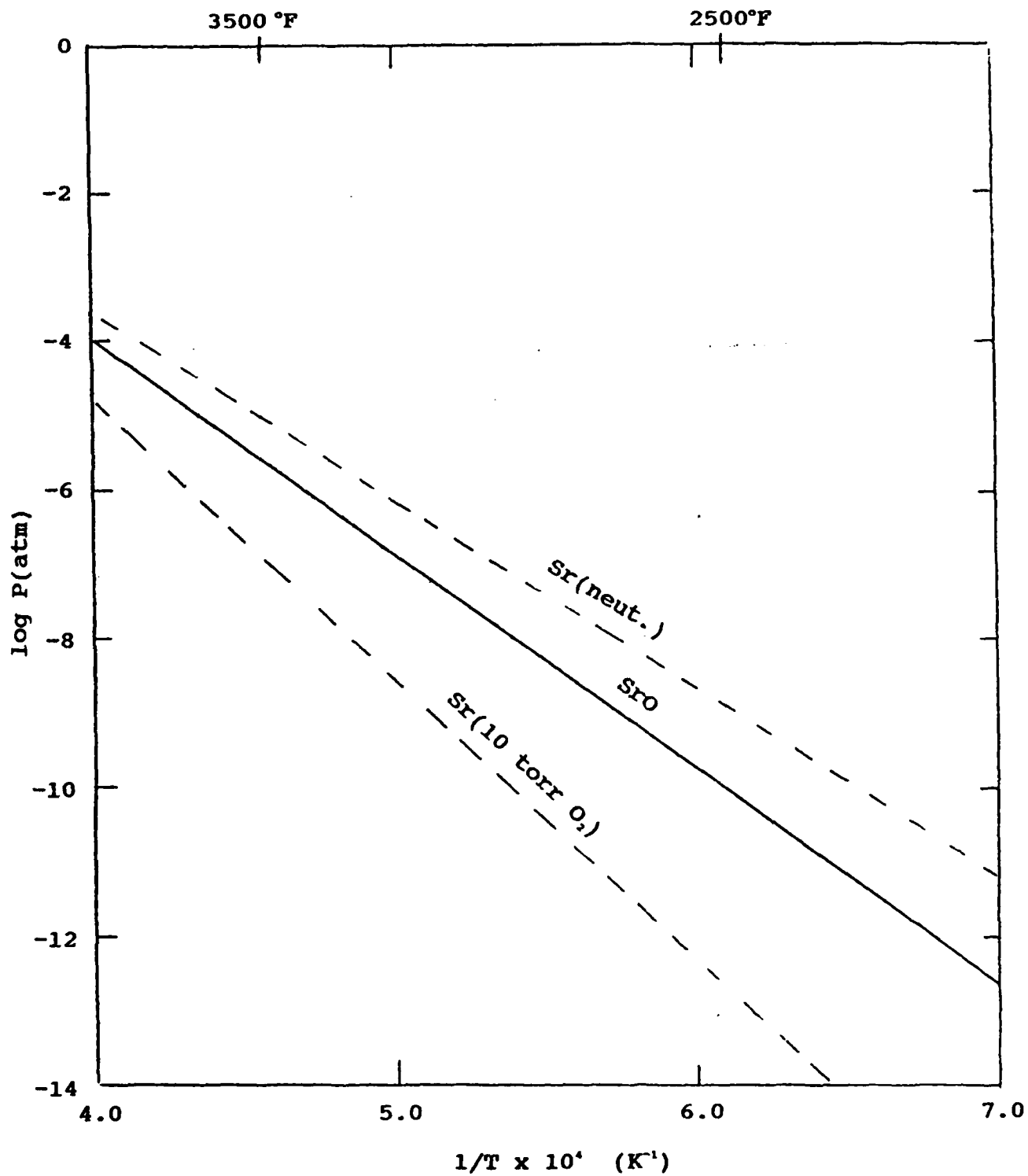


FIGURE 4-5. EQUILIBRIUM VAPOR PRESSURES OVER SrO

temperature. It will also be noted that the O and O₂ pressures are comparable. It is this near equivalence of concentration that requires the inclusion of the O/O₂ equilibrium in the solution of the problem.

The corresponding results for SrO·HfO₂ are shown in Figure 4-6. The pressures are lower, as expected from the lower free energy of SrO in SrO·HfO₂ compared with SrO. It is also noted that the Sr/SrO ratio is larger. The dissociation of SrO(g) proceeds to a greater extent at low pressures. Also, and for the same reason, the concentration of O relative to O₂ is larger.

In the presence of an oxidizing atmosphere, the dissociation of SrO(g) via (2) or (2') and the dissociation of O₂ via (3) will be reduced. At 10 torr O₂, the dissociation reaction (3) only proceeds to about 6% at the 3333K extreme taken. To a close approximation, (2') and (3) can be ignored. The SrO(g) concentration remains determined by the equilibrium of (1) and the Sr concentration is now determined by the equilibrium of (2), with the O₂ pressure fixed at 1.3×10^{-3} .

The results for both SrO and SrO·HfO₂ are presented in Figure 4-7. The SrO pressures are the same as in Figures 4-5 and 4-6, but the Sr concentration is suppressed by the ambient O₂ concentration. This results in a substantial reduction in the total Sr plus SrO concentration, i.e., a decrease in the volatility of SrO. In addition, the [Sr]/[SrO] is now much less than unity at lower temperatures and only approaches unity at the highest temperatures. (In the case of SrO, the plot has been cut off at approximately the temperature at which [O₂] in the neutral atmosphere case equals 10 torr, since the 10 torr condition loses its significance.)

4.2 LASER PROBE SPECTROSCOPY

The major goal of this program was the development of a laser probe spectroscopy method suitable for studies on laser heated materials held in vacuum and low partial pressure oxidizing environments. HARC's efforts were directed toward spectroscopic measurements of ultrahigh temperature species produced from CO₂ laser heating of model constituent materials. The HARC CO₂ Laser Test Resource, described Section 4.2.1.1, was used to record data. The laser probe spectroscopy method proved to be particularly well suited for the detection of atomic and diatomic species produced during laser heating of model materials. Additionally, a Princeton Instruments optical multichannel analyzer (OMA) system [equipped with Instruments SA Model HR320 0.32 meter monochromator and low resolution (150 lines/mm) grating] was used by HARC to record emission spectra of vapor species close to the sample surface during laser heating of materials. Though not quantitative, the OMA recorded emission spectra which were used to identify some of the vapor species constituents produced from the heated sample (not all of the vapor species may be emitting at a wavelength detected by

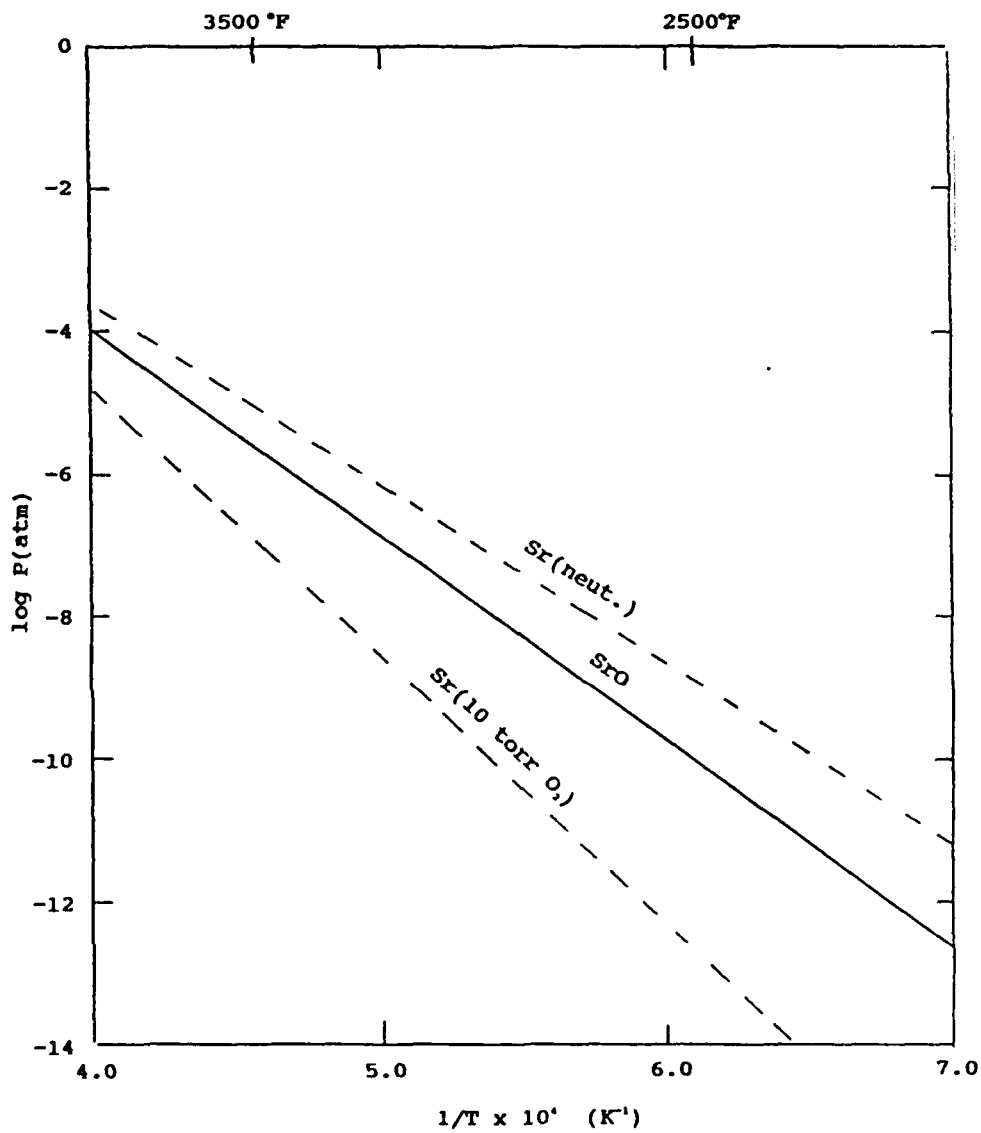


FIGURE 4-6. EQUILIBRIUM VAPOR PRESSURES OVER SrO·HfO₂

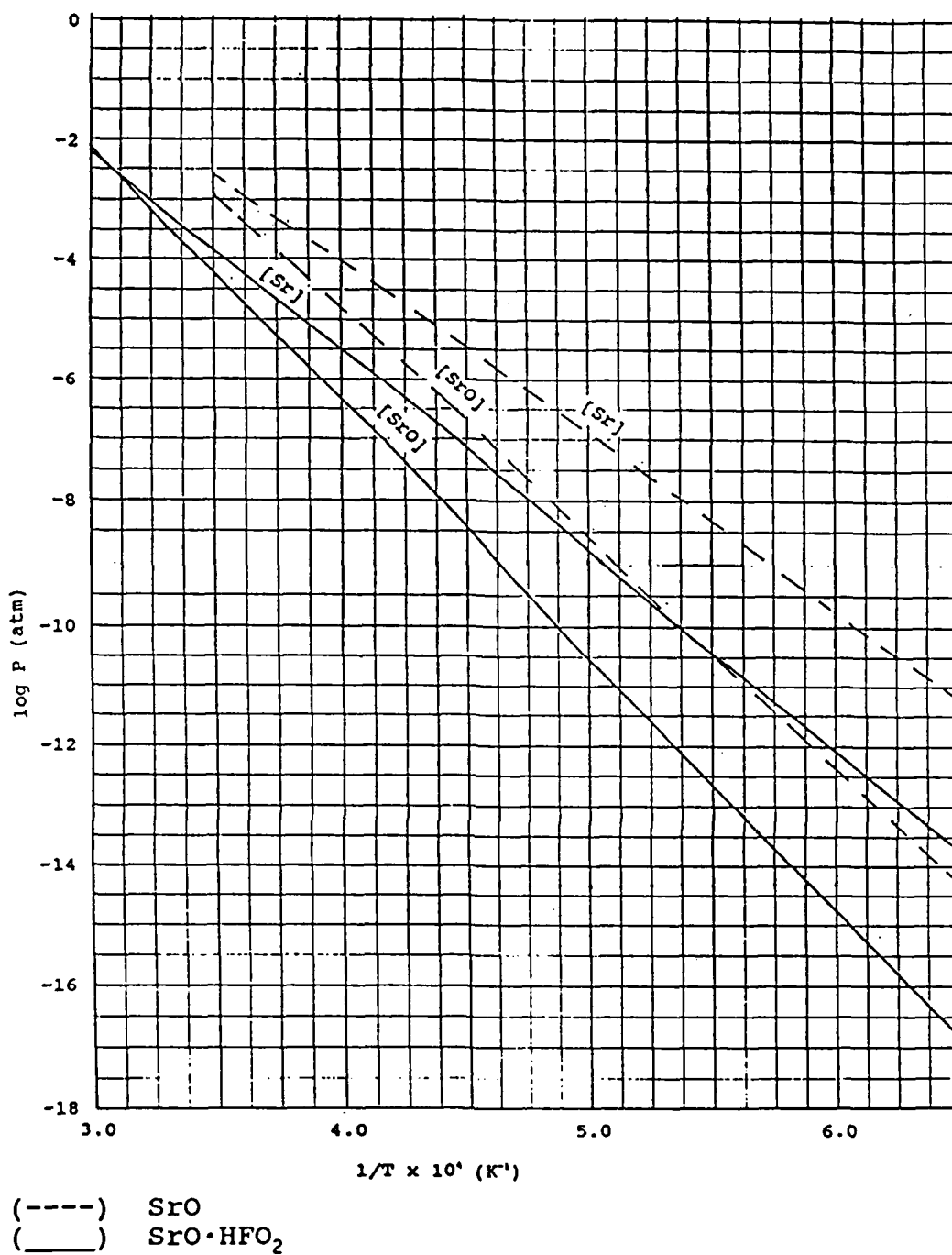


FIGURE 4-7. CALCULATED PRESSURES OVER SrO AND SrO·HfO₂ UNDER 10 TORR O₂

the current OMA system). Table 4-1 lists the materials, environment (vacuum or 10 torr O₂), and type of spectra (plume optical emission and/or laser probe absorption) recorded.

Generally, the emission spectra recorded by the OMA provided spectroscopic evidence to identify the vapor species produced from the heated sample. Emission spectra of constituent materials (those labeled "for ID purposes" in the comments column of Table 4-1) were recorded to help identify emission features of candidate materials. The laser probe spectrometer was then used as an analytical tool to quantitatively measure the vapor species abundance. The laser probe absorption spectrometer (the CCLAS system) and the OMA system are described in Sections 4.2.1.2 and 4.2.1.3, respectively. Spectroscopic data are presented in Section 4.2.2.

TABLE 4-1. PRELIMINARY LASER SPECTROSCOPIC OBSERVATIONS

<u>Material</u>	<u>Environment</u>	<u>Emission/Absorption</u>	<u>Comments</u>
Al ₂ O ₃	Vacuum	Emission & absorption	Baseline material
TiB ₂	Vacuum, 10 T O ₂	Emission	Candidate material
Y ₂ O ₃	Vacuum	Emission	For ID purposes
HfO ₂	Vacuum	Emission	For ID purposes
HfO ₂ -Y ₂ O ₃	Vacuum, 10 T O ₂	Emission	Candidate material
SrO	Vacuum	Emission	For ID purposes
SrHfO ₃	Vacuum, 10 T O ₂	Emission	Candidate material
HfC	Vacuum, 10 T O ₂	Emission	Candidate material
ZrC	Vacuum, 10 T O ₂	Emission	Candidate material
Ir _x Al _y	Vacuum, 10 T O ₂	Emission & absorption	Candidate material

4.2.1 Experimental Apparatus

4.2.1.1 HARC Carbon Dioxide Laser Test Resource. For the experiments conducted during this program, only a part of the HARC CO₂ Laser Test Resource apparatus was required. However, the entire apparatus is described here and shown in Figure 4-8. A cw CO₂ laser irradiates samples contained within the vacuum chamber at the far right of the figure. Portions of the laser beam are directed by a beamsplitter (BS 1) and a wedged chamber window onto beam diagnostics equipment (a power meter, a fast response power monitor, and a fast response beam profile monitor). A fast-acting shutter (S) controls irradiation times on target. An optical delivery system [comprising attenuators, beam steering mirrors (M1 and M2), and a focusing lens] provides accurately positioned beams on target with controlled and measured irradiance distributions. An alignment scope facilitates accurate positioning of the focused

CO₂ LASER TEST RESOURCE

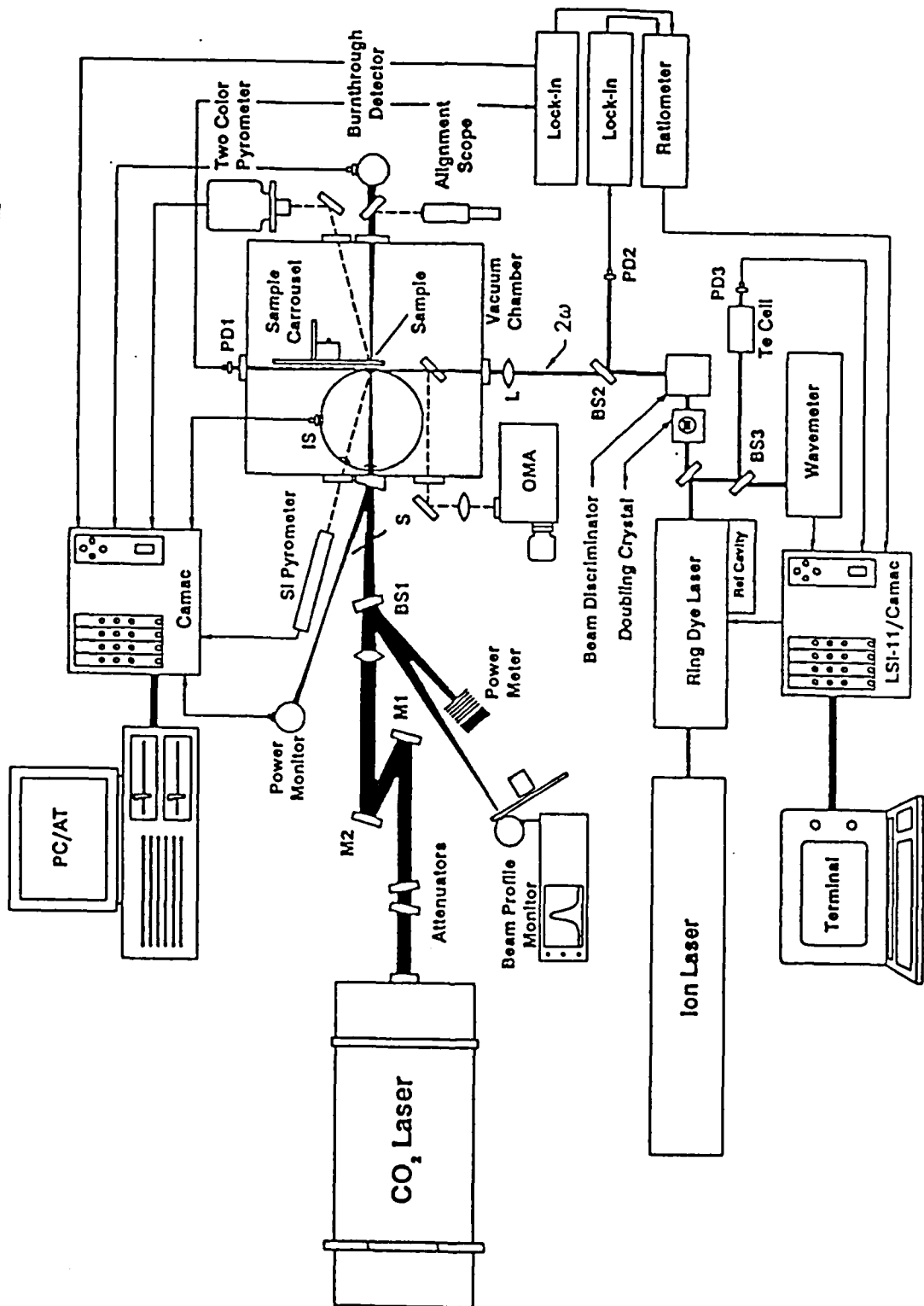


FIGURE 4-8. HARC CO₂ LASER TEST RESOURCE

laser beam onto the target surface. Real time target responses are monitored with time-resolved target diagnostics instrumentation [optical pyrometers for front and back surface temperature measurements, a burnthrough detector, an integrating sphere (IS) with a filter plus fast response detector for reflectance measurements, camera systems (both video and fast framing camera, not shown), and an OMA system for plume emission measurements]. Signals from the beam, the target, and the plume diagnostics are digitized, recorded, and processed using transient digitizers, digital oscilloscopes, and a minicomputer system.

4.2.1.2 Laser Probe Absorption Spectrometer. A computer controlled laser absorption spectrometer (CCLAS), shown in Figure 4-9, was used in conjunction with the laser/materials interaction apparatus to provide spectroscopic measurements on plume vapor species. The laser probe absorption spectrometer provides tunable cw dye laser probe beams with near-Doppler-limited spectral resolution. In the right part of the figure, a cw ion laser pumps a single frequency tunable dye laser system [Coherent, Inc. Model 699-21, optical cavity defined by mirrors M1 through M4 and the output coupler (OC)] which produces spectral outputs (ω_1) over the entire visible/near infrared (400-900 nm) spectral regions. The dye laser can also be combined with intracavity (not shown) and external cavity second harmonic generation crystals (lower left part of the figure) to produce tunable ultraviolet (200-400 nm) spectral output ($2\omega_1$). The visible spectral region of the cw dye laser system is scanned electronically and is passed through an electro-optical modulator (a "noise eater", not shown) to obtain stable low noise probe signals. A reference cavity within the dye laser system is used to verify single frequency operation during scans. The low noise scanning (or fixed frequency) dye laser probe beam is directed toward the sample by the beam discriminator (used to isolate the frequency doubled beam from the fundamental dye laser beam), focused to a narrow beam waist in front of the target surface and within the plume, and detected by a filter and/or small monochromator plus fast photodiode PD combination. Beamsplitters direct small portions of the probe beam to photodiodes for monitoring output power (for ratioed absorption measurements) and through wavelength monitoring reference cells (Te or I₂, not shown). The dye laser wavelength is also calibrated using an interferometric measurement system (wavemeter); a scanning Fabrey-Perot (FP) monitors the dye laser mode in real time. The probe beam can be positioned accurately within the vapor plume for spatial resolution of plume absorptions as functions of distance from the sample surface and of distance from the plume centerline. The laser probe absorption spectrometer and all the detection electronics are computer controlled by an LSI-11/Camac-based system. Absorption spectra recorded with the laser probe absorption spectrometer are reported in Section 4.2.2.2.

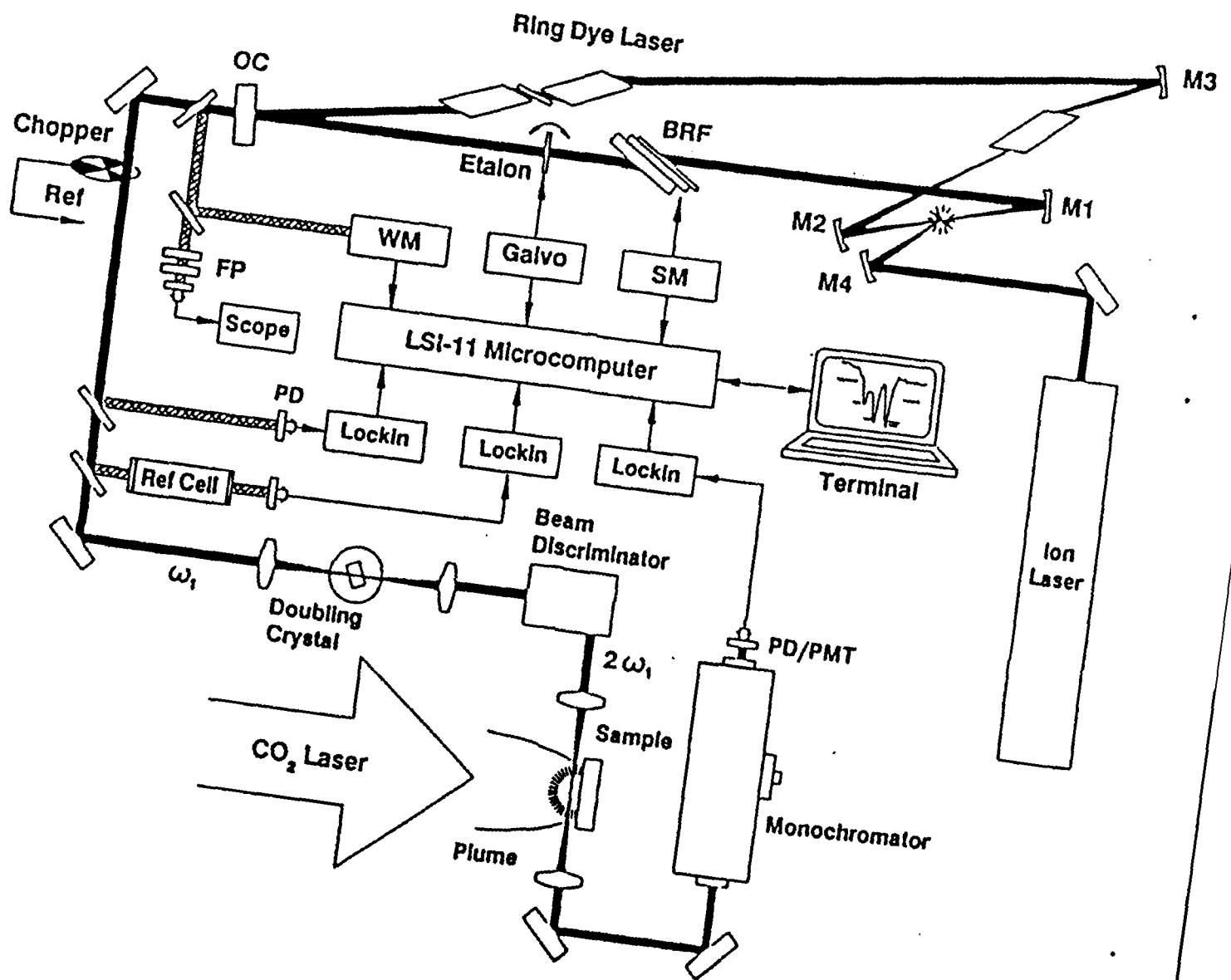


FIGURE 4-9. COMPUTER CONTROLLED LASER ABSORPTION SPECTROMETER (CCLAS)

4.2.1.3 Optical Multichannel Analyzer (OMA) System. Figure 4-10 shows the OMA system (Princeton Instruments Optical Multichannel Analyzer with Instruments SA Model HR320 0.32 meter monochromator) used to obtain survey emission spectra in the 340-660 nm spectral region during CO₂ laser heating of materials. The monochromator was equipped with a low resolution (150 lines/mm, blaze $\lambda = 500$ nm) grating. Reference light sources (e.g., Hg lamps) were used to calibrate wavelength scales. An intensified CCD array mounted on the exit slit plane was used to record spectra in "cw" mode; the OMA system can record a single emission spectrum every 30 ms. None of the emission spectra, reported in Section 4.2.2.1, are corrected for the spectral detection efficiency of the OMA system. However, near the end of the program, a tungsten strip lamp traceable to NBS spectral radiance standards was acquired and used to obtain an instrumental correction function⁷ for future data processing.

4.2.2 Spectroscopic Data

4.2.2.1 Emission Spectra. Figures 4-11 through 4-19 show emission spectra recorded with the HARC CO₂ Laser Test Facility and OMA system. Samples were held in a small (ca 8 in. x 8 in. x 8 in.) chamber. For vacuum experiments, the chamber was pumped down to ca 200 μ m pressure and then purged three times with N before laser heating. Small samples were either cut/broken from the stock material (i.e., Al₂O₃, TiB₂, HfO₂, Y₂O₃, Ir_xAl_y) or pressed into pellets from powder stock (i.e., SrO, SrHfO₃) with a simple nut and bolt press. HfO₂-Y₂O₃ and HfC could not be pressed into pellets and therefore were heated in the powder form. When laser heated in the powder form, some materials (particularly SrHfO₃) "exploded," sending powder all over the vacuum chamber. However, no "explosions" occurred during laser heating of HfO₂-Y₂O₃ and HfC powders in either vacuum or 10 torr O₂ environments.

An IRCON two color pyrometer [$\lambda_1 = 0.95$ μ m (wide bandwidth), $\lambda_2 = 1.05$ μ m (narrow bandwidth), spatial resolution ca 0.5 mm] monitored the sample front surface temperature during CO₂ laser heating. However, these optically measured temperatures are subject to error from (1) unknown emittance values and (2) contaminations from plume emissions in either or both of the pyrometer's detection bandwidths. [HARC has recently developed an advanced multi-color (six wavelength) optical pyrometer system to measure target front surface temperatures. This six color system will be extremely useful in future high temperature experiments.] In all emission spectra reported here, the OMA system viewed an area ca 4 mm in front of the sample.

Figure 4-11 shows the plume emission spectrum recorded during CO₂ laser heating of Al₂O₃ in a vacuum environment. The emission features are due to the well-known 1.10 B-X bands (Ref. 8, pp. 28-31). The 451.4 nm, 467.1 nm, 485.8 nm, and 510.0 nm features are

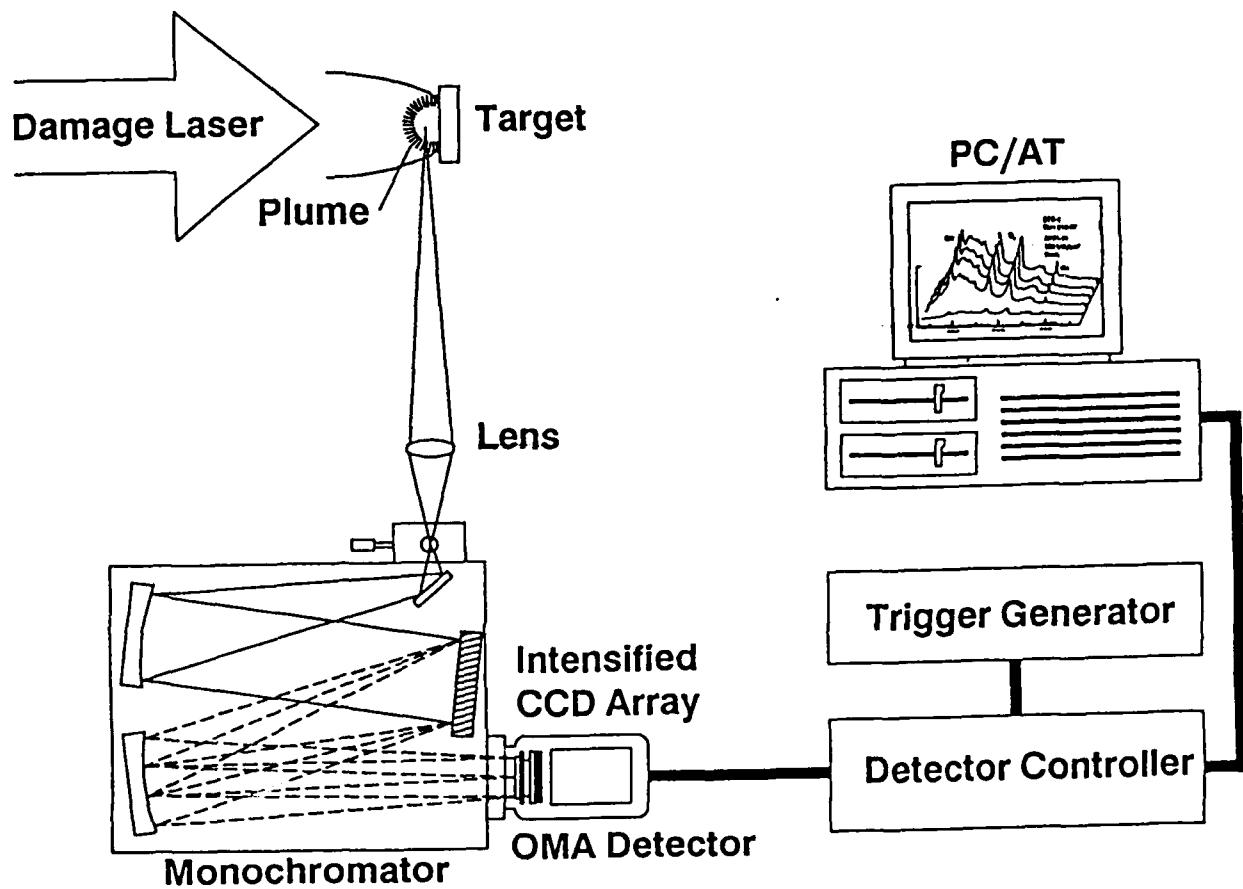


FIGURE 4-10. OPTICAL MULTICHANNEL ANALYZER (OMA) SYSTEM

EMISSION SPECTRUM: Al_2O_3

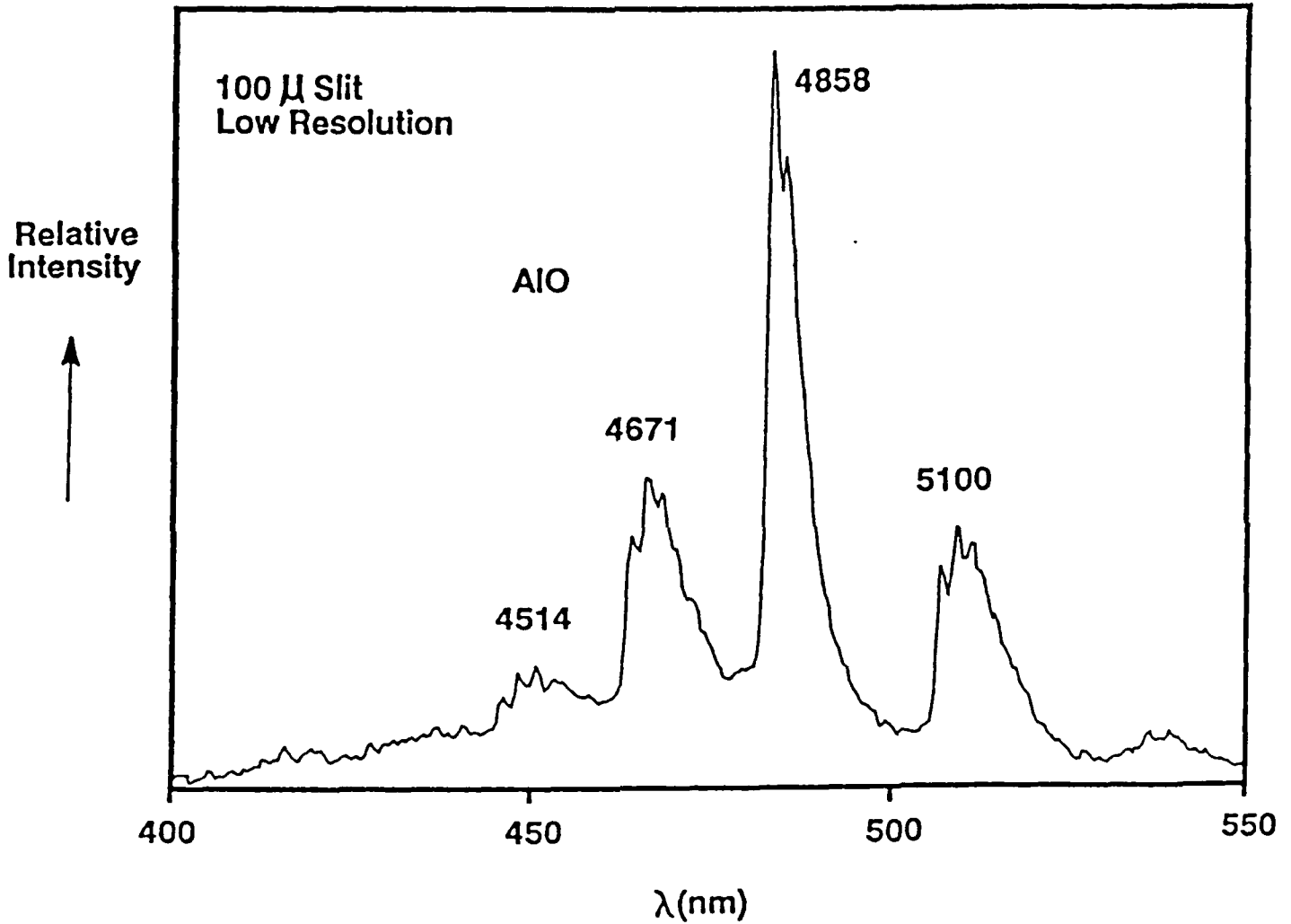


FIGURE 4-11. PLUME EMISSION SPECTRUM FROM LASER HEATED Al_2O_3

due to $\Delta v = +2, +1, 0,$ and -1 vibrational transitions, respectively.

Figure 4-12 shows the plume emission spectrum recorded during laser heating of TiB_2 in vacuum (top panel) and 10 torr O_2 (bottom panel) environments. The emission features observed in the bottom panel are due to the linear symmetric molecule BO_2 .⁹

Figure 4-13 shows the plume emission spectrum recorded during laser heating of Y_2O_3 (top panel) and HfO_2 (bottom panel) in vacuum. The emission features observed from laser heating Y_2O_3 are due to B-X (short wavelength features) and A-X (long wavelength, strong features) bands of YO (Ref. 8, p. 674 ff., and Ref. 10). The emission features observed from laser heating HfO_2 are due to HfO (Ref. 8, pp. 310-311).

Figure 4-14 shows the plume emission spectrum recorded during laser heating of $HfO_2-Y_2O_3$ in vacuum (top panel) and 10 torr O_2 (bottom panel) environments. From comparison with the emission spectrum shown in the top panel of Figure 4-13, the emission features observed from laser heating $HfO_2-Y_2O_3$ in a 10 torr O_2 environment are attributed to YO.

Figure 4-15 shows the plume emission spectrum recorded during laser heating of SrO in a vacuum environment. The emission features at the red end of the spectrum are currently attributed to SrO (Ref. 8, pp. 630-631). However, several bands of SrOH occur in this spectral region, so the assignment of the emission features is somewhat tentative. The low intensity peak at ca 460 nm is most likely due to the $^1P^o \rightarrow ^1S$ transition of atomic Sr.¹¹

Figure 4-16 shows the plume emission spectrum recorded during laser heating of $SrO \cdot HfO_2$ in vacuum (top panel) and 10 torr O_2 (bottom panel) environments. From comparison of Figure 4-16 with both the bottom panel of Figure 4-13 (HfO_2 plume emission spectrum) and Figure 4-15 (SrO plume emission spectrum), the emission features observed from laser heating $SrO \cdot HfO_2$ in a vacuum environment are identified as SrO.

Figure 4-17 shows the plume emission spectrum recorded during laser heating of HfC in vacuum (top panel) and 10 torr O_2 (bottom panel) environments. From comparison of Figure 4-16 with the bottom panel of Figure 4-13, the emission features observed from laser heating HfC in a 10 torr O_2 environment are identified as HfO.

Figure 4-18 shows the plume emission spectrum recorded during laser heating of ZrC in vacuum (top panel) and 10 torr O_2 (bottom panel) environments. The complex emission spectrum observed under vacuum conditions is probably due to the maze of atomic Zr transitions.¹¹

TiB₂ EMISSION SPECTRUM

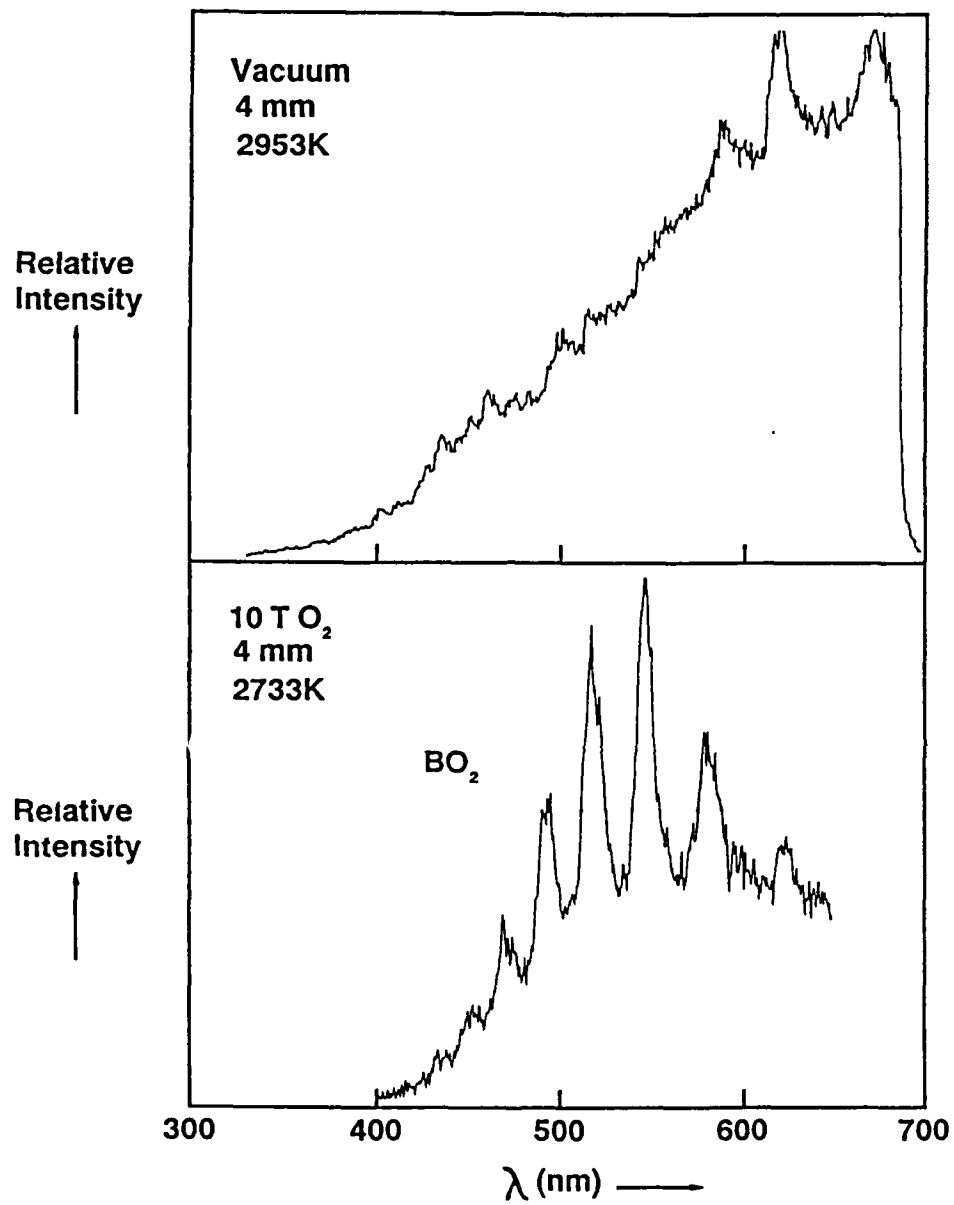
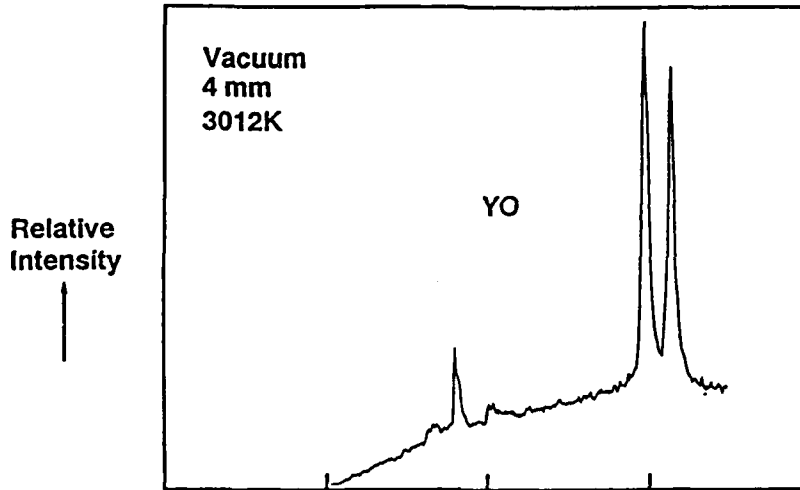


FIGURE 4-12. PLUME EMISSION SPECTRUM FROM LASER HEATED TiB₂

Y_2O_3
EMISSION SPECTRUM



HfO_2
EMISSION SPECTRUM

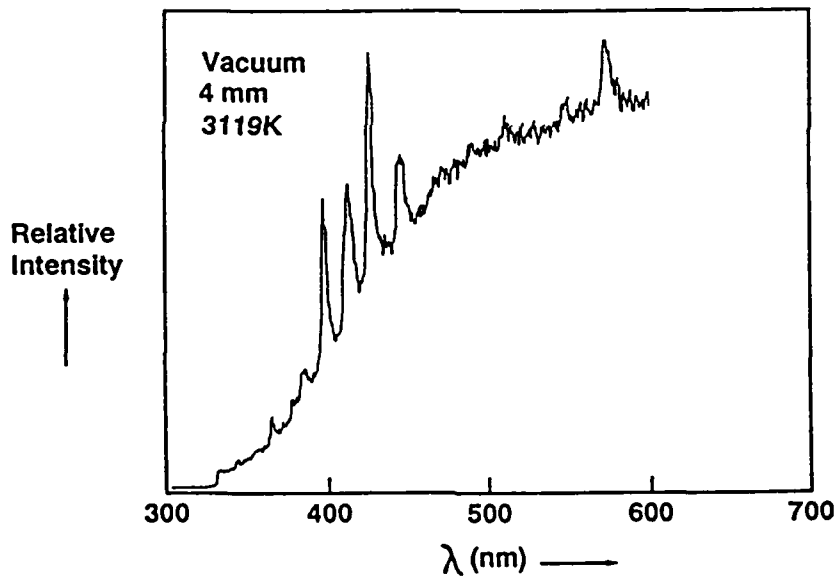


FIGURE 4-13. PLUME EMISSION SPECTRUM FROM LASER HEATED Y_2O_3 AND HfO_2

$\text{HfO}_2\text{-Y}_2\text{O}_3$
EMISSION SPECTRUM

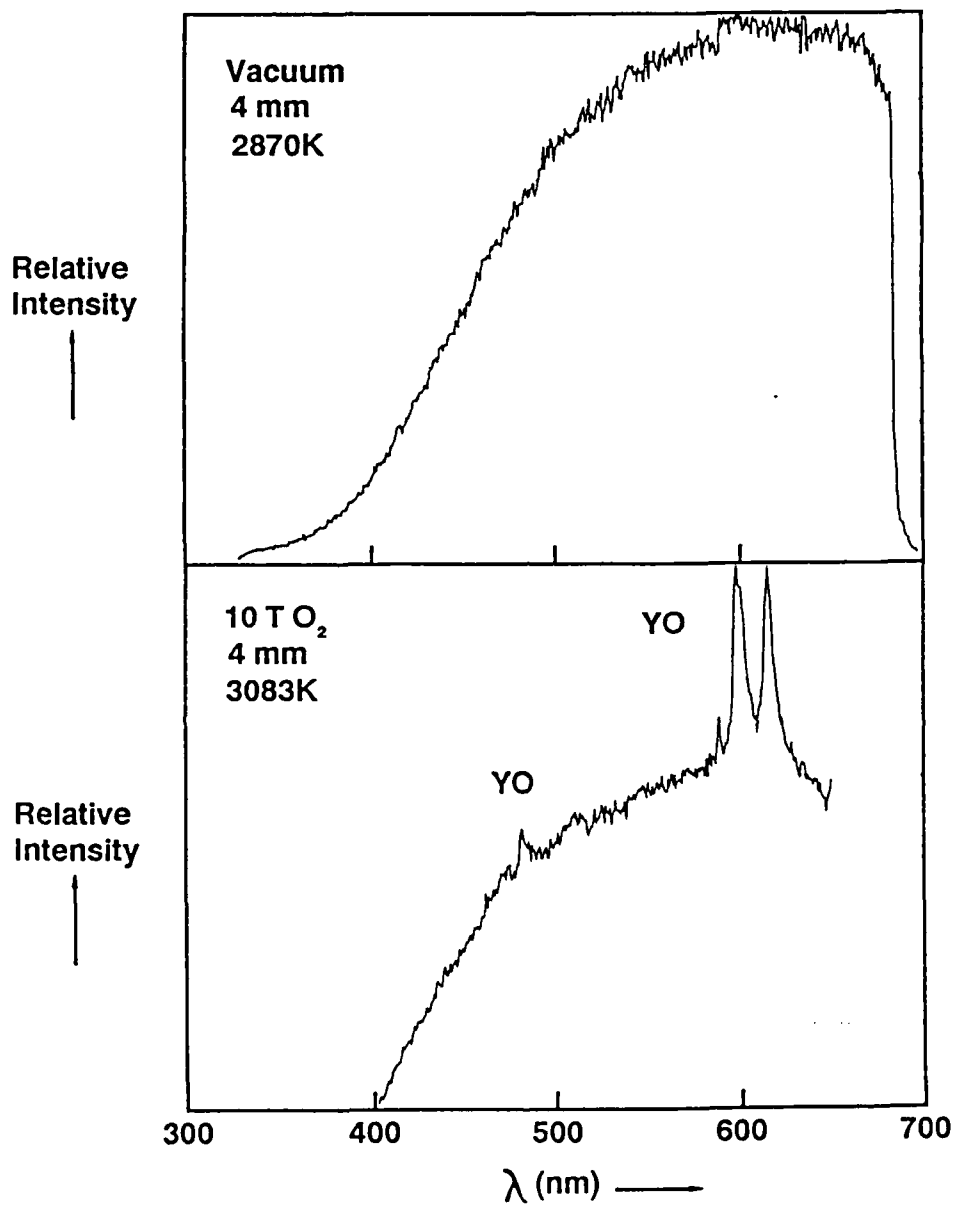


FIGURE 4-14. PLUME EMISSION SPECTRUM FROM LASER HEATED $\text{HfO}_2\text{-Y}_2\text{O}_3$

SrO EMISSION SPECTRUM

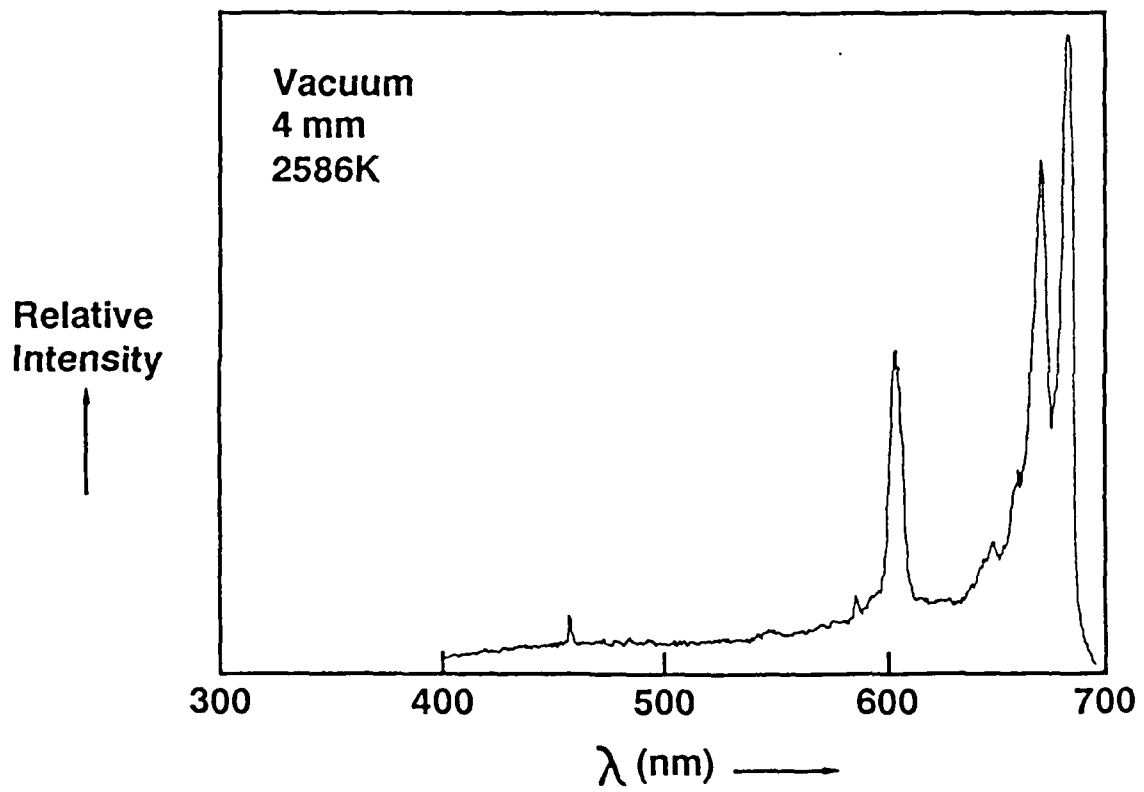


FIGURE 4-15. PLUME EMISSION SPECTRUM FROM LASER HEATED SrO

SrHfO₃
EMISSION SPECTRUM

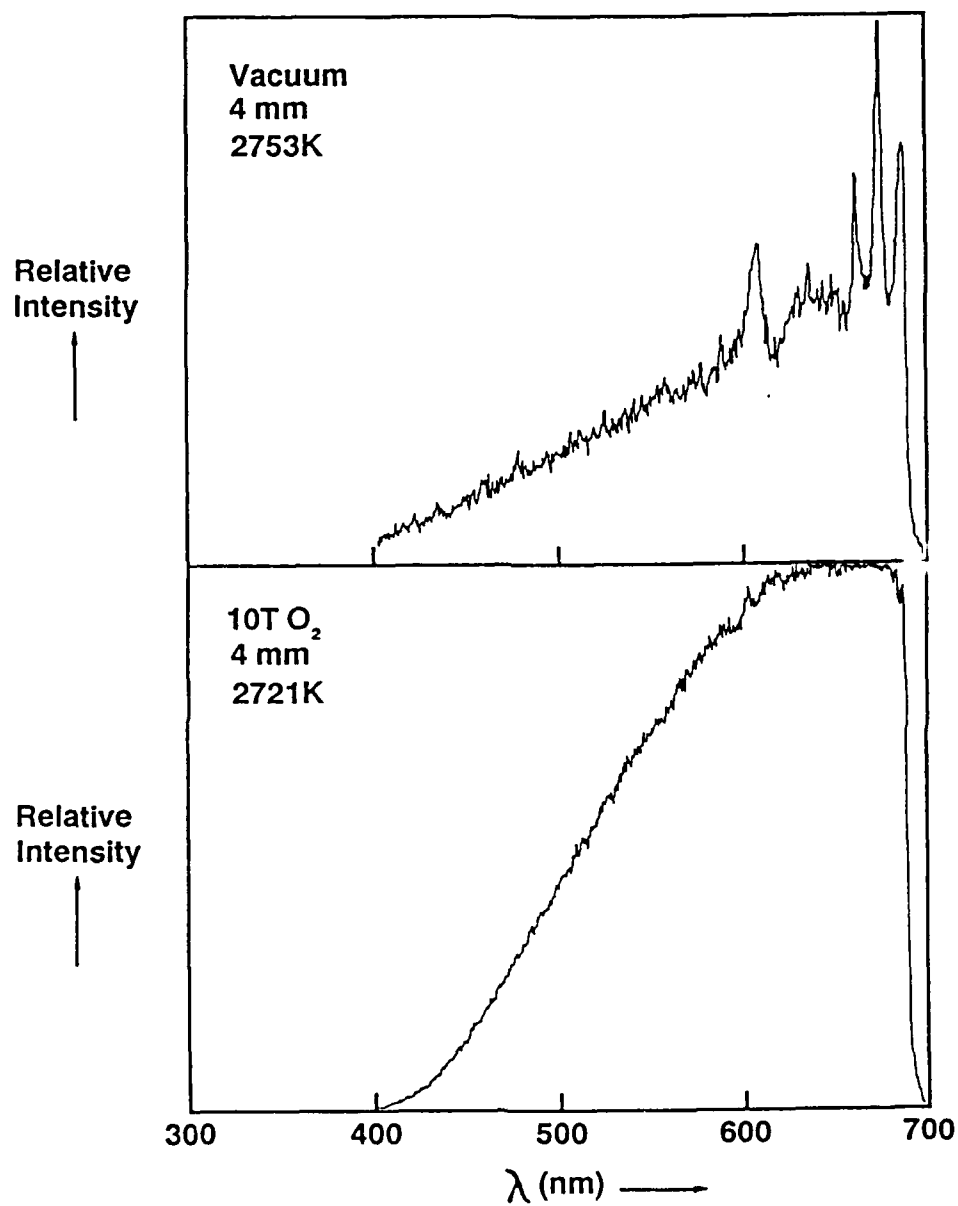


FIGURE 4-16. PLUME EMISSION SPECTRUM FROM LASER HEATED SrO·HfO₂

HfC EMISSION SPECTRUM

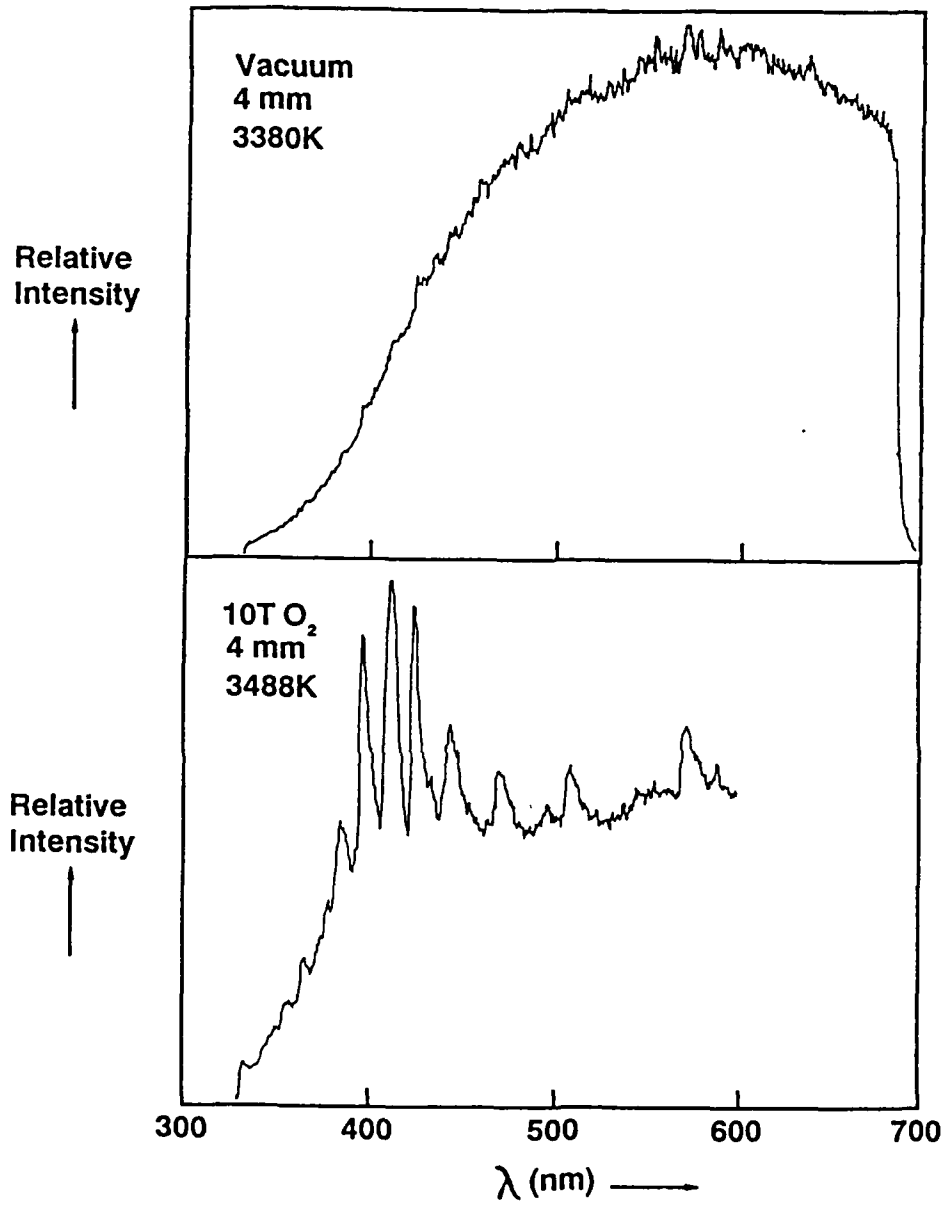


FIGURE 4-17. PLUME EMISSION SPECTRUM FROM LASER HEATED HfC

ZrC EMISSION SPECTRUM

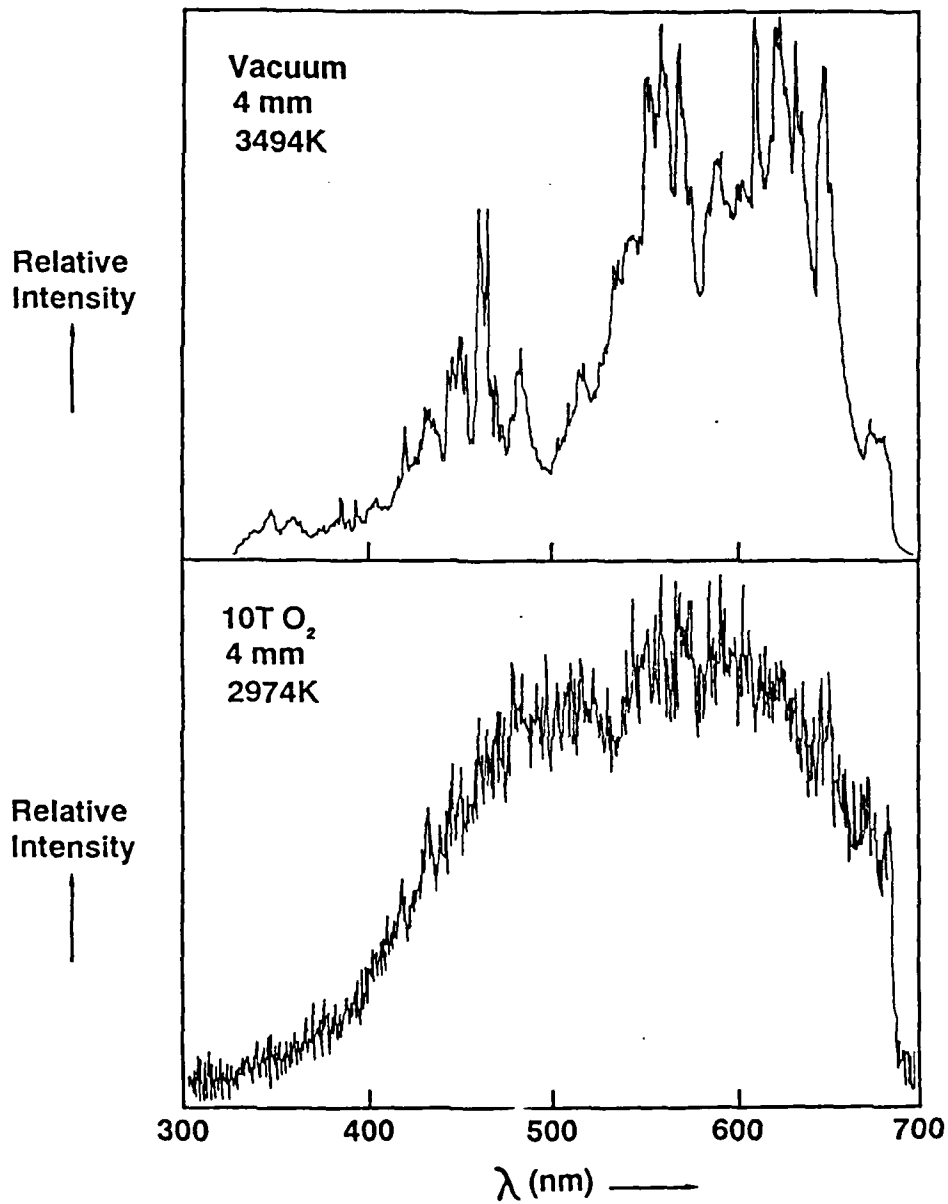


FIGURE 4-18. PLUME EMISSION SPECTRUM FROM LASER HEATED ZrC

Figure 4-19 shows the plume emission spectrum of the intermetallic Ir_xAl_y in a 10 torr O_2 environment. The emission features of the plume vapor produced from laser heating Ir_xAl_y are readily recognized as the $\text{AlO B-X } \Delta v = +2, +1, 0, -1, \text{ and } -2$ vibrational bands. These emission features were also observed during laser heating of Al_2O_3 (Figure 4-11). The emission spectrum of Ir_xAl_y in a vacuum environment appeared as a featureless "blackbody" source.

4.2.2.2 Laser Probe Absorption Spectra. Laser probe absorption studies were conducted to detect AlO during laser heating of Al_2O_3 . Al_2O_3 was chosen as a reference/calibration material to test the CCLAS system. Laser absorption studies were also performed to detect atomic Al during laser heating of both pure Al metal (reference material) and the intermetallic Ir_xAl_y .

The bottom panel of Figure 4-20 shows the experimental absorption spectrum of AlO recorded by the CCLAS during laser heating of Al_2O_3 to 2700°C ; individual absorption features are due to rotational transitions in the $\text{AlO B-X } 0,0$ band and are labeled in the experimental spectrum. The top panel of Figure 4-20 is a computer simulation of the rotational transitions using rotational constants from the literature.¹² Intensities of individual transitions were calculated from a Boltzmann distribution at 2700°C and rotational line strengths for a ${}^2\Sigma + {}^2\Sigma$ electronic transition.¹³ Each rotational transition has a 0.125 cm^{-1} Lorentzian FWHM lineshape.

Figure 4-21 shows the calculated partial pressures of all the major species produced from heating Al_2O_3 . The calculations were performed using the computer code "SOLGASMIX with HETTA," which was obtained from Dr. R. Behrens at Los Alamos National Laboratory.

From the known Einstein A-coefficient for the entire AlO B-X electronic transition ($A_{ki} = 6.34 \times 10^6 \text{ s}^{-1}$),¹⁴ the Doppler-broadened peak absorption cross section σ (including the vibrational partition function) is

$$\sigma = 1.85 \times 10^{-6} A_{ki} \nu^{-3} (M/T)^{1/2} = 9.4 \times 10^{-16} \text{ cm}^2,$$

where ν is the transition energy (in cm^{-1} units), M is the atomic mass (in amu), and T is the temperature (in K). Referring to Figure 4-21, at 2700°C (2973K), the number of AlO molecules, n , in the $\nu = 0$ state is ca $1.4 \times 10^{-4} \text{ atm}$, or $3.58 \times 10^{14} \text{ molecules/cm}^3$. The predicted absorption, using $l = 0.4 \text{ cm}$ (the effective pathlength assumed identical to the longitudinal sample dimension), from the Beer Lambert relation is then

$$A = 1 - \exp(-\sigma n) = 1 - \exp[-(9.4 \times 10^{-16} \text{ cm}^2)(3.58 \times 10^{14} \text{ cm}^{-3}) \times (0.4 \text{ cm})] = 13\%.$$

Ir_xAl_y
EMISSION SPECTRUM

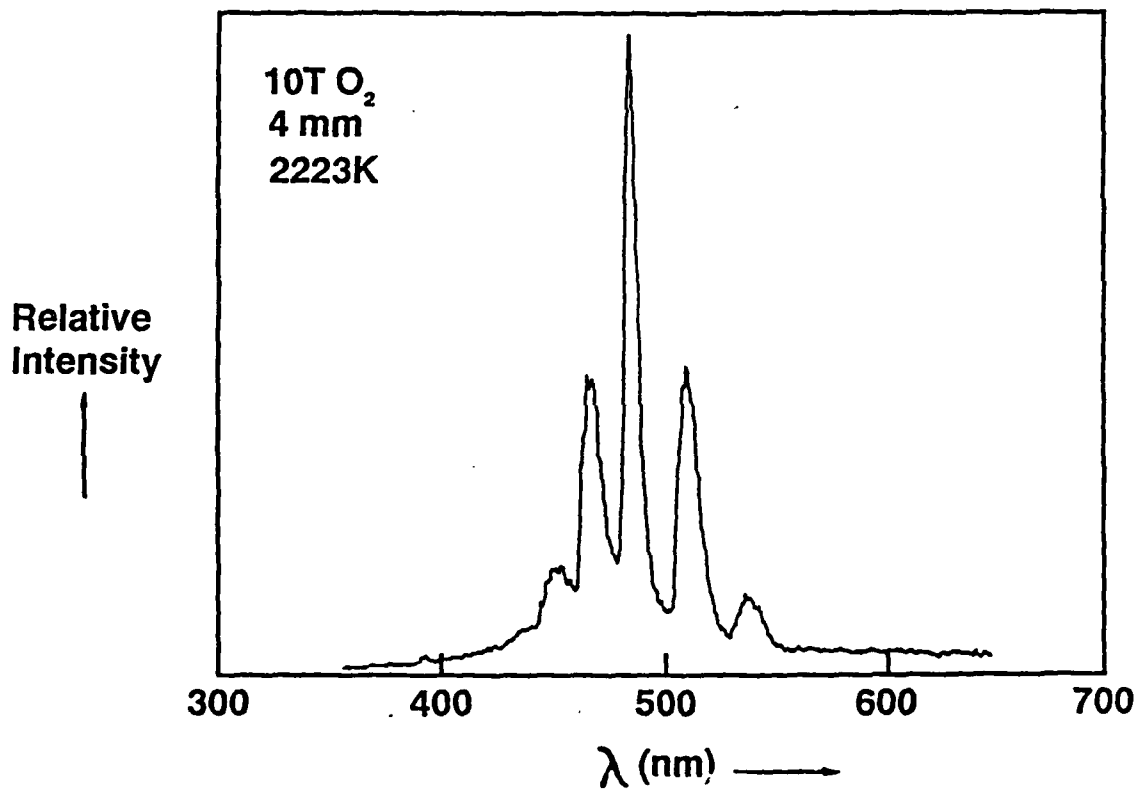


FIGURE 4-19. PLUME EMISSION SPECTRUM FROM LASER HEATED Ir_xAl_y

AlO Plume Spectrum

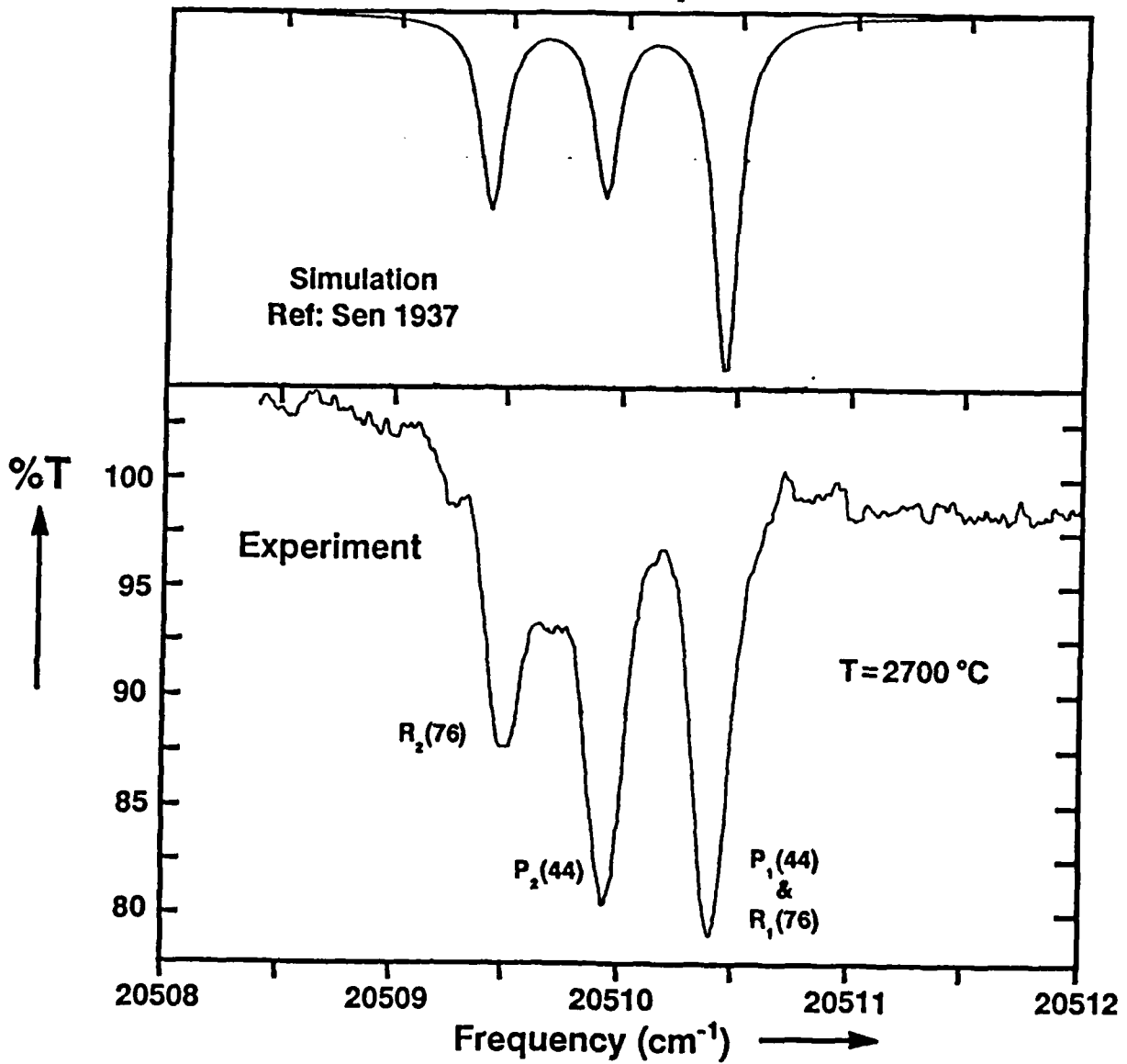


FIGURE 4-20. PLUME EMISSION SPECTRUM FROM LASER HEATED Al₂O₃

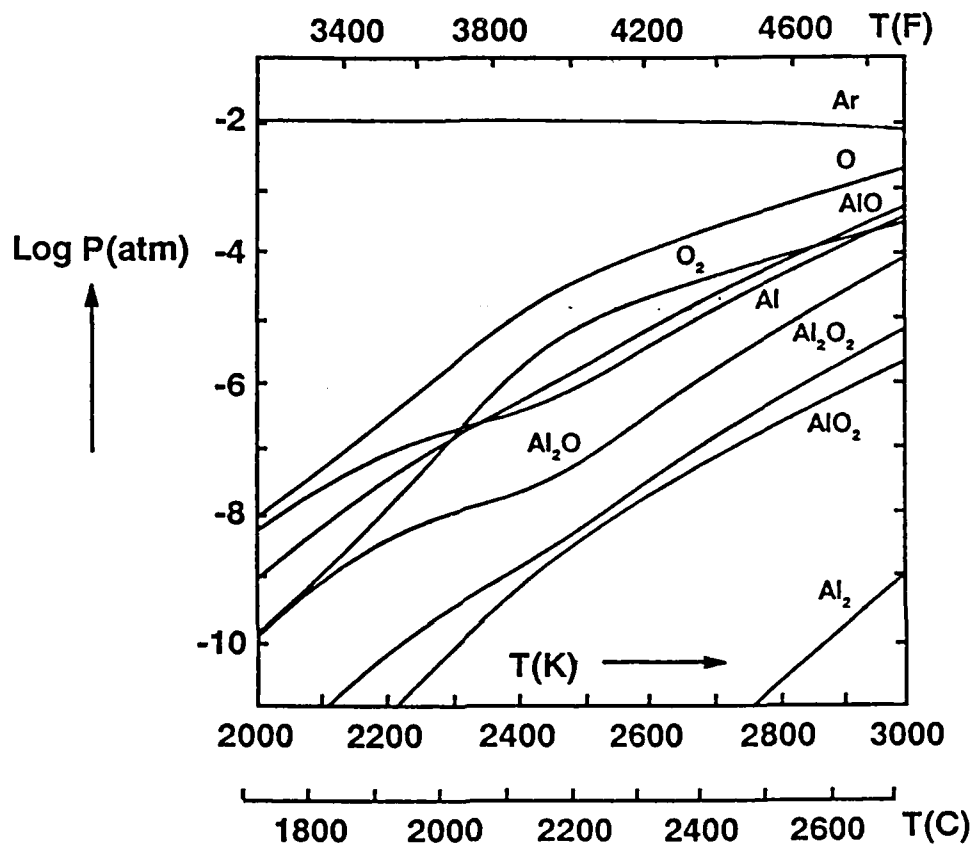


FIGURE 4-21. CALCULATED VAPOR SPECIES PRESSURE OVER LASER HEATED Al_2O_3

In the experimental spectrum shown in Figure 4-20, the $P_2(44)$ rovibronic transition shows an absorption of 20%. Principal uncertainties in this quantitative comparison are the front surface temperature and the plume pathlength. (See Section 5 for additional discussion.)

The top panel of Figure 4-22 shows the experimental absorption spectrum of atomic Al recorded during laser heating of pure Al metal. The pure Al was held in a boat machined from C. The boat measured ca 6 mm x 3 mm x 2 mm (length x width x height) with a small center section notched out on the side for a thermocouple contact to the Al sample; small fragments of Al were placed in the center cavity. The 308 nm ($2\omega_1$) laser probe beam was generated by frequency doubling the dye laser [616 nm (ω_1); DCM laser dye, pumped by 6 W blue-green output of an Ar ion laser] with a 31° z-cut beta Ba borate (BBO) crystal (phase match angle ca 38 degrees). The Al was held in a vacuum environment (ca 0.5 torr background pressure) and laser heated. An IRCON infrared 7000 series pyrometer measured the front surface temperature, and a Chromel-Alumel thermocouple measured the temperature of the Al sample.

The atomic Al transitions shown in Figure 4-22 are the ${}^2D_{5/2} \leftarrow {}^2P_{3/2}^0$ (Einstein A-coefficient = $7.3 \times 10^7 \text{ sec}^{-1}$) and ${}^2D_{3/2} \leftarrow {}^2P_{3/2}^0$ (Einstein A-coefficient = $1.2 \times 10^7 \text{ sec}^{-1}$) transitions at $32,324.75 \text{ cm}^{-1}$ and $32,323.41 \text{ cm}^{-1}$, respectively. The 64% absorption by the Al ${}^2D_{5/2} \leftarrow {}^2P_{3/2}^0$ peak at ca 1300K corresponds to a number density of $5.2 \times 10^{12} \text{ atoms/cm}^3$ (with a pathlength, l , assumed to be equal to the sample size = 0.34 cm). The calculated atomic Al number density at 1300°C (1303K) is ca $1.7 \times 10^{12} \text{ atoms/cm}^3$,¹⁵ which translates to an expected 28% absorption. Therefore, the experimental and calculated values disagree by approximately a factor of 2.3. Again, principal uncertainties in this quantitative comparison are the front surface temperature and the plume pathlength. (See Section 5 for additional discussion.)

Figure 4-23 shows the results of probing for Al during laser heating of Ir_xAl_y in vacuum (top panel) and 5 torr O_2 (bottom panel) environments. The 61% absorption by the Al ${}^2D_{3/2} \leftarrow {}^2P_{3/2}^0$ peak at ca 2183K corresponds to a number density of $4.0 \times 10^{13} \text{ atoms/cm}^3$. Note that no Al was detected during the 5 torr O_2 environment experiment (see Section 5.2 for additional discussion).

4.3 MASS SPECTROMETRY AND MATRIX ISOLATION FTIR SPECTROSCOPY

4.3.1 Experimental Apparatus

Schematics of the Rice University mass spectrometry and matrix isolation FTIR equipment are shown in Figures 4-24 and 4-25. Mass spectrometric sampling permitted the identification of both simple and complex species, possessed high dynamic range and high sensitivity, and provided real time monitoring of species. This

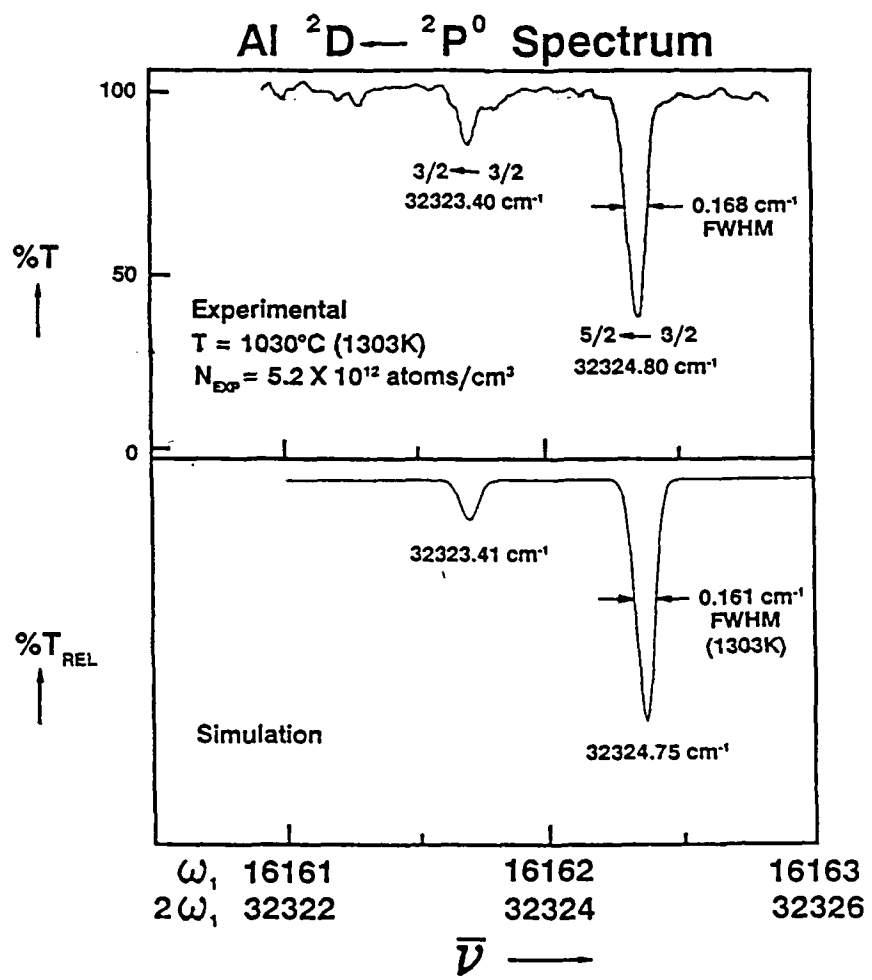


FIGURE 4-22. ABSORPTION SPECTRUM OF LASER HEATED Al

Ir_xAl_y : Al ²D — ²P⁰ Spectrum

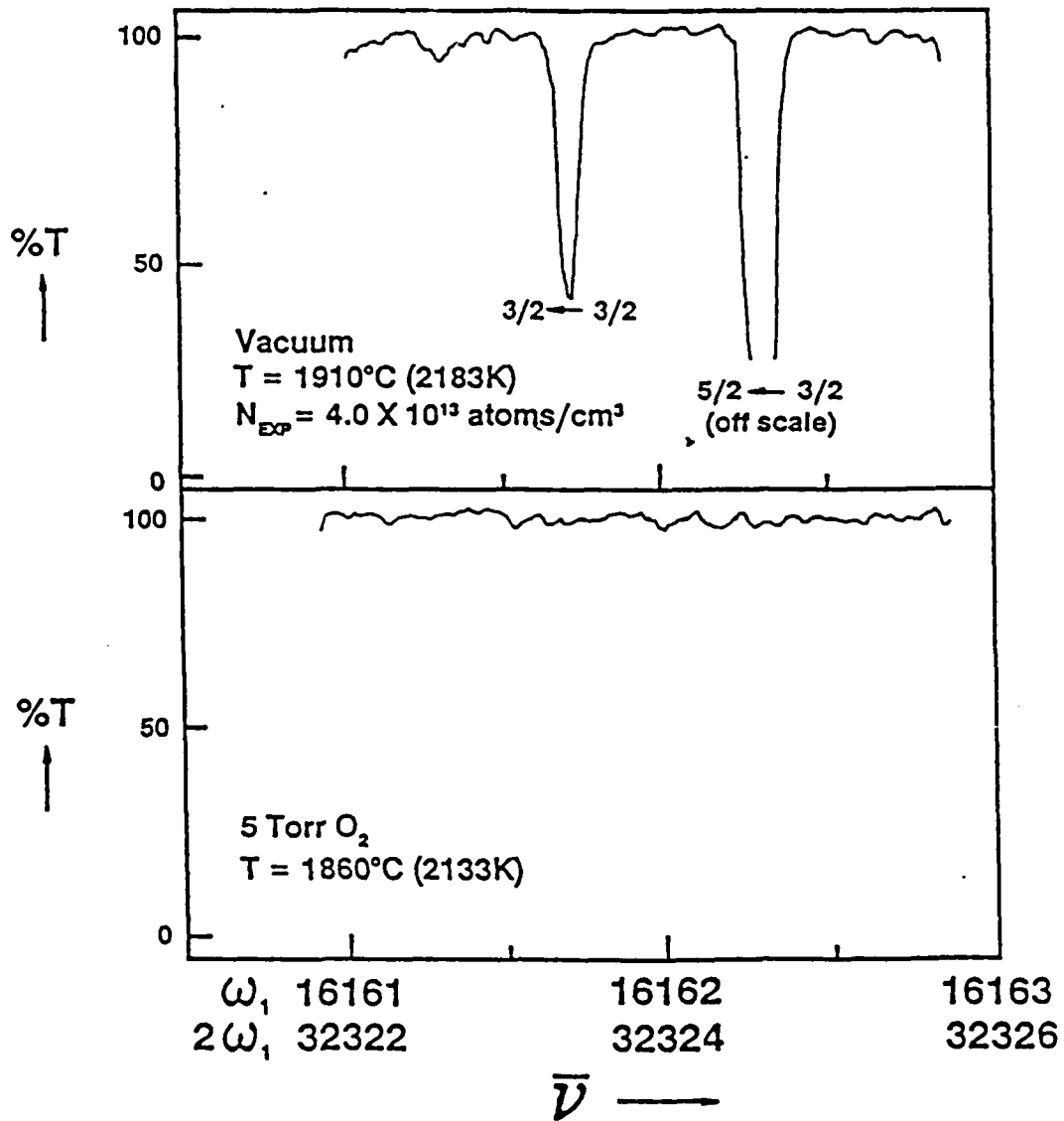


FIGURE 4-23. ABSORPTION SPECTRUM OF LASER HEATED Ir_xAl_y

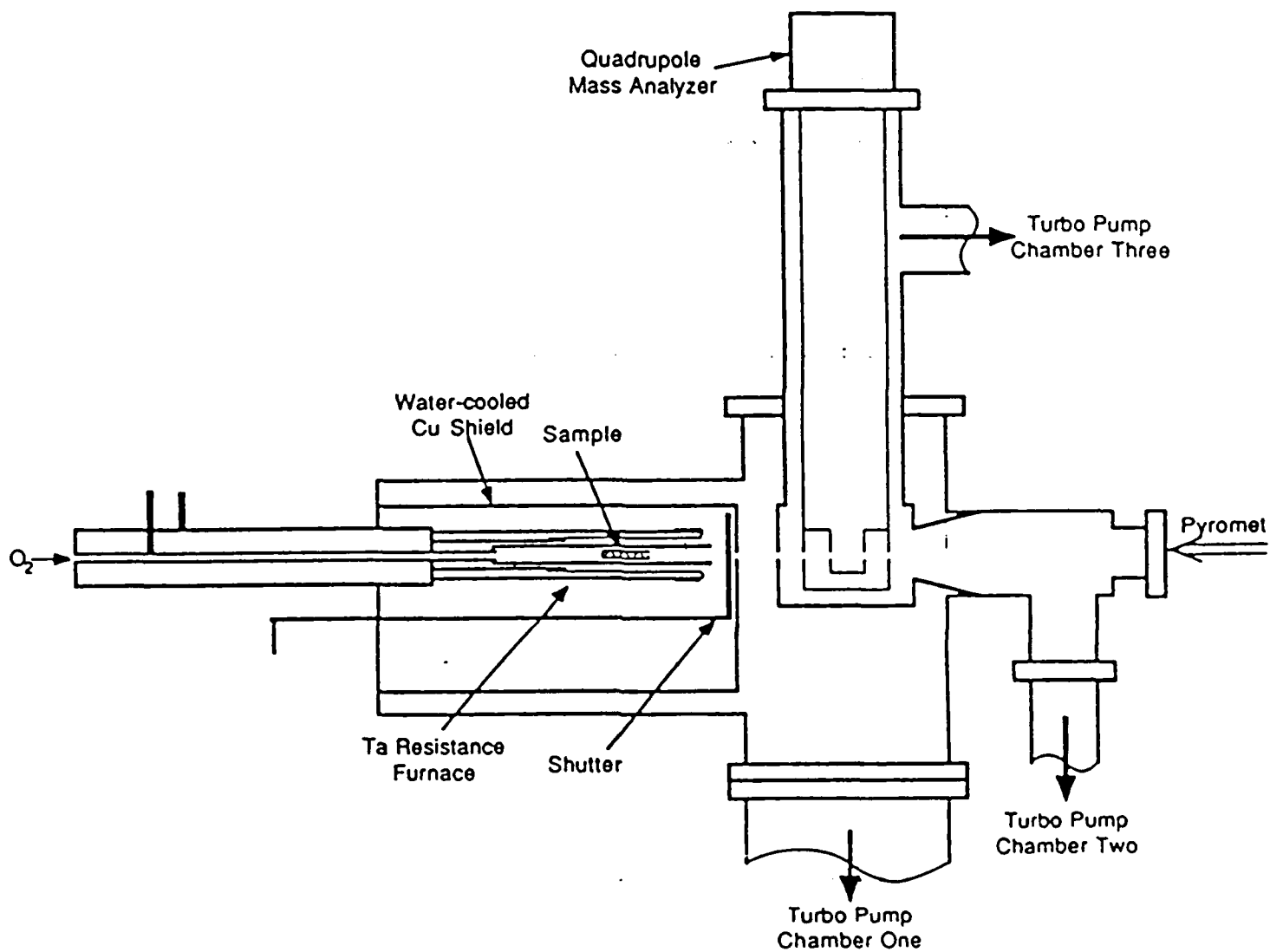


FIGURE 4-24. SCHEMATIC OF RICE UNIVERSITY MASS SPECTROMETRY SYSTEM

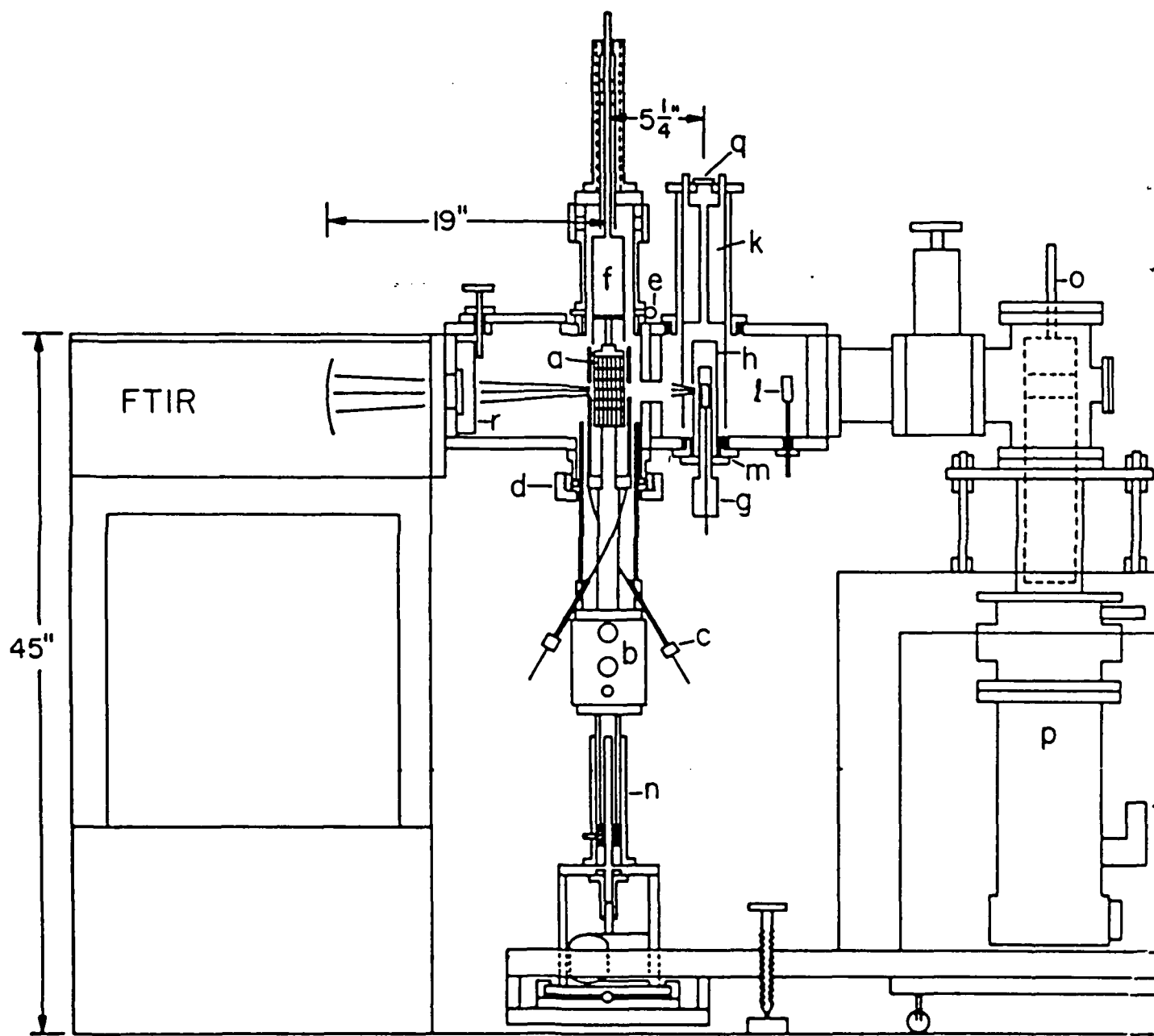


FIGURE 4-25. SCHEMATIC OF MATRIX ISOLATION FTIR APPARATUS

technique was used to obtain quantitative measures of volatile species as a function of temperature. The single quadrupole mass spectrometer has low mass resolution. As a result, species of very similar mass, such as SiO and CO₂, were indistinguishable.

Matrix isolation FTIR sampling permitted differentiation between species of like mass with moderate sensitivity. Monatomic vapor species could not be detected unless complexation reactions with species such as CO were initiated prior to matrix deposition. In addition, real time data could not be taken with the matrix isolation FTIR technique.

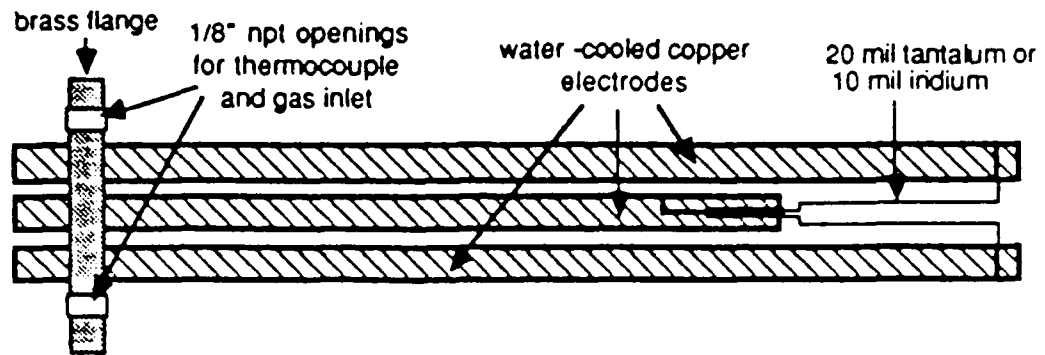
Resistively heated furnaces were used to vaporize the samples. The reactivity of furnace components and their melting points or sublimation temperatures were of considerable concern. Three basic furnace types, illustrated in Figure 4-26, were utilized as dictated by the samples and the experimental conditions.

The type one filament heater was primarily used with expensive heating element materials, such as Ir, or with materials which were difficult to form, such as W. Iridium was the preferred filament material in cases where oxidation was of concern; however, temperatures were limited to less than 2300K. Temperature nonuniformities were a major problem encountered with the type one design.

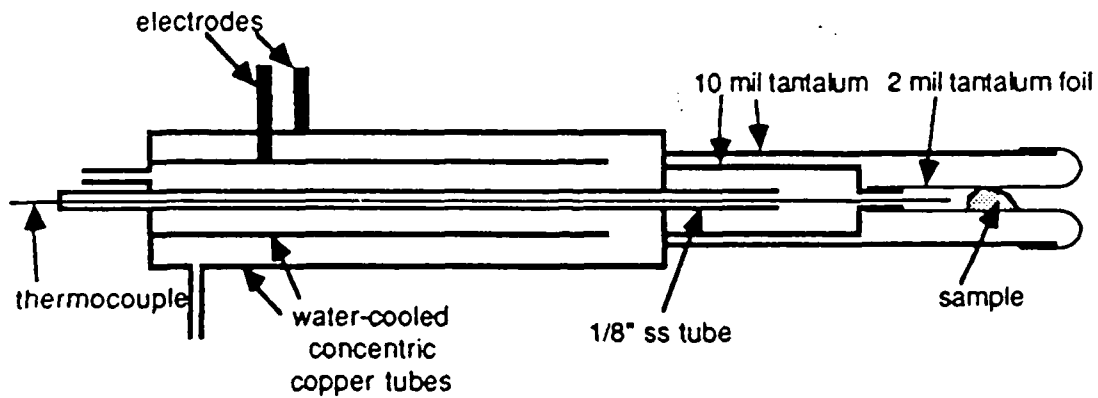
The type two design was constructed with a Ta heating element. Tantalum produced a reducing environment which resulted in enhanced loss of the elemental metals from their oxides. As a result, heats and temperatures of sublimation of metal oxides could not be determined using this furnace design. Tantalum did not react with Sr or Y at the temperatures of interest. Therefore, comparisons of the metal activity between the single and mixed component oxides were possible.

The type three tubular heater, with an interior oxide cell, was used for passage of O₂ over the samples at high temperature. Tantalum was used for the heater material, and three types of oxide containers were investigated: Al₂O₃, calcia-stabilized zirconia, and yttria-stabilized zirconia. A gas-tight seal between the oxide tube and 0.125 in. stainless tubing was made with a high temperature epoxy. This seal was kept near room temperature by using a 6 in. long oxide tube filled up to the 1 in. long hot zone with chips of the cell material. Studies were carried out with and without chips of the cell material placed in front of the sample. The melting points of the cell materials and their inertness with respect to the samples were evaluated. In addition, operation in an oxidizing environment required that the cell provide an effective O₂ barrier between the reducing environment of the heater and the oxidizing environment of the sample. Repeated experiments with different sample-cell combinations revealed the following with respect to the oxide cell materials considered. Stabilized zirconia did not provide an effective O₂ barrier when it directly contacted

(1) Filament Heater



(2) Tubular Heater



(3) Tubular Heater with Cell

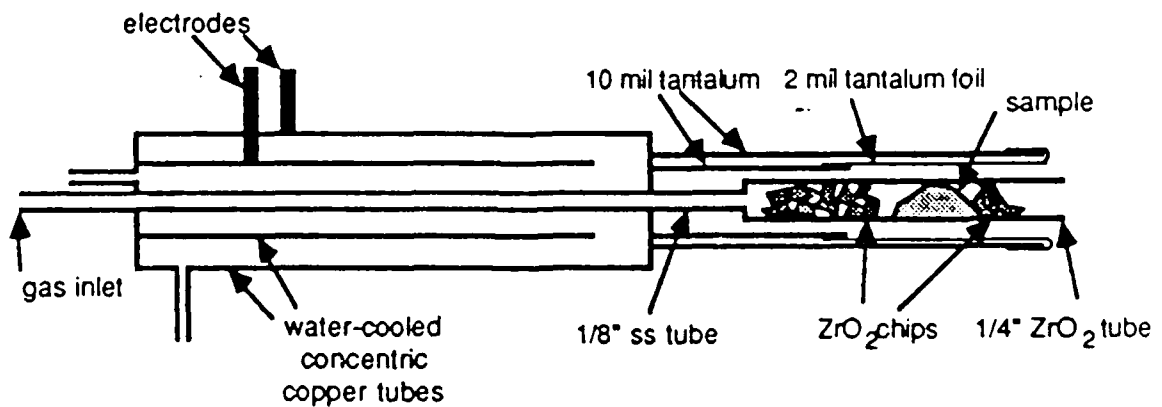


FIGURE 4-26. FURNACE CONFIGURATIONS USED TO VAPORIZE SAMPLES

the Ta heating element. An effective O₂ barrier could be achieved by separating the zirconia from the Ta with an alumina sleeve, but the highest useful temperature was then limited to about 2050K. This configuration was used for vaporization studies of SrO·ZrO₂ and SrO·HfO₂. Lining the zirconia cell with Pt as an O₂ barrier proved unattractive due to extensive reaction of the Pt foil with Sr vapor. Attempts to use Al₂O₃ as the container resulted in extensive reaction of the SrO·ZrO₂ with the Al₂O₃, leading to a lower melting mixed oxide and loss of the heating element.

Temperatures were measured with a disappearing filament Micro-dot pyrometer and W/Re or Pt/Rh thermocouples.

4.3.2 Experimental Results

4.3.2.1 Al₂O₃ and B₂O₃ Vaporization Studies. Al₂O(g) and B₂O(g) were chosen as preliminary materials for investigation, since their thermodynamic properties have been well studied and they were species of likely interest when aluminides and borides were examined.

Alumina was heated in a neutral environment to 2100K using a type one Ir filament heater. Monatomic Al was the only vapor species identified under these conditions. A background of water in the mass spectrometer resulted in a peak at m/z = 16 (O⁺). This obscured any monatomic O which might have been produced by the Al₂O(g) vaporization. In these preliminary experiments, the signal to noise ratio was low. Species of lower expected vapor pressures, such as AlO, could not be readily detected. A study of alumina vaporization under reducing conditions was conducted using a type two furnace with an alumina cell containing Al metal. Al, Al₂O, and AlO were the principal vapor species identified. Figure 4-27 shows a plot of the intensities of these species with respect to 1/T.

The vaporization of B₂O₃ was studied in a type one Ir furnace and a type two furnace with an alumina cell to 1600K. Five ions were identified in the mass spectrum: B₂O₃⁺, B₂O₂⁺, BO₂⁺, BO⁺, and B⁺. The dependencies of the intensities of these ions with respect to temperature are shown in Figure 4-28. Since the product of the ion intensity and the temperature is proportional to the pressure of the neutral species, the slope of the line in Figure 4-28 can be used to calculate a second law heat of vaporization for B₂O₃.

The observed value, 70.8 kcal/mole, was slightly lower than the range of values reported in the JANAF Thermochemical Tables (73.27-101.67 kcal/mole).⁴

4.3.2.2 TiB₂ Vaporization Studies. The vaporization behavior of TiB₂ was studied in both reducing and oxidizing environments. When TiB₂ was heated in a type one Ta furnace, only Ti and B were evolved, with vaporization beginning at 2300K.

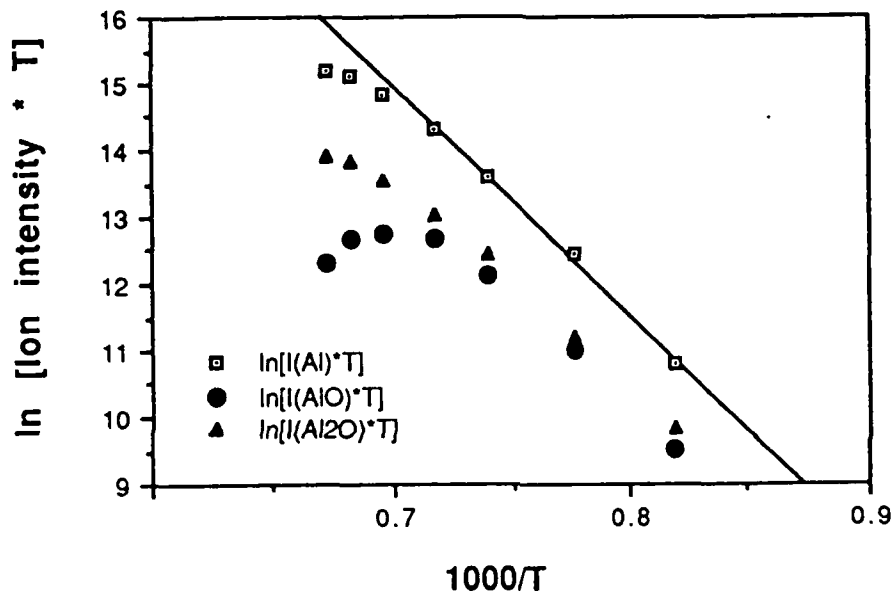


FIGURE 4-27. VAPORIZATION OF Al IN AN Al_2O_3 CELL

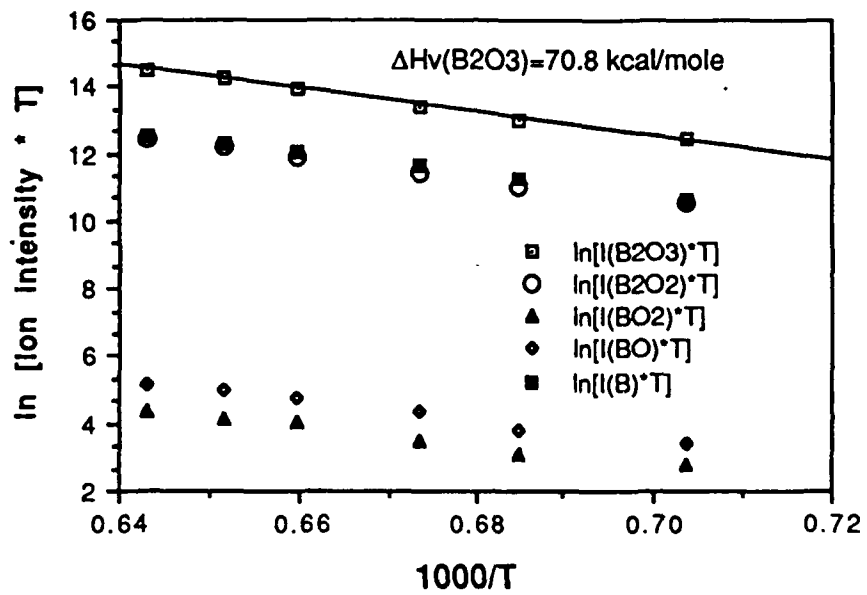


FIGURE 4-28. VAPORIZATION OF B₂O₃ IN AN Al₂O₃ CELL

Vaporization experiments with TiB_2 were also run in a type two furnace, using either an alumina or a calcia-stabilized zirconia cell. TiB_2 was found to react with Al_2O_3 when heated to 1900K. Reduction of the Al_2O_3 cell occurred, producing primarily Al_2O and Al vapor species with a much smaller amount of elemental B. Very low intensity ions were also observed at $m/z = 43$ (AlO or B_2O), $m/z = 54$ (Al_2 or AlB or B_2O_2), and $m/z = 69$ (B_2O_2 or $AlBO_2$). The intensity of the ions and the resolution of the mass spectrometer did not permit differentiation between the possible ion assignments. The ZrO_2 cell produced an almost neutral environment. Elemental B was the only vapor species detected and was first noted below 2000K.

When B_2O_3 was added to TiB_2 in an alumina cell, B_2O_3 , B_2O_2 , BO , B , and BO_2 (probably a fragment ion) were the dominant species. Figure 4-29 is a plot illustrating the relative ratios of the $B_2O_3^+$ and $B_2O_2^+$ ions which were produced. Passing O_2 over TiB_2 in a type three furnace with a zirconia tube led to the production of B_2O_3 , B_2O_2 , and B . Figure 4-30 shows the relative ratios of the $B_2O_3^+$ and $B_2O_2^+$ ions which were produced. Rather intense ions were also observed at $m/z = 28$ and $m/z = 44$. The matrix isolation spectra shown in Figure 4-31 revealed that these ions arose from a silica impurity in the zirconia. A drop in the O_2 intensity occurred at low temperatures, beginning at 800K, while evolution of B_2O_3 did not begin until 1400K. Evidently, diffusion of O_2 through the zirconia tube and subsequent oxidation of the Ta furnace became significant at the low temperature.

4.3.2.3 SrO·ZrO₂ and SrO·HfO₂ Vaporization Studies. Studies of the vaporization behavior of $SrO·ZrO_2$ and $SrO·HfO_2$ were carried out in both reducing and oxidizing environments. Incongruent vaporization was observed for both materials, with the evolution of atomic Sr beginning at a temperature more than 500K below that for the evolution of ZrO_2 or HfO_2 . No SrO was detected in the vapor phase at intensity levels one hundredth those of the atomic Sr and at ionization energies as low as 20 eV. When a type two furnace was used, Sr was first detected in the vapor phase at roughly 1400K. Containment of the samples in a zirconia cell, which was in direct contact with the Ta heater, gave essentially the same onset of Sr evolution and temperature dependence. No evolution of O_2 was observed, presumably due to its rapid reaction with the heater. The evolution of Sr as a function of temperature is shown in Figure 4-32. The reaction $SrO = Sr + 1/2 O_2$ was assumed and the equilibrium constant was defined as $K_p = [(intensity\ of\ Sr) * T]^{3/2}$. The vaporization of $SrO·ZrO_2$ in the presence of O_2 was investigated using a type three heater with a zirconia inner tube. Oxygen introduced into the zirconia cell caused rapid oxidation of the Ta heater. If a vacuum barrier or an Al_2O_3 sleeve was inserted between the zirconia cell and the Ta heater, an oxidizing environment could be maintained within the cell. Under these conditions both O_2 and Sr pressures within the cell were monitored. The variation with

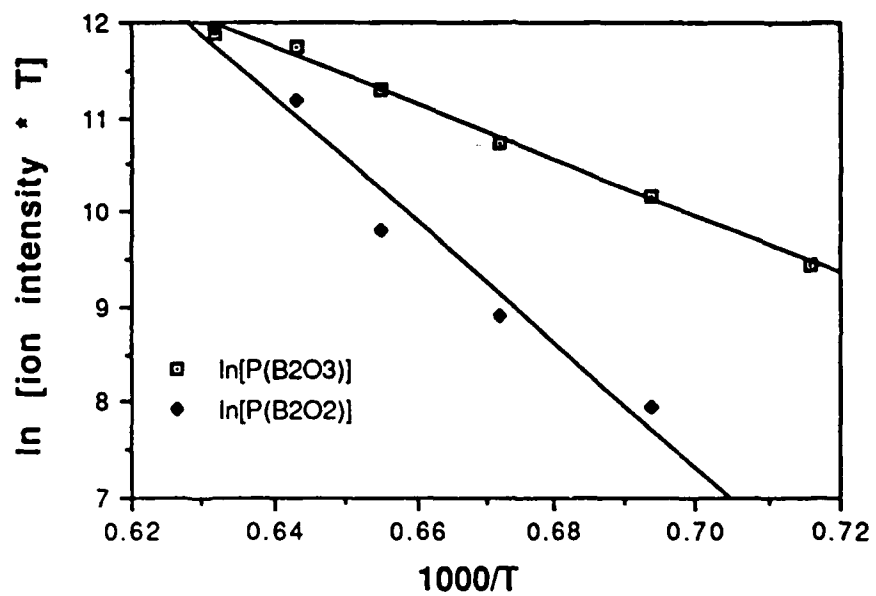


FIGURE 4-29. VAPORIZATION OF $TiB_2 + B_2O_3$ FROM Al_2O_3

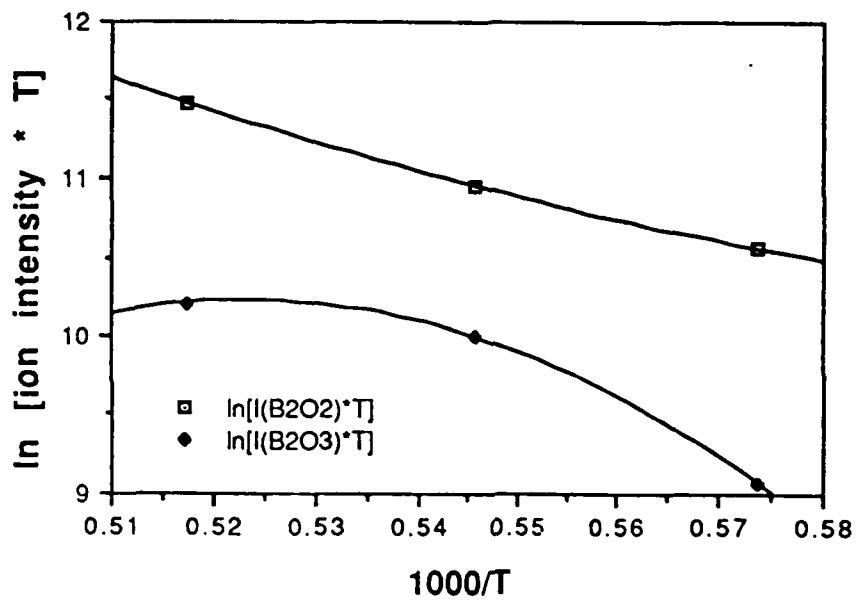


FIGURE 4-30. VAPORIZATION OF TiB_2 WITH O_2 IN ZrO_2

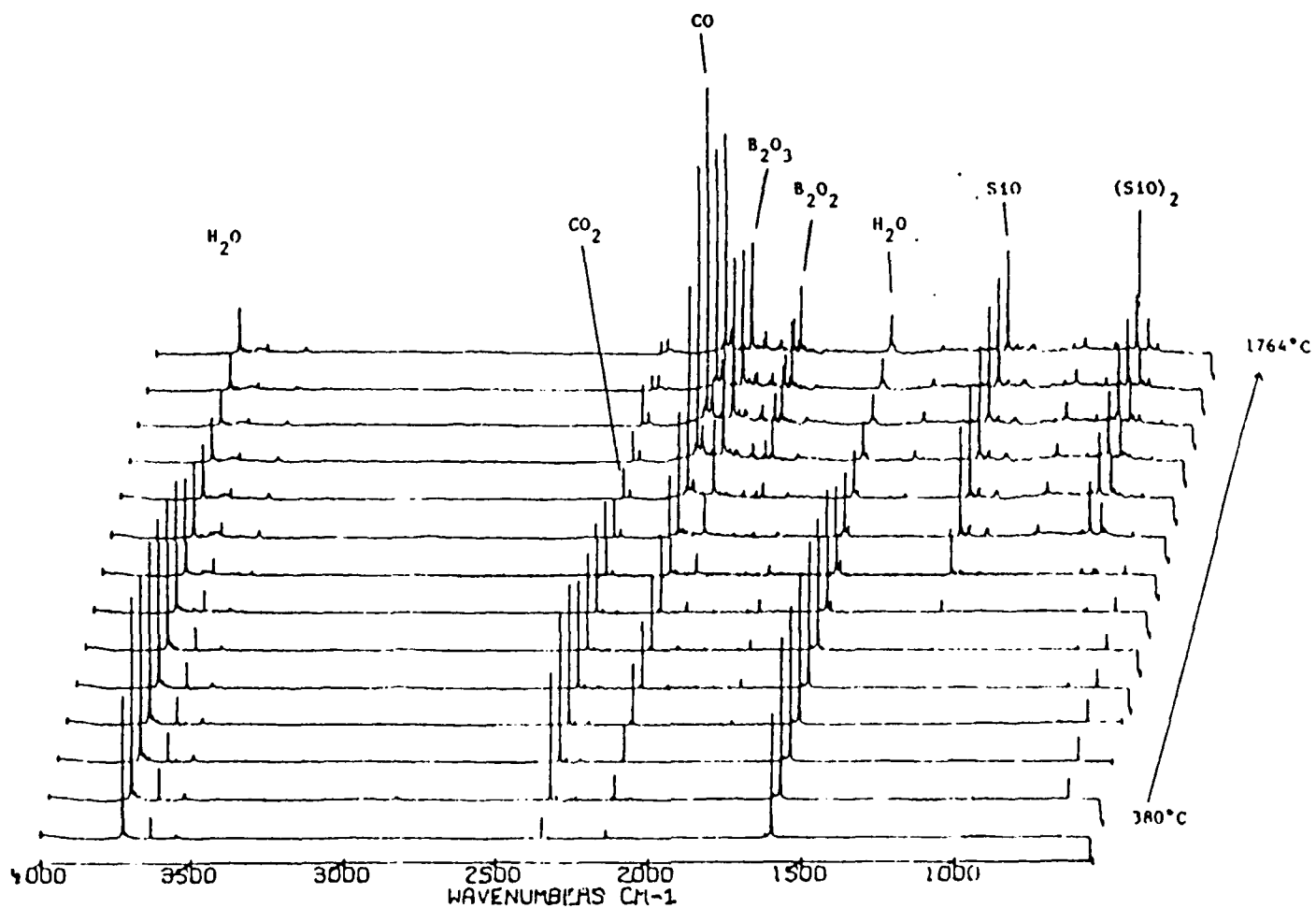
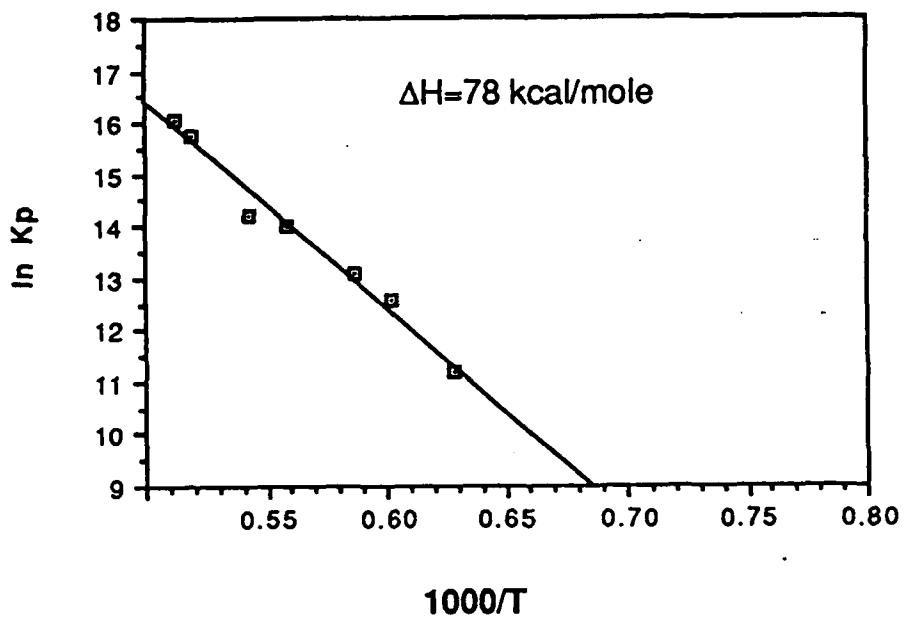
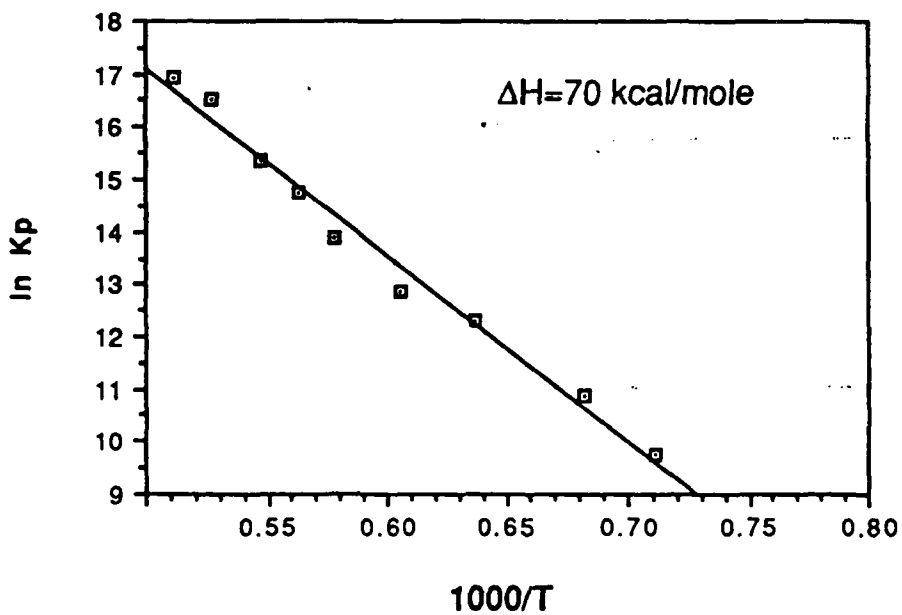


FIGURE 4-31. MATRIX ISOLATION FTIR SPECTRA OF $TiB_2 + O_2$ IN ZrO_2 CELL



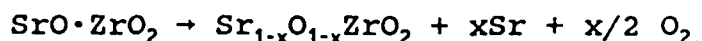
Vaporization of Sr + O₂ from SrHfO₃



Vaporization of Sr + O₂ from SrZrO₃

FIGURE 4-32. VAPORIZATION OF Sr + O₂ FROM SrHfO₃ AND SrZrO₃

variation with temperature of K_p is shown in Figure 4-33, where $K_p = P(\text{Sr}) \times P^{1/2}(\text{O}_2)$, for the reaction



The measured heat of reaction for the above reaction was approximately 130 kcal/mole. Although this value was higher than that measured in the type two furnace (reducing environment), it was still less than expected. The heat of vaporization should be greater than that for SrO, which is 173 kcal/mole at 2000K. Evidently, the reaction process was not simply as stated above. An x-ray microprobe analysis of a cross section of the zirconia tube and sample after the experimental run revealed the presence of Ca in the sample near the tube walls. Calcium from the calcium-stabilized zirconia had diffused into the sample, forming some new mixed oxide of composition $\text{Ca}_w\text{Sr}_x\text{Zr}_y\text{O}_z$. The enthalpy of this reaction was not known.

Finally, when the $\text{SrO} \cdot \text{ZrO}_2$ and $\text{SrO} \cdot \text{HfO}_2$ samples were heated above 2300K, their respective atomic metals and diatomic metal oxides were evolved, with the diatomic monoxide most abundant. Appearance potential curves were determined for atomic Zr and ZrO as shown in Figure 4-34. The rapid rise of ZrO at electron energies from 50 to 70 eV suggested that possible fragmentation of another molecule was contributing to the ZrO ion intensity in this ionization energy range.

4.3.2.4 Vaporization Studies of Yttria, Zirconia, and Hafnia.

Samples of pure (>99.5%) yttria, zirconia, and hafnia, as well as yttria-stabilized hafnia and hafnia with 5% to 10% yttria, were studied. Type one Ta furnaces and type two furnaces were used to heat the samples as high as 2700K. The required vaporization temperatures exceeded cell capabilities for all oxide cell materials except ThO. Thoria tubes were ordered but arrived at the conclusion of the program. Vaporization of the oxides began between 2400K and 2500K. The samples were observed to vaporize as atomic Y, Zr, and Ha and their respective monoxides. More atomic metal was produced in the type two furnace, presumably as a result of the larger hot Ta surface area (reducing environment) exposed to the sample vapors.

Matrix isolation FTIR experiments revealed small extinction coefficients for the oxides. Observation of the monatomic metals required codeposition with a low concentration of CO. The resulting spectra contained a number of unidentified peaks.

Since the IR spectroscopy literature on the heavy metal oxides and carbonyls is rather limited, a complete assignment of the spectra would require the development of a more extensive data base.

Vaporization of Sr + O₂ from SrZrO₃

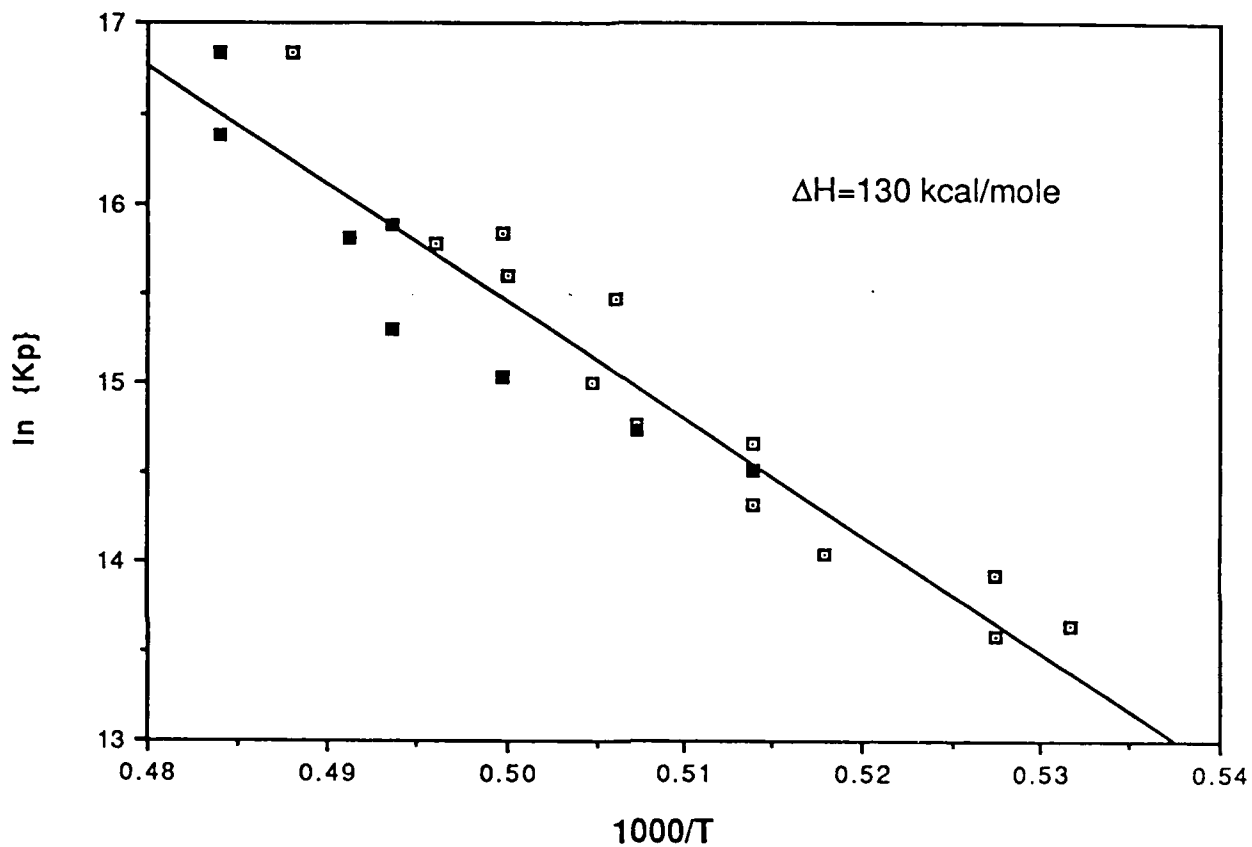


FIGURE 4-33. VAPORIZATION OF Sr + O₂ FROM SrZrO₃ WITH VACUUM SEPARATION BETWEEN ZIRCONIA CELL AND Ta HEATER

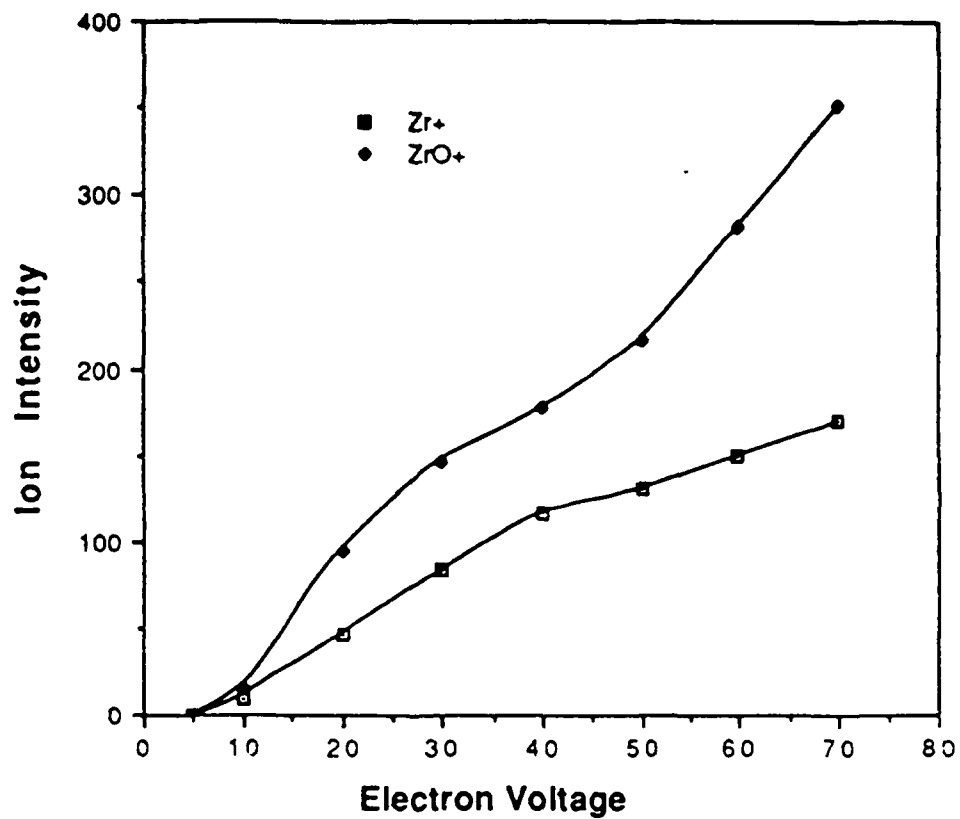
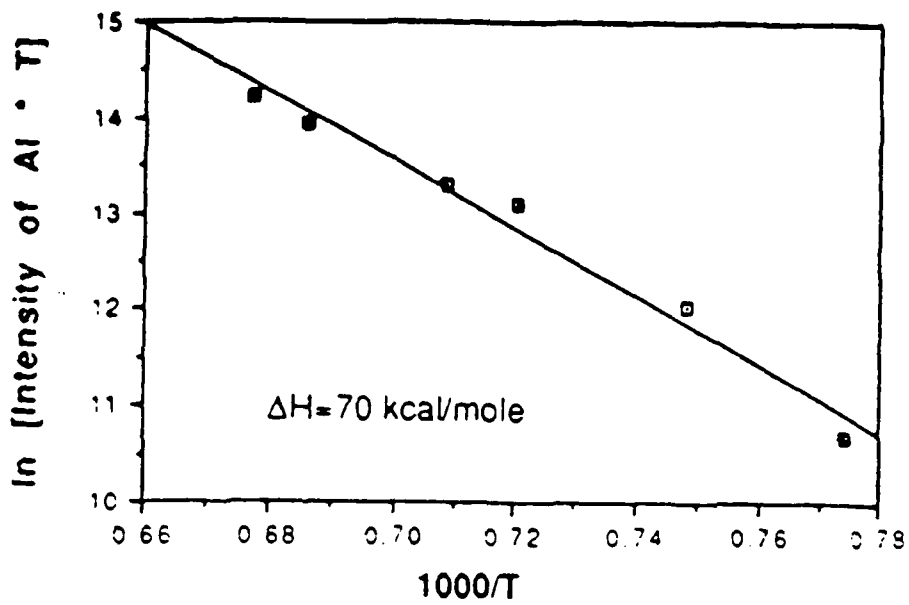


FIGURE 4-34. APPEARANCE POTENTIAL OF Zr AND ZrO FROM THE VAPORIZATION OF SrZrO_3

4.3.2.5 Vaporization Studies of $\text{Ir}_{0.4}\text{Al}_{0.6}$. The vaporization of $\text{Ir}_{0.4}\text{Al}_{0.6}$ was studied under both neutral and oxidizing conditions in the temperature range of 1100K to 1700K. In both cases the loss of Al was observed through vaporization of the Al and Al_2O species, with Al vapor first detected at 1390K. The Al_2O species may have resulted from an oxide surface layer. Elemental Al and a piece of an $\text{Ir}_{0.4}\text{Al}_{0.6}$ sample, which was inserted as a single piece, were studied in a type two furnace containing a zirconia cell. The data are shown in Figure 4-35. The partial pressure of Al showed a much greater temperature dependence at the lower temperatures than at the higher temperatures. This is illustrated by the two lines which are fitted to the upper four points and lower three points in Figure 4-35 for $\text{Ir}_{0.4}\text{Al}_{0.6}$. The points of two additional vaporization studies are shown in Figure 4-36. In both of these studies, the $\text{Ir}_{0.4}\text{Al}_{0.6}$ samples were crushed prior to the experiment to expose more sample surface. In the study without added O_2 (using a type two furnace with a zirconia cell), the Al ion intensity showed a greater temperature dependence in the first heat cycle than in the second heat cycle. After the first heating, the temperature dependence was very similar to that of elemental Al (shown in Figure 4-35). This behavior suggested that in the early heating period, an oxide layer existed which inhibited the vaporization process, thus producing a temporary higher temperature dependence. This was supported by a study of the loss of Al while O_2 was passed over the sample (using a type three furnace with a zirconia tube), as shown in Figure 4-36. The temperature dependence of the Al pressure in a low partial pressure of O_2 ($< 10^{-5}$ torr) was greater than for the studies without O_2 . At low inlet rates of O_2 , the pressure of Al was similar to that for the case without O_2 and the pressure of Al_2O was enhanced. This resulted in a more rapid depletion of Al from the sample, as evidenced by the drop in Al pressure in the second heating cycle of the sample after the O_2 was turned off.

The experimental enthalpies of vaporization of Al from the Ir-Al alloy were disturbingly low, almost suggesting that free Al was vaporizing. Optical microscopy revealed that the sample consisted of two phases. An x-ray microprobe analysis of an untreated sample of the alloy revealed that roughly two thirds of the material had an approximate stoichiometry of Ir_3Al_8 . The stoichiometry of the remaining one third of the sample was roughly Ir_5Al_6 . After a sample of the alloy was heated several times, the sample appeared homogeneous with a stoichiometry of Ir_5Al_6 . Because of container limitations, the samples were not heated to sufficient temperatures to vaporize the Ir or to investigate the vaporization of Al from the "homogeneous" phase.



Vaporization of Al from Al

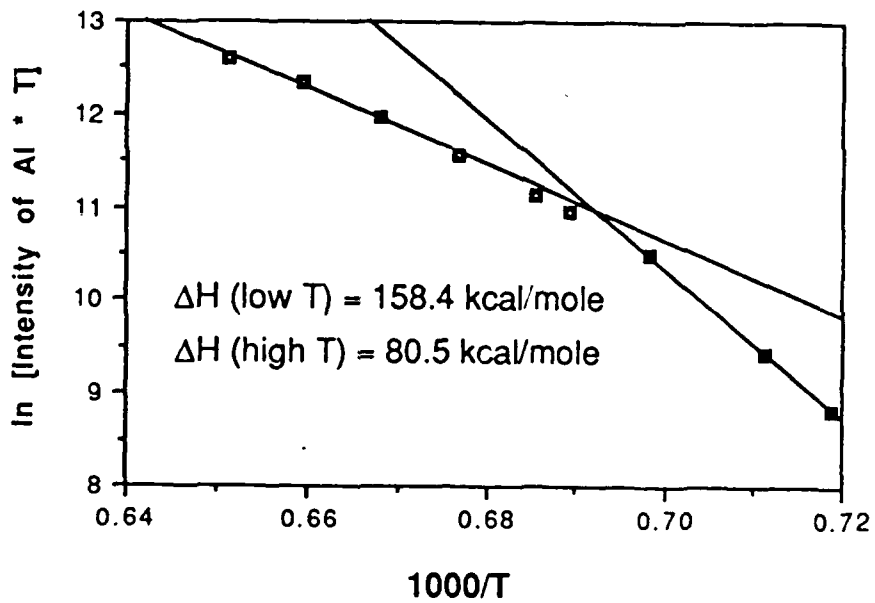
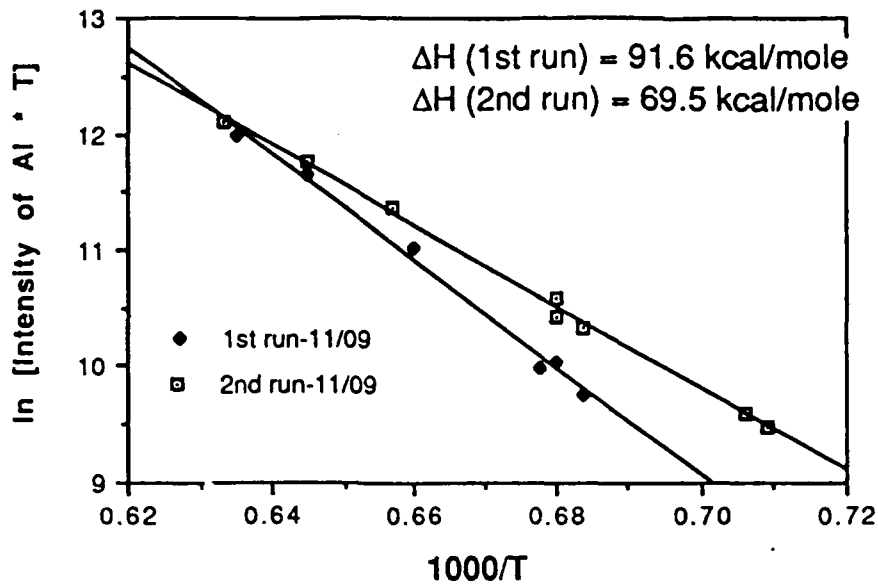


FIGURE 4-35. VAPORIZATION OF Al FROM ELEMENTAL Al AND FROM $\text{Ir}_{0.4}\text{Al}_{0.6}$



Vaporization of Al from $\text{Ir}_{0.4}\text{Al}_{0.6}$

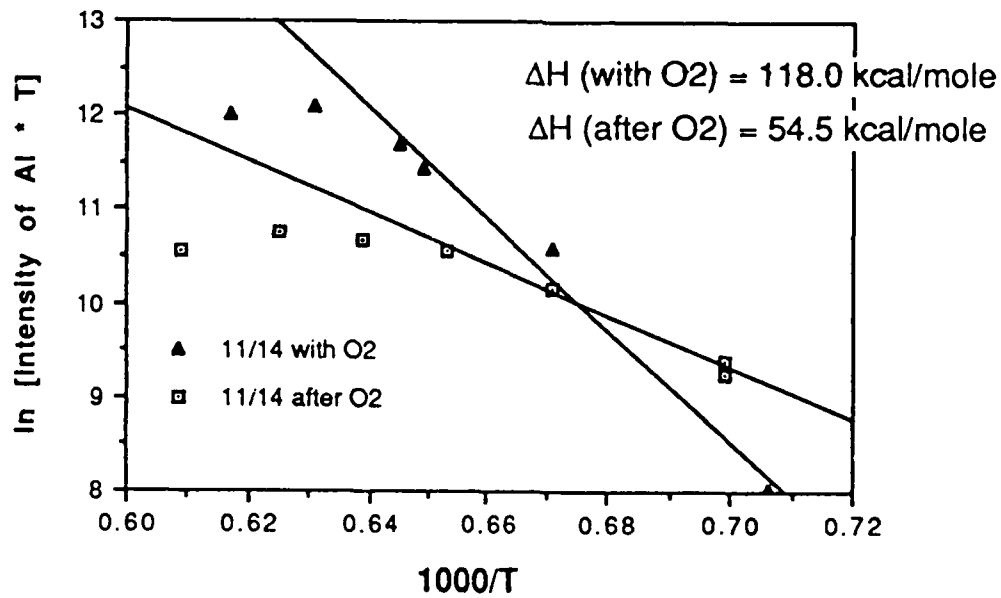


FIGURE 4-36. VAPORIZATION OF Al FROM $\text{Ir}_{0.4}\text{Al}_{0.6}$ WITH AND WITHOUT ADDED O₂

CHAPTER 5

DISCUSSION

5.1 MODELING

For the most part, thermochemical analysis based upon data available in the literature, primarily the major compilations, has proved adequate to provide useful estimates of the behavior expected for the single constituent systems examined in this program.

There are major deficiencies in the data base available for refractory intermetallic systems. In many cases, one has no more to work with than a lower limit on the free energy of formation based on qualitative observations of formation reactions at elevated temperatures.

More subtle limitations exist for systems involving compounds with a range of composition. Compiled data, in general, apply to compositions of simple combining proportions. As illustrated in the discussion of the vaporization behavior of HfC, this results in some ambiguities in the interpretation of systems of changing composition. However, these problems are second order in nature.

Modeling efforts indicate that the impact of oxidizing environments can be readily determined at very low O_2 pressures, even as low as say 10^{-3} atm, provided only that the O_2 pressure is well defined. This is significant in assessing potential experimental approaches. For example, mass spectrometric sampling is much easier to achieve at 10^{-3} atm than at full atmosphere. The reason that relatively low O_2 pressures can provide an adequate experimental basis for assessing behavior under oxidizing conditions is that even these low pressures far exceed the decomposition pressures of oxides of interest in the reaction of refractory materials. Further, the thermodynamic response to pressure change is intrinsically logarithmic. The extrapolation of data in the range 10^{-4} to 10^{-3} atm to 1 atm involves an extrapolation from -3 to 0, not from 10^{-3} to 1.

Material assessment based on thermochemical methods takes the form of the prediction of a reaction, for example, the formation of an oxide, or the estimation of the pressure in a volatilization process. Reaction events are usually clear-cut. Where the result is the estimation of a vapor pressure, there remains a question of how large a pressure can be accepted.

5.2 LASER PROBE SPECTROSCOPY

Optical pyrometry was used to measure the sample front surface temperature during laser heating of all the materials studied.

Though an IRCON two color system was used, the temperature readings are subject to error. Temperature errors could result from unknown material emissivities and/or plume emission contamination within the detector bandwidth. To address these problems, HARC, in an independent effort, is developing an advanced six color optical pyrometer system to accurately measure the sample front surface temperature. The six color system is constructed and currently undergoing checkout and validation. Additionally, HARC may be funded (by a separate program) to develop an advanced 32 color optical pyrometer system. If funded, the system would be available in the summer of 1989.

5.2.1 Emission Spectra

Generally, optical emission spectra measurement has been extremely useful in determining what species are produced from laser heated materials. This quick and simple method has detected atomic, diatomic, and polyatomic species in the visible portion of the spectrum. The identity of the species in the vapor plume provides important information on the high temperature degradation reactions of the candidate materials. For example, the emission spectrum of $\text{HfO}_2\text{-Y}_2\text{O}_3$ (Figure 4-14) shows YO (not HfO) vaporizing from the substrate when heated in a 10 torr O_2 environment. When $\text{SrO}\cdot\text{HfO}_2$ was laser heated in a vacuum environment, SrO was detected in the vapor plume; however, when $\text{SrO}\cdot\text{HfO}_2$ was heated in a 10 torr O_2 environment, SrO was not detected (Figure 4-16). Additionally, HfO was detected from laser heated HfC in a 10 torr O_2 environment (Figure 4-17), and atomic Sr was detected only during laser heating of ZrC in a vacuum environment (Figure 4-18).

However, the OMA studies could be extended further. Many strong atomic transitions lie in the ultraviolet (UV) and vacuum ultraviolet (VUV) portion of the spectrum. HARC has recently acquired high resolution UV diffraction gratings that should extend the short wavelength capability to ca 225 nm. Additionally, a scintillator could be added to the OMA detector to enhance the UV/VUV response.

5.2.2 Absorption Spectra

Generally, the laser absorption method should be able to produce accurate, quantitative results that agree with theoretical predictions if the absorption cross section (σ or, equivalently, the Einstein A-coefficient), the temperature, and the effective pathlength are known. The assumption that the effective pathlength is the same as the longitudinal sample dimension may be incorrect and the primary source of error in the calculation of the vapor species number density. Indeed, the factor of ca 2.3 difference between the calculated and observed atomic Al number densities (see discussion of Figure 4-22) could be accounted for by such a probe

pathlength error. Clearly, the pathlength must be better defined in future experiments.

Figure 4-23 shows the absorption spectrum of atomic Al obtained during CO₂ laser heating of Ir_xAl_y to 1910°C in a vacuum environment (top panel); the experimental atomic Al number density (calculated from the Beer Lambert relation and the 3/2 → 3/2 transition data) is 4x10¹³ atoms/cm³. However, no atomic Al was detected during laser heating at 1860°C in a 5 torr O₂ environment (bottom panel). Most likely, atomic Al quickly reacts with O₂ at the sample-vapor interface to efficiently produce AlO. Simultaneous observation of Al and AlO under varying temperature and O₂ pressure and as a function of position relative to the interface could provide information on the dynamics of that reaction.

5.3 MASS SPECTROMETRY AND MATRIX ISOLATION FTIR SPECTROSCOPY

Mass spectrometric sampling with Ta heating elements has been shown to be capable of monitoring vapor species evolved at temperatures up to 2700K with O₂ pressures up to a few microns with an open ended cell. Pressures of a few hundred microns can be achieved when specially fabricated cell caps with small (0.5 mm) orifices are used. As discussed in Section 6.3, higher environmental pressures can be investigated with provision of differentially pumped, high pressure sampling nozzles.

For Ta and metallic W resistance heating, the reducing environment near the heating element must be isolated chemically from the oxidizing environment of the sample container. For containers which exhibit high oxide conductivity, such as the stabilized zirconia cells, a vacuum gap and a secondary oxide barrier were required for adequate separation of the reducing and oxidizing environments. Achieving the required isolation was found to be a demanding and somewhat limiting requirement in the present study, which strongly supports the desirability of self-contained material configurations to the extent possible.

As expected, mass spectrometry, with its sampling of all volatile species, high sensitivity, and wide dynamic range, was the most versatile experimental tool. Matrix isolation FTIR spectroscopy remains a useful adjunct for situations of mass/charge ambiguity.

The general behavior across the range of materials studied can be summarized as follows:

Metal Borides and Carbides

- (1) Metal borides and carbides vaporize under neutral conditions as the atomic metal, B, and C species.

- (2) TiB_2 and HfC react readily with O_2 at temperatures below 1300K. At higher temperatures, B_2O_3 and B_2O_2 are evolved from the boride and CO from the carbide.

Metal Oxides

- (1) Strontium zirconate and hafnate lose Sr and O_2 over the temperature range from 1800K to 2300K. Above 2300K Zr oxides and Hf oxides are evolved. The onset temperature of Sr evolution is observed to increase with O_2 pressure. Under reducing conditions the Sr will evolve at temperatures as low as 1500K.
- (2) Yttria stabilized zirconia and hafnia vaporize with loss of Y, YO, and the respective metals, metal monoxides, and metal oxides. Vaporization begins above 2500K in a Ta cell.

Alloys

- (1) The heat of vaporization of atomic Al from the Ir-Al alloy initially appears approximately two times as high as that for elemental Al, presumably due to an initial oxide surface layer. Once the oxide layer is removed, the heat of vaporization of Al from $Ir_{0.4}Al_{0.6}$ approximates that for elemental Al. Passage of O_2 over the sample causes an apparent increase in the heat of vaporization of Al. At low O_2 flow rates, the sample completely consumes the O_2 and the loss of Al is enhanced, apparently by the resultant evolution of Al as Al_2O in addition to atomic Al.

The combined control of the O_2 activity as a consequence of the strongly reducing properties of the resistance heating elements has precluded achieving a well enough controlled O_2 activity to fully compare results with literature values in some cases.

5.4 MATERIALS AND METHODS COMPARISON

The laser spectroscopic and mass spectrometric methods were found to be complementary, although cell reaction problems with the mass spectrometer limited the range of direct comparisons available.

HfC was examined only via laser spectroscopy. Up to 3400K, no distinct spectrum was observed in vacuum, but an identifiable HfO emission spectrum was obtained in 10 torr O_2 . In related experiments with ZrC , a complex spectrum attributed to atomic Zr was observed in vacuum at 3500K. These results are in accord with the expectation of very low volatility as the metal under neutral conditions and vaporization as HfO under oxidizing conditions.

TiB₂ was studied by both laser spectroscopic and mass spectrometric techniques, although the mass spectrometric measurements were limited by cell interactions. Under vacuum conditions, the emission spectrum showed only a few irregular features up to 2950K. Under 10 torr O₂, a well-characterized emission from BO₂ was obtained. Under vacuum, or actually reducing, conditions, the mass spectra showed Ti and B as vapor species above 2300K. Measurements attempted in Al₂O₃ and stabilized ZrO₂ cells resulted in reaction with the cell. BO, B₂O₂, B₂O₃, and BO₂ were all observed in these experiments. These results illustrate some of the relative advantages of the approaches. The laser spectroscopic methods can readily attain high temperatures without problems of cell reactions, but the mass spectrometric approach readily monitors the full range of gaseous species.

Y₂O₃ stabilized HfO₂ was measured only via laser tests. ThO₂ cells needed for mass spectrometric measurements were not delivered in time to attempt such measurement. The laser tests provided a YO emission spectrum at 3083K in O₂. No YO was observed in vacuum, but that spectrum was obtained at 2870K. The absence of HfO emission qualitatively suggests that Y₂O₃ is being preferentially vaporized. However, sufficient data are not available to assess the relative emission strengths of YO and HfO.

SrO·HfO₂ was investigated by both laser spectroscopy and mass spectrometry. An SrO emission spectrum was recorded for SrO·HfO₂ in vacuum at a temperature of 2750K. Identification was through comparison with a spectrum obtained from pure SrO at 2590K. The SrO features were not observed at 2721K in a 10 torr O₂ atmosphere. This result is not fully understood since vaporization as SrO should not be suppressed by O₂. The volatility was qualitatively lower from SrO·HfO₂ than from SrO, but the difference was not quantified. The mass spectrometric measurements clearly showed the preferential volatility of Sr, but apparent interactions with cell and heater materials prevented quantitative interpretation. In particular, only Sr was observed as a volatile species, although calculated abundances for SrO in equilibrium under neutral conditions should have been detectable. Further, the apparent heat of vaporization of Sr from SrO·HfO₂ was less than the calculated value from SrO, an unphysical result. If the cell/heater interactions were overcome, mass spectrometric measurements could provide direct measurement of the free energy of formation of SrO·HfO₂ from SrO and HfO₂.

The IrAl sample was also investigated using both laser spectroscopic and mass spectrometric methods. In this case, the strong absorption band of Al was available and measurement could be made in absorption. Analysis of the spectrum under vacuum provides an estimated number density of $4.0 \times 10^{13}/\text{cm}^3$ at 2183K. If this number density is converted to a pressure and compared with the vapor pressure of pure Al, one obtains a one point estimate of the free energy of formation of IrAl of -35 kcal. Previously

available thermodynamics for IrAl consisted of an estimate of <-17 kcal at 1500K.¹⁶ Under 10 torr O_2 , no Al absorption was observed at 2133K. This is the expected result since Al_2O_3 would form. The mass spectrometric results also provided an initial indication of strongly reduced Al pressure, but subsequent results suggest that surface oxides present on the samples are creating artifacts. It also appears uncertain that the relatively large, low surface area sample particles are attaining or maintaining equilibrium.

CHAPTER 6

RECOMMENDATIONS

6.1 MODELING

Extension of modeling to the evaluation of composite systems, in contrast to constituents, will place increased emphasis on the interaction of condensed phases. This has been done to some extent in the consideration of constituents forming additional condensed phases upon exposure to O. In the assessment of composite systems, consideration must be given both to the principal, desired phases and any probable impurity phases.

The basic analytical approach should also be extended to "dynamic testing," where that term is taken to mean the assessment of gas phase concentration data from open systems. The classical thermochemical analysis primarily used in the present modeling effort is most simply applied to enclosed, equilibrium systems. The Knudsen cell is the classic example. In the present program, the laser probe spectroscopy investigations were carried out in an open system. The results of the mass spectrometric studies suggest that a self-contained, laser heated sample configuration would provide a less ambiguous approach for some materials, again a more open system. The requirement will provide appropriate thermochemical, mass transport, and heat transfer models to interpolate between the Knudsen cell, i.e., perfectly closed system, and a Langmuir evaporation condition of vaporization into a perfect vacuum.

Some of the same questions that must be addressed in the interpretation of "dynamic testing" should also be considered in quantifying the use of vapor pressures, whether experimental or from thermodynamic calculation, in assessing the usefulness of ultrahigh temperature materials. The estimation of a material loss rate from a vapor pressure requires the definition of a mass transport problem very analogous to the treatment of open system vaporization processes.

6.2 LASER PROBE SPECTROSCOPY

One of HARC's major goals in this program was the development of a laser probe spectroscopy method suitable for studies on laser heated materials held in vacuum and low partial pressure oxidizing environments. HARC has developed a procedure for systematically testing ultrahigh temperature materials. The flow diagram for the recommended procedure is shown in Figure 6-1. Initially, the environmental conditions to which the material will be subjected are defined and a pre-test characterization is conducted. Next, thermodynamic calculations are performed to predict what vapor species are expected, and atomic and/or molecular spectra are simulated based on these predictions. Qualitative plume emission

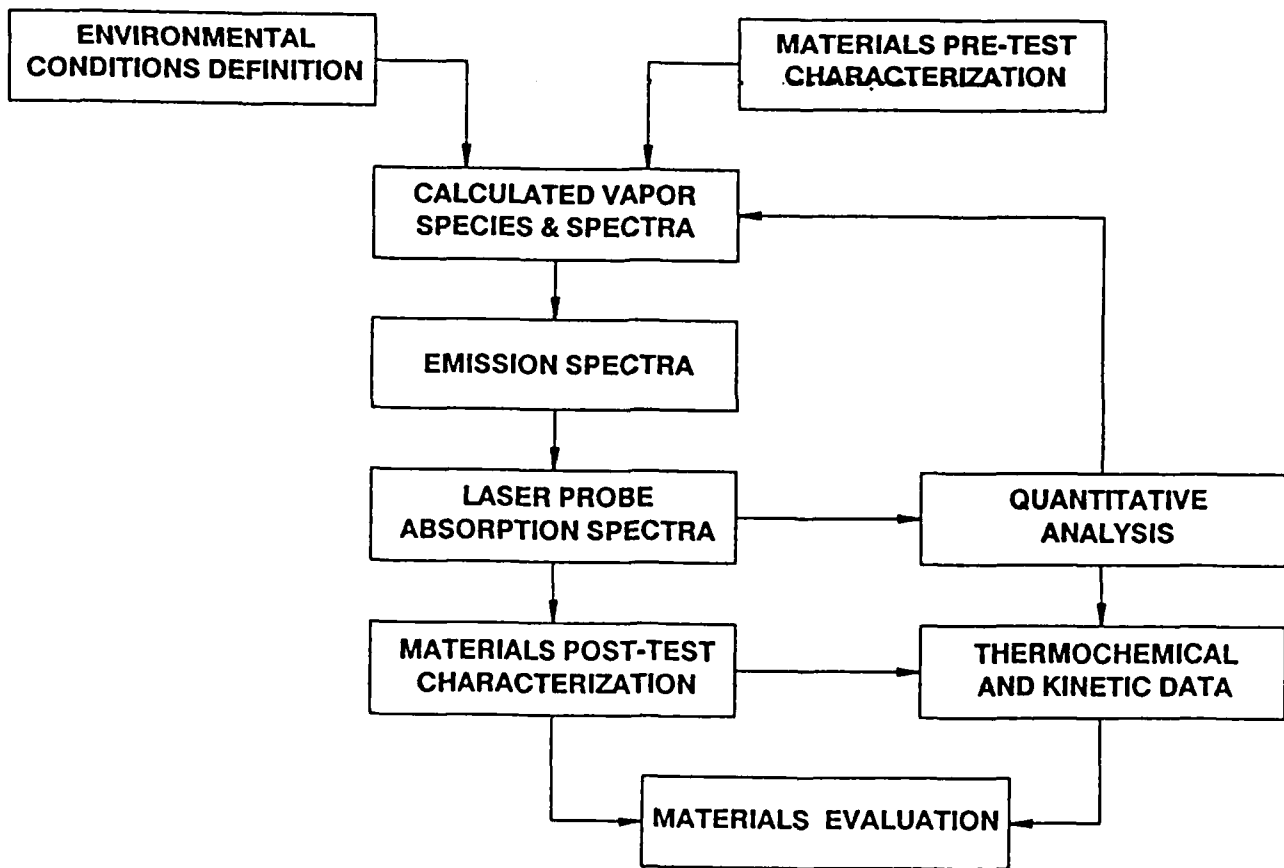


FIGURE 6-1. HIGH TEMPERATURE MATERIALS EVALUATION APPROACH

spectra from the laser heated material are then recorded and the atomic/molecular plume species are identified. The laser probe spectrometer can then intelligently probe the vapor plume to quantitatively measure vapor species abundance as a function of temperature and environment. Finally, the data and post-test analysis are used to evaluate the performance of the material.

In addition to the procedure outlined above, recommendations for extending and improving the laser probe spectroscopy technique for future high temperature materials evaluation studies are:

Flat-Top CO₂ Beam Profile

The CO₂ laser profile should be converted to a flat-top profile to eliminate any steep temperature gradients in the sample temperature. HARC has recently acquired a mirror integrator from Spawr Optical for this purpose. The mirror will supply uniform irradiance on target and possibly aid in defining the effective pathlength of the probe laser.

Defined Probe Pathlength

As mentioned Section 5.2.2, additional steps must be taken to accurately define the effective pathlength of the probe laser. This issue requires immediate attention.

"Computer Controlled" Sample Temperature

An active feedback circuit is required to control the temperature of the sample. The feedback signal should originate from the optical pyrometer (or thermocouple) to control CO₂ laser power on target (and hence sample temperature).

Multiple Wavelength Probing

With a second tunable dye laser system (i.e., another CCLAS system), two vapor species could be monitored simultaneously via the direct absorption method. For example, in the Ir_xAl_y oxidation experiment, the evolution of atomic Al and the formation of AlO could be simultaneously recorded and studied as a function of temperature and O₂ pressure. HARC has all the laser equipment (ion lasers and dye lasers) on hand but would require an additional PC and time for setup, interfacing, checkout, etc.

Laser Induced Fluorescence (LIF)

If greater sensitivity is required beyond the detection limits of the direct absorption method, LIF is the technique of choice. LIF would enhance detection sensitivity three to five orders of magnitude.

6.3 MASS SPECTROMETRY AND MATRIX ISOLATION FTIR SPECTROSCOPY

Mass spectrometric sampling provides versatile detection of volatile species evaporating from ultrahigh temperature materials or formed by reaction of other vapor species with those materials. Operation with resistively heated sample systems, however, complicates and/or compromises control of the gaseous environment. Modified Knudsen cell approaches are limited to pressures in the micron range.

To extend the capabilities of this method, a differentially pumped sampling system combined with laser heating is recommended. By sampling through a differentially pumped orifice chamber, the pressure of the sampled environment can be increased to near atmospheric. By using a high wattage cw laser as the heat source, samples can be self-contained; i.e., only the sample material need be brought to the experimental temperature. In some cases it may be possible to design the self-containment to attain equilibrium vapor pressures, but the interpretation of results will, in general, involve open or semi-open systems.

A system developed along these lines is nearing completion in the Rice University laboratories and is shown schematically in Figure 6-2.

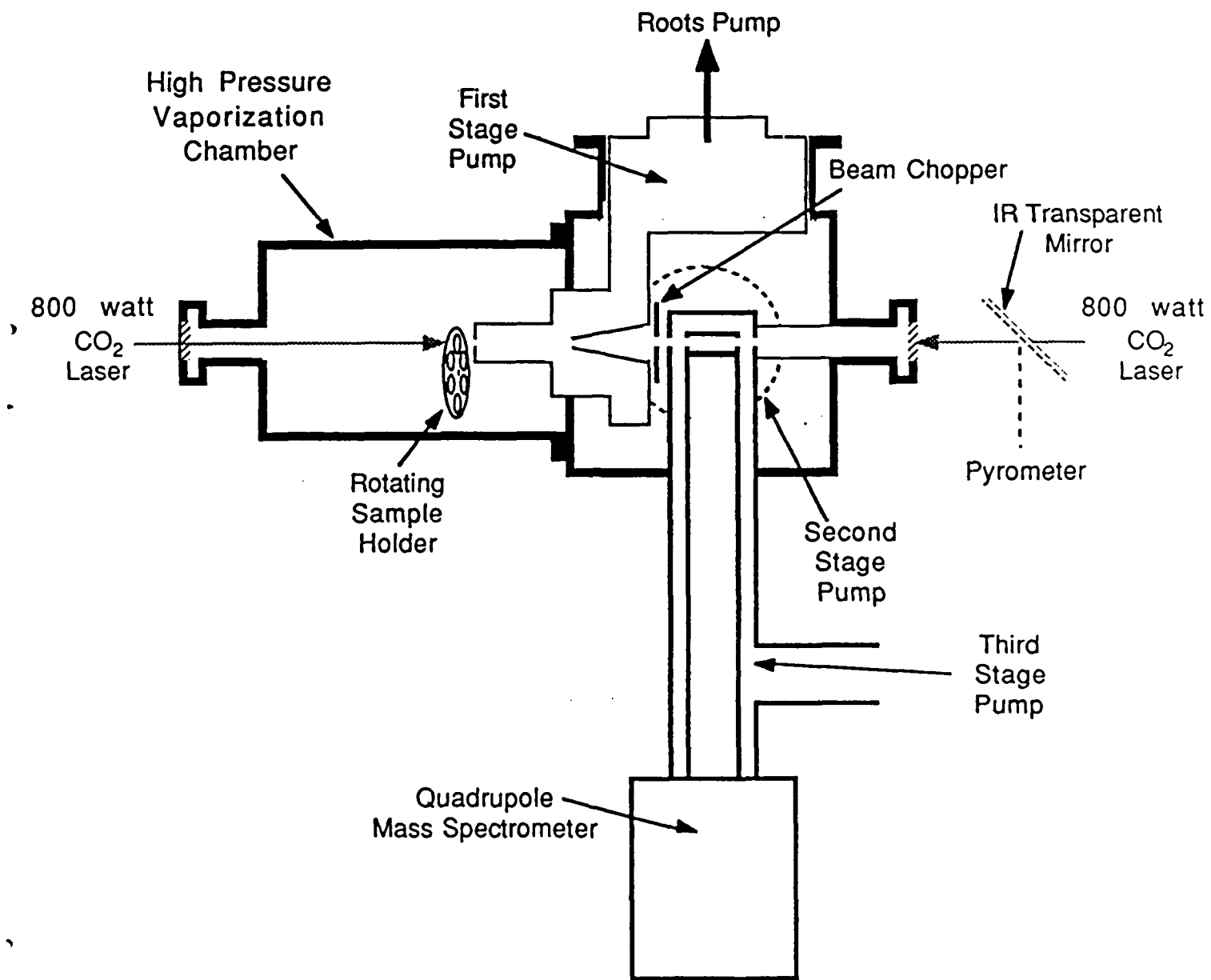


FIGURE 6-2. HIGH PRESSURE MOLECULAR BEAM MASS SPECTROMETER PROBE

CHAPTER 7

REFERENCES

1. Worrell, Wayne L., "Experimental Evaluation of New Alloys for Protective Coatings for Carbon-Carbon Composites at Ultra-High Temperatures," Air Force Materials PRDA Programs Review, Dayton, Ohio, November 18-19, 1987.
2. Kubaschewski, O., and C.B. Alcock, Metallurgical Thermochemistry, 5th ed. Pergamon, Oxford, 1979, pp. 193.
3. Belov, A.N., and G.A. Semenov, Russ. J. Phys. Chem. 59, 342 (1985).
4. Chase, M.W., et al., "JANAF Thermochemical Tables, Third Edition," J. Phys. Chem. Ref. Data 14, Suppl. 1 (1985).
5. Schick, H.L., Thermodynamics of Certain Refractory Compounds, Vol. II, Academic Press, New York, 1966.
6. L'vova, A.S., and N. N. Feodos'ev, Russ. J. Phys. Chem. 39, 1091 (1965).
7. Kosta, L.F., K.D. Mielenz, and F. Grum, "Correction of Emission Spectra," Chapter 4 of K.D. Mielenz (ed.), Optical Radiation Measurements, Vol. 3, Measurement of Photoluminescence, Academic Press, New York, 1982, pp. 139-174.
8. Huber, K.P., and G. Herzberg, Molecular Spectra and Molecular Structure, IV, Constants of Diatomic Molecules, Van Nostrand Reinhold Company, New York, 1979.
9. Johns, J.W.C., Can. J. Phys. 39, 1738 (1961).
10. Bernard, A., and R. Gravina, Astr. J. Supp. Ser. 44, 223 (1980).
11. Reader, J., C. Corliss, W.L. Wiese, and G.A. Martin, "Wavelengths and Transition Probabilities for Atoms and Atomic Ions," NSRDS-NBS #68, U.S. Government Printing Office, Washington, DC, 1980.
12. Sen, M.K., Ind. J. Phys. 11, 251 (1937).
13. Herzberg, G., Molecular Spectra and Molecular Structure, I, Spectra of Diatomic Molecules, Van Nostrand Reinhold Company, New York, 1950, p. 208.
14. Herbert, G.R., and R.W. Nicholls, J. Quant. Spectrosc. Radiat. Trans. 23, 229 (1980).

15. Wiese, W.L., M.W. Smith, and B.M. Miles, "Atomic Transition Probabilities," Vol. II, "Sodium Through Calcium," NSRDS-NBS 22, U.S. Government Printing Office, Washington, DC, 1969.
16. Gibson, J.K., and P.R. Wengert, High Temp. Sci. 17, 371 (9184).